Università degli Studi di Cagliari

PHD DEGREE

Neuroscience

Cycle XXXIV

TITLE OF THE PHD THESIS

Cerebral white matter status and resting state functional MRI

Scientific Disciplinary Sectors

MED/36 – MED/37

PhD Student: Dr. Michele Porcu

Supervisor Prof. Giovanni Defazio

Final exam. Academic Year 2020/2021
Thesis defence: February 2022 Session

This thesis is dedicated to my father, Guido Porcu.

I will always try to carry on your example as a man and medical doctor.

Acknowledgements

I want to thank my hospital tutor, scientific mentor and friend, Prof. Luca Saba, for always believing in me and for the passion he transmitted to me for scientific research.

I want to thank my academic tutor, Prof. Giovanni Defazio, for his support in this PhD course.

I want to thank my colleague and friend, Dr. Luigi Cocco, my "partner in crime" in this project, and all the other co-authors of the mentioned studies.

I want to thank Dr Luigi Barberini for teaching me the basics of functional MRI analysis.

I want to thank all the colleagues, radiographers, nurses and the administrative stuff of the Radiological Department of the A.O.U. of Cagliari for their support in our daily clinical activities.

I want to thank my clinical mentor, Dr. Paolo Siotto, for the passion that he transmitted to me for radiology.

I want to thank all the colleagues of the Radiologisk Klinik of the Rigshospitalet in Copenhagen, in particular Dr. Vibeke André Larsen and Prof. Carsten Thomsen, for the great opportunity that they give me as resident in Radiology in 2016 and their precious teaching in Neuroradiology. For all of you, Tusind Tak!

I want to thank all the colleagues of the Emergency Radiology Department of the University Hospital of Turku (Finalnd), in particular Dr. Kimmo Mattila, for their precious teaching in the emergency radiology department and the great professional experience I had in 2014. For all of you, Kiitos!

I want to thank my radiologist colleagues and friends, Vitanio, Carlo, Francesco, Stella, Elisa, Giulio, Antonio, Giulio, Francesco, Paolo, Riccardo, Annunziata, Annapaola, Carla, Elisa, Serena, Rosi, Virgilio, Giuseppe, Silvia, Angelo, Stefano, Giovanni, Gildo, Stefano, Dino, Maria Angelica and Mauro for their true friendship that goes beyond the ordinary working activities.

I want to thank my university colleagues and friends Federico, Francesco, Roberto, Giulio, Gian Mario, Sergio, Fabio, Federica, Elisa, Chiara, Bruna and Daniela for their friendship and the incredible funny moments we had together.

I want to thank my "Erasmus" friends Kalypso, Luca, Jesus, Alina, Fernando, Alberto, Emilia, and Giovanni for their friendship that goes beyond every boundary.

I want to thank Agostino and Genoveffa, my second parents.

I want to thank my lifetime friends, Francesco and Mario, for their friendship and loyalty.

I want to thank my mom, Patrizia, for the motherly love she gives me every day, and my family for their support.

I want to thank my life partner, Gloria, for her precious support and the love she always showed me in these years.

A tutti voi, grazie di cuore!

"*What is a scientist after all? It is a curious man looking through a keyhole, the keyhole of nature, trying to know what's going on.*"

Jacques Yves Cousteau

Index

1. **Introduction – page 7**

1.1. **Abstract** - page 8

1.2. **Organization of central nervous system: grey and white matter** – page 8

1.3. **Resting-state functional connectivity: an MRI tool for the study of neural activity and brain networking** - page 10

1.4. **Brain activity and networking in fMRI: the cognitive circuits** – page 16

1.5. **The white matter: from microscopic to macroscopic organization** – page 19

1.6. **Aging and white matter degeneration** – page 22

1.7. **The analysis of white matter status on MRI** – page 25

1.8. **The correlation between MRI markers of white matter degeneration and the cognitive sphere** - page 28

1.9. **Aging-related cognitive decline - the disconnection hypothesis** – page 31

2. **The PhD project – page 33**

2.1. **Background and general design** – page 34

2.2. **The LEMON dataset** – page 36

2.3. **The extrapolation of the markers of white matter degeneration through the analysis of MRI structural and DWI data** – page 39

2.4. **Preprocessing and processing of the rs-fMRI data** – page 43

2.5. **Study 1 - The association between white matter hyperintensities, cognition and regional neural activity in healthy subjects** – page 45

2.5.1. *Study population* – page 45

2.5.2. *Statistical analysis: relationship between demographic, cognitive and volumetric data* – page 46

2.5.3. *Statistical analysis: rs-fMRI* – page 46

2.5.4. *Results: neuropsychological evaluation and volumetric analysis* – page 47

2.5.5. *Results: rs.fMRI analyses* – page 50

2.5.6. *Discussion* – page 53

2.5.7. *Limits* – page 56

2.6. **Study 2 - Effects of white matter hyperintensities on brain connectivity and hippocampal volume in healthy subjects according to their localization** – page 57

2.6.1. *Study population* – page 57

2.6.2. *Statistical analysis: relationship between demographic and volumetric data* – page 59

2.6.3. *Statistical analysis: rs-fMRI* – page 60

2.6.4. *Results: relationship between demographic and volumetric data* – page 61

2.6.5. *Results: rs-fMRI* – page 63

2.6.6. *Discussion* - page 65

2.6.7. *Limits* – page 68

2.7. **Study 3 - Global fractional anisotropy: effect on resting-state neural activity and brain networking in healthy participants** – page 70

2.7.1. *Study population* – page 70

2.7.2. *Statistical analysis: relationship between demographic data and gFA value* – page 72

2.7.3. *Statistical analysis: rs-fMRI* – page 73

2.7.4. *Results: relationship between demographic and volumetric data* – page 74

2.7.5. *Results: rs-fMRI analyses* – page 76

2.7.6. *Discussion* – page 80

2.7.7. *Limits* – page 84

3. **General considerations and conclusion – page 85**

4. **Literature – page 89**

1. Introduction

1.1. Abstract

White Matter (WM) is a pivotal component of the Central Nervous System (CNS), and its main role is the transmission of the neural impulses within the CNS and between CNS and Peripheral Nervous System (PNS). It is note from literature that changes in the WM affects the function of the CNS with effects on the higher neurological function [Walhovd et al., 2014], included cognition [Filley et al., 2016]. Further, it has been theorized in the last decades that ageing-associated decline in higher neurological functions, in particular in the neurocognitive sphere, could be at least partly explained by the "disconnection" of the cortical areas of the brain due to the WM degeneration [O'Sullivan et al., 2001; Salat, 2011; Bennett et al., 2014; Filley et al., 2016].

Although standard "in-vivo" imaging biomarkers of WM integrity have not been validated yet for clinical purposes, several researches have demonstrated the correlation between different potential imaging biomarkers and WM integrity [Wardlaw et al, 2015].

The aim of the PhD project is to explore and better understanding the effects of WM status on the brain structure, networking and cognition. In particular, we designed three distinct explorative and cross-sectional studies; more specifically, we analyzed the effects of two Magnetic Resonance Imaging (MRI) markers of WM degeneration (the global Fractional Anisotropy (gFA) and the white matter hyperintensities burden (WMHb), respectively) on the brain activity measured with the Resting-State Functional Magnetic Resonance Imaging (rs-fMRI) technique. The project was conducted by analyzing a human population of healthy subjects extracted from the public available dataset "Leipzig Study for Mind-Body-Emotion Interactions" (LEMON) [Babayan et al., 2019]. The results of these studies have been published during the PhD course on three distinct international scientific papers [Porcu et al., 2020a, 2021a and 2021b].

1.2. Organization of central nervous system: grey and white matter

The central nervous system (CNS) is a complex structure that controls most functions of both the body and mind, including cognition, mood, memory, sensory perception and movement [Thau et al., 2021]. It consists of a specialized tissue, the nervous tissue (NT), able to generate, receive, integrate and transmit impulses within the CNS and to the peripheral nervous system (PNS) [Thau et al., 2021]. From an anatomical point of view, the NT has been traditionally divided into grey matter (GM) and white matter (WM) [Garman, 2011; Thau et al., 2021]. The GM consists mainly of neuronal cell bodies and neuropils, astrocytes and it is located mainly on the surface of the cerebrum and cerebellum (cerebral and cerebellar cortices, respectively) and in "nuclei" located deeply in the brain and in the spinal cord [Garman, 2011; Mercadante et al., 2020]. The WM consists mainly of axons covered by myelin sheath provided by oligodendrocytes, and it is organized in fiber bundles that link the different GM regions [Garman, 2011; Mercadante et al., 2020]. The different histological composition of GM and WM reflect the different specialization of these two components; in particular, the GM is responsible for the reception, integration and generation of the neural impulses, whereas the WM, which is heavily myelinated, is responsible for the transmission of the impulses within the CNS and between CNS and PNS [Thau et al., 2021, Mercadante et al., 2020].

1.3. Resting-state functional connectivity: an MRI tool for the study of neural activity and brain networking

Functional MRI was firstly described in literature by *Biswal et al.* in 1995, that observed how it was possible to reveal the activity of the sensorimotor cortex during a finger tapping task by registering the fluctuations of signal intensity on MRI with the so-called Blood Oxygen Level-Dependent (BOLD) contrast imaging approach [Biswal et al., 1995; Lv et al., 2018]. Although several aspects of this phenomenon are still a matter of research, it is known that the physiological phenomenon underlying the signal fluctuations registered with the BOLD approach is the so called "hemodynamic response" [Nasrallah et al., 2015; Lv et al., 2018]. This phenomenon is due to the increased regional cerebral blood flow in order to satisfy the metabolic demands the active areas of the brain [Nasrallah et al., 2015; Lv et al., 2018]. The local changes of the relative levels of oxyhemoglobin and deoxyhemoglobin, generate a signal detectable on MRI with the BOLD approach on the basis of the different magnetic susceptibility of hemoglobin status detected with T2*-weighted sequences, like for example the Echo-Planar Imaging (EPI) sequences [Kwong et al., 1992; Nasrallah et al., 2015; Lv et al., 2018].

During rs-fMRI is a functional MRI, the low-frequency fluctuations of the BOLD signal are acquired on resting state, i.e. in absence of a stimulus or a task; this technique is suitable for research purposes in order to analyze brain activity in various pathological and physiological conditions [Lv et al., 2018].

For better understanding how the rs-fMRI data can be analyzed, we can compare the brain to a map [Dance, 2015; Lv et al., 2018]. If we look at a map, we can focus our attention on the cities or on the highways that connect one city to each other, and similarly in rs-fMRI we can extract information relative to the activity and function of a specific cerebral region, or the functional connectivity between cerebral regions [Dance, 2015; Lv et al., 2018]. Following what above mentioned, the analytic methods for rs-fMRI data can be categorized in two big groups, the functional segregation and the functional integration methods [Tononi et al., 1994; Lv et al., 2018].

The functional segregation approach allows to analyze the local function of specific brain regions with no information about their interconnections [Lv et al., 2018]. The main analysis methods that belong to this category are the Regional Homogeneity (ReHo) [Zang et al., 2004], the Amplitude of Low Frequency Fluctuation (ALFF) [Zang et al., 2007] and the derived fractional ALFF (fALFF) [Zou et al., 2008]. All these approaches are voxel-based and they are usually calculated within a low-frequency range (0.01 - 0.1 Hz) [Lv et al., 2018]. The ReHo technique measures the synchronicity of adjacent brain regions by calculating the Kendall coefficient of concordance of the BOLD time-series between a given voxel and its nearest neighbors [Zang et al., 2004; Lv et al., 2018]. The ALFF technique measures the total power of the BOLD signal, and the ALFF signal results proportional to regional neural activity [Zang et al., 2007; Lv et al., 2018]; the derived fALFF technique measures the power of the BOLD signal within the low-frequency range divided by the total power of the BOLD signal in the entire detectable frequency range, and the fALFF signal represents the relative contribution of the low-frequency oscillations in the whole spectrum of BOLD frequency oscillations, and it has been reported to be more specific for the analysis of the activity of GM when compared to ALFF [Zou et al., 2008; Lv et al., 2018]. The advantages of the functional segregation approach rely on their relative simplicity and long-term test-retest reliability (about six months) [Zuo et al., 2014, Lv et al., 2018], but they cannot provide information about the brain networking.

The functional integration approach allows to analyze the interaction between different cerebral regions directly or indirectly anatomically connected between them by measuring the degree of synchronicity of the BOLD signal time-series fluctuations [Lv et al., 2018]. The analysis techniques that belongs to this category are the Functional Connectivity Density (FCD), the Region of Interest (ROI) based functional connectivity analysis, the Independent Component Analysis (ICA), and the graph analysis [Lv et al., 2018].

FCD identifies the highly connected functional hubs by calculating the correlation of the BOLD signal time-series fluctuations between each voxel and all the other voxels [Tomasi et al., 2010; Lv

et al., 2018]. FCD is straightforward but the data obtained with this approach must be interpreted with caution due to the low test-retest reliability [Zuo et al., 2014, Lv et al., 2018].

The ROI-based functional connectivity approach is able to find the regions whose activity is correlated with the activity of other cerebral regions by computing the cross-correlations between the BOLD signal time-series fluctuations of a ROI (also called seed) and the other cerebral regions [Lv et al., 2018]. Several metrics can be used to analyze these correlations, included cross-correlation coefficient, synchronization likelihood, partial correlations and multiple regressions, and the overall results can be visualized using a connectivity matrix [Lv et al., 2018]. In this case the ROI must be a priori defined on the basis of literature evidences, like for example by using brain atlases like the Harvard-Oxford [Desikan et al., 2006] and the Automated Anatomical Labelling (AAL) [Tzourio-Mazoyer et al., 2002], or on the basis prior results such as those derived from ALFF or ReHo analyses [Lv et al., 2018]. The advantages of this technique relies on the simplicity of computation and interpretation of the results, but the disadvantage is its intrinsic dependence on the selection of the a-priori selection of the seed, that makes it vulnerable to bias [Lv et al., 2018].

The ICA approach exploits multivariate decomposition in order to identify and to separate the BOLD signal into several independent temporally correlated functional networks in form of spatial maps of the z-scores derived from the correlation of the BOLD time-series of each voxel and the mean time series of the given brain network [Kiviniemi et al., 2003; Lv et al., 2018]. With this approach it has been possible to identify and to characterize several fundamental brain networks [Uddin et al., 2019], such as for example the Default Mode Network (DMN) [Raichle et al., 2001; Raichle, 2015].

The advantage of this approach is that it is data-driven and that it can be performed without any a-priori assumption, with high short (< 45 minutes) and long-term (5-16 months) test-retest reliability [Zuo et al., 2010; Lv et al., 2018]. However, the interpretation of the data can be difficult because the underlying cause of perceived synchronicity within a functional network may be of non-neural origin

and because this technique only presents brain networks one by one and do not allow to analyze the interactions between different brain networks [Bertolero et al., 2015; Lv et al., 2018].

The graph analysis exploits the graph theory [Barabási et al., 2011; Bullmore et al., 2009; Bassett et al, 2017; Liao et al., 2017; Bassett et al., 2018] for the study of the cerebral networking. According to the graph theory, a network can be represented as a graph (G) consists of nodes (N), that represent the constituents unit of the system, and edges (E) that connect one node to the other ones as reflection of the interconnections between them [Liao et al., 2017], and the properties of the graph can be analyzed as a function of the nodes and edges according to the following formula [Achard et al., 2007; Lv et al., 2018]:

$$G = f(N, E)$$

In the case of brain networks analyzed with the rsfMRI technique, the nodes can be the single voxels or the ROI, defined according to anatomical landmarks, functional significance, connectivity profiles and/or multi-modal and random parcellation, whereas the edges are defined as the interregional statistical coherence between the BOLD signal time-series fluctuations of the nodes, expressed in terms of cross-correlation coefficient, synchronization likelihood, partial correlations or multiple regressions [Liao et al., 2017; Lv et al., 2018]. This result in the creation of an adjacency matrix on which we can assess the topological properties of the graph by applying the metrics developed in the graph theory [Bullmore et al., 2009; Bassett et al, 2017; Liao et al., 2017; Lv et al., 2018; Bassett et al., 2018]. Among these properties, that can be calculated both for the network and for its single nodes, it is noteworthy to mention the following [Barabási et al., 2011; Bullmore et al., 2009; Bassett et al, 2017; Liao et al., 2017; Lv et al., 2018; Bassett et al., 2018]:

- Average path length: the average number of connections that link one node to the others, as an expression of the tendency to which the neighboring nodes of a node are interconnected.
- Clustering coefficient: the ratio of the number of existing connections between its nearest neighbors and the maximum number of potential connections.

- Degree: the number of connections that connect a node to the others
- Cost (also known as "connection density"): the actual number of links of the network as a proportion of the total number of possible connections.
- Betweenness centrality: the measure of node centrality within a graph.
- Local efficiency: the ability of a node to transfer information between nodes at the local level.
- Global efficiency: the ability of a node to transfer information between nodes at the global level.

A fundamental concept to underline in the graph analysis of cerebral circuits is the fact that in physiological conditions brain networks, as well as many other biological, social and technical networks, are organized according to a "small-world" architecture [Watts et al., 1998]. The small-world architecture is characterized by an optimal balance between information segregation and integration, and it presumably developed in this way following natural selection under the pressure of a cost-efficiency balance [Watts et al., 1998; Liao et al., 2017]. In fact, this network model characterized by a combination of high-clustering coefficient and short characteristic path length, so that most nodes result to be not connected one to each other, but they can be reached from every other node through few connections [Watts et al., 1998; Liao et al., 2017; Lv et al., 2018]. These features make it possible to efficiently transmit local information because of the high clustering coefficient, and to efficiently deliver global information due to the short characteristic path length with low wiring costs [Watts et al., 1998; Liao et al., 2017; Lv et al., 2018]. It has been demonstrated in several researches that the disruption of the small-world architecture of brain networks is a characteristic of several pathological conditions such as for example schizophrenia [Liu et al., 2008] or leukoaraiosis [Zhu et al., 2020], and physiological aging as well [Sun et al., 2012].

The main advantage of the graph analysis relies on the ability to analyze brain networking without any a priori assumptions, but the results can vary a lot on the basis of the node definition and can be not intuitive [Liao et al., 2017; Lv et al., 2018].

Finally, it is important to underline that although rs-fMRI is extensively used for research purposes, its applicability in clinical scenarios is still not feasible due to various factors, including acquisition protocol (MR scanner, scan timing, sequence parameters) and analysis methods [Cole et al., 2010]. For example, in a recent research by *Botvnik-Nezer et al.* [Botvinik-Nezer et al., 2020], the authors asked to 70 independent teams to analyze the same dataset testing the same 9 ex-ante hypotheses, and no two teams chose the identical workflows to analyze the data, resulting in sizable variation in the results of hypothesis tests. For this reason, the research community advocates for further technical implementation and experimental refinement in order to overcome of these limitations [Cole et al., 2010].

1.4. Brain activity and networking in fMRI: the cognitive circuits

The complexity of the cerebral system do not allow an easy comprehension of its functioning due to the presence of uncountable variables that must be taken into account during the analysis of a specific phenomenon, like for example the comprehension of the mechanisms underlying the cognitive sphere. This field represents an extensive matter of research in neuroscience, both at microscopic to macroscopic level.

Regarding the macroscopic level, it is known that the cortical areas and subcortical structures plays a specialized role according to their topological localization, and this has been possible basing on the analysis of the neurological effects of a localized anatomical brain damage, as happened for example for the definition of the function of the Broca's area [Mohr et al., 1978]. In the last years, fMRI allowed us to better understand the functioning mechanisms of the brain, by describing both the activity of the single brain structures and the relationships between them; in particular, several researches pointed out that the brain works as a single network, that can be further divided into different subnetworks that interact one to each other, even if there is no unique consensus on the general organization due to the heterogeneity and ongoing introduction of new and updated analysis methods for research [Damoiseaux et al., 2006; De Luca et al., 2006; Uddin et al., 2019].

One of the most recent brain networking organization model have been developed and purposed by *Uddin et al. in 2019* in order to harmonize the current knowledges about this topic [Uddin et al., 2019]. This models provides six major cognitive networks, and it has been generated on the bases of observations from resting state functional connectivity, functional task-based and cross-modal convergence MRI studies [Uddin et al., 2019]. These six networks are the following [Uddin et al., 2019]: 1) Occipital Network (ON), also referred as "visual network"; 2) Pericentral Network (PN), also referred as "somatomotor network"; 3) Dorsal Fronto-Parietal Network (D-FPN), also referred as "attention network"; 4) Lateral Fronto-Parietal Network (L-FPN), also referred as "control network"; 5) MiCingulCingulo-Insular Network (M-CIN), also referred as "salience network"; 6) Medial Fronto-Parietal Network (M-FPN), also referred as "default network".

The ON is involved in visual processing, and can be further divided into two distinct subsystem, one located more medially associated with the primary visual cortex, and one more laterally, involved in the visual processing [Haxby et al., 1994; Uddin et al., 2019]. The PN is involved in motor process and somatosensory processing [Uddin et al., 2019]. The D-FPN, also referred in literature as dorsal frontoparietal network" [Corbetta et al., 2002], "dorsal attention system" [Fox et al., 2006] and "dorsal attention network" [Yeo et al., 2011], is involved in visuospatial attention, included the voluntary deployment and maintenance of visuospatial attention [Uddin et al., 2019]. The L-FPN is responsible for the control of information flow in the brain, and its functions include the executive functions, the working memory, inhibition and task switching [Uddin et al., 2019]. The M-CIN, also referred in literature as "ventral attention network" [Corbetta et al., 2002], "ventral attention system" [Fox et al., 2006],"ventral attention network" [Yeo et al., 2011]", and "empathy network" [Kennedy et al., 2012], is responsible for the identification of important, or "salient" information, and it is involved in detecting behavioral relevant environmental stimuli and internally generated information [Uddin et al., 2019]. Regarding the function of the M-FPN, also referred in literature as DMN [Raichle et al., 2001; Raichle, 2015], comprised also the so-called "limbic network" [Yeo et al., 2011; Uddin et al., 2019]; there is not unique consensus in literature: it is probable that this network is involved in the development, temporal binding and dynamic reconfiguration of associative representations based on current goal-states, as well as in the detection of the associative relevance of internal and external stimuli, semantic association, and environmental monitoring [Uddin et al., 2019]. A resume table of this brain networking model is shown in Table 2.

Cognitive Networks			
Anatomical name	***Cognitive domain***	***Core regions***	***Main functions***
Occipital	Visual network	• Occipital cortex (striate and extrastriate cortex included) • Lateral geniculate nucleus of thalamus*	• Visual processing
Pericentral	Somatomotor network	• Somatomotor coritces (anterior and posterior to the central sulcus) • Juxtapositional lobe • Auditory cortex* • Superior temporal gyrus*	• Motor processes • Somatosensory processing

Dosal Fronto-Parietal	Attention network	• Superior parietal lobule extending into the the intraparietal sulcus • Middle temporal complex • Right-lateralized dorsolateral prefrontal cortex* • Superior colliculus*	• Visuospatial attention
Lateral Fronto-Parietal	Control network	• Prefrontal cortex along the middle frontal gyrus • Anterior-inferior parietal lobule into the intraparietal sulcus • Midcingulate gyrus • Dorsal precuneus* • Posterior inferior temporal lobe* • Dorsomedial thalamus* • Head of the caudate*	• Executive functions • Working-memory • Inhibition and task-switching
MidCIngulo-Insular	Salience network	• Bilateral anterior insula • Anterior cingulate cortex • Inferior parietal cortex* • Right temporal parietal junction* • Several subcortical strucutres*	• Identification of behavioral relevant environmental stimuli and internally generated information
Medial Fronto-Parietal	Default network	• Medial prefrontal cortex • Posterior cingulate cortex • Posterior extent of the inferoparietal lobule • Areas located dorsally and ventrally to the posterior cingulate, the precuneus and the retrosplenial cortex* • Hippocampus* • Superior and middle frontal gyrus* • Ventral frontal cortex and anterior temporal lobees* • Temporoparietal junction*	• Formation, temporal binding and dynamic reconfiguration of associative representations based on current goal-states • Detection of the associative relevance of internal and external stimuli • Semantic association and enviromental monitoring.
*less well characterized			

Table 1: Cognitive network taxonomy according to Uddin et al. [Uddin et al., 2019].

Besides these circuits, it is important to recall also the cerebro-cerebellar circuits, that bidirectionally connects the neocortex and the cerebellum, important not only for the motor function, but also in the regulation of nonmotor cortical areas (including prefrontal, associative, sensory and limbic areas) and of hypothalamus [Banagiano et al., 2018].

1.5. The white matter: from microscopic to macroscopic organization

As we have already seen in the previous section, from an histological point of view the WM consists mainly of axons that originate from neurons located in the GM [Garman, 2011; Mercadante et al., 2020]. The main role of WM is to conduct electric pulses generated from the GM through the axons thanks to a rapid saltatory conduction system sustained by voltage-dependent sodium channels located in the nodes of Ranvier and guaranteed by the presence of myelin sheaths provided by support cells known as oligodendrocytes [Standelman et al., 2019]. Other cell types contribute to the organization of WM in particular other glial cells such as astrocytes, microglia and oligodendrocytes progenitor cells (OPC), and the metabolic supply is guaranteed by a local cerebral microvascular network [Walhovd et al., 2014; Yang et al., 2017]. It is known that the main structural feature of the cerebrovascular network is the so called blood-brain barrier, thanks to the presence of tight junctions between the endothelial cells [Abbott et al., 2010; Yang et al., 2017]. This system avoids that harmful molecules could directly enter in the nervous tissue acting as an active in & out filter, it participates in removing neurotoxic molecules such as amyloid-β from the interstitial fluid, and it promotes or prevents thrombosis under special circumstances [Abbott et al., 2010; Hainsworth et al., 2015; Yang et al., 2017]. Further, it plays a major role in regulating the cerebral blood flow (CBF) [Yang et al., 2017]. The CBF is regulated by three distinct mechanisms: a) metabolic, according to the fluctuations of the pressure of arterial carbon dioxide; b) cerebral autoregulation in response to blood pressure fluctuations; and c) autonomic regulation under the stimulation of sympathetic and parasympathetic fibers [Yang et al., 2017].

In the last decades the knowledges about the structure and the organization of WM sensibly increased: it has been demonstrated in particular the existence of complex interactions between the axons and the oligodendrocytes, in which the oligodendrocytes not only provide the myelin sheaths to the axons, but they also provide metabolic support to the neurons [Standelman et al., 2019]. It is note for example that oligodendrocytes, which are mostly located intrafascicularly, are able to generate up to 80 different types of myelin sheaths to the axons [Standelman et al., 2019; Williamson

et al., 2018], and that there is a huge variability among myelin thickness and internodal length (i.e. the distance between) two nodes of Ranvier, both between axons and along an individual axon [Walhovd et al., 2014]. Microglia are the resident immune cells within WM and they are responsible for the maintenance of WM homeostasis [Rawji et al., 2013; Liu et al., 2017], whereas astrocytes are able to promote myelination and myelin maintenance by removing extracellular ions and by producing and releasing pro-myelination factors [Lundgaard et al., 2014; Liu et al., 2017].

Regarding the WM development, it is note that the production of myelin sheaths begins in mid-to-late gestation period (starting at approximately 20 weeks), and this process advances rapidly throughout the early childhood in the first 5 years of life according to a specific pattern in a caudo-cranial and posterior-to-anterior direction [Lebel et al., 2018]. There is a growing body of evidence that suggests that the microstructural development and the myelin organization not only change with development and ageing, but also that its metabolic activity tends to change in order to regulate phenomena such as experience and learning [Zatorre et al., 2012; Lebel et al., 2018; Williamson et al., 2018], with mechanisms partly mediated by neuronal activity [Lundgaard, 2013; Walhovd et al., 2014].

From a macroscopic point of view, the WM is organized in a complex architecture that consists of bundles of fibers crossed with each other [Mandonnet et al., 2018]. Several organizational model of the WM have been purposed in the past centuries and this topic is still a matter of research [Mandonnet et al., 2018]. One of the simplest model is the one purposed by Meynert in the 19th century, that divided WM bundles into three distinct groups: a) projection fibers, that connect a cortical region to a subcortical GM nucleus (brainstem, deep nuclei, cerebellum and spinal cord), b), commissural fibers, that connects interhemispheric cortical regions and c) association fibers, that connects intrahemispheric cortical regions, that can be further divided into short association fibers (that connect area within the same lobe) and long association fibers [Meynert T, 1888; Wycoco et al., 2013; Mandonnet et al., 2018]. There are also other fibers that cannot be included in the categories above mentioned, i.e. the limbic system fibers, the temporal stem and the brainstem fibers [Wycoco

et al., 2013]. A resume table of the main WM fibers and of their respective known function is reported in Table 1 [Wycoco et al., 2013].

White matter fibers			
Fibers groups	***Tracts***	***Connections***	***Primary known functions***
Projection fibers	Corticospinal tracts	Tracts that connect the motor area to the spinal cord	Motor
	Corticobulbar tracts	Tracts that connect the motor area to cranial nerve nuclei in the brainstem	Motor
	Corticopontine tracts	Tracts that connect the precentral and postcentral gyri to the pontine nuclei	Coordination of planned motor functions
	Internal capsule	Main conduit for projection fibers	Motor
	Thalamic radiations	Reciprocal interconnections between thalamus and cortex - from lateral thalamic nuclei to cortex passing through internal capsule	Transmission and integration of sensory and motor data to precentral and postcentral fibers
	Geniculocalcarine tract (optic radiation)	Lateral geniculate body to the primary visual cortex	Vision
Commissural fibers	Corpus callosum	Connections of homologous areas of the both hemispheres, although there is a significant proportion of asymmetry	Interhemispheric sensorimotor and auditory connectivity
	Anterior commissure	Connections between the temporal lobes (included amygdala, inferior temporal, parahippocampal, and fusiform gyri) and inferior occipital cortex.	Smell and data integration
Association fibers	U-fibers	Adjacent gyri	Integration of the data
	Superior longitudinal fasciculus	Bidirectional connections between frontal lobe and parietal, temporal and occipital lobes	Integration of auditory and speech nuclei
	Middle inferior fasciculus	From the angular gyrus to the superior temporal gyrus	Language (dominant hemisphere) and attention (non-dominant hemisphere)
	Inferior longitudinal fasciculus	Connections between temporal and occipital lobes	Visual emotion and memory
	Superior occipitofrontal fasciculus	Connections between frontal and parietal lobes	Spatial awareness and symmetric processing
	Inferior occipitofrontal fasciculus	Connections between frontal lobe and both temporal and parietal lobes (posterior part)	Integration of data of both auditory and visual association cortex with prefrontal cortex
	Uncinate fasciculus	Connections between frontal and temporal lobes	Auditory-verbal memory
Limbic system fibers	Cingulum	From the cingulate gyrus to the enthorinal cortex	Affective control, visceromotor control, skeletomotor control, visuospatial processing and memory access
	Fornix	From the hippocampus, the septal area, the hypothalamus and the mamillary body to the dorsal regions of the hippocampi	Cognition and episodic memory recall
	Stria terminalis	Interconnections between amygdala, septal area and hypothalamus	Integration of limbic data; emotional and behavioral responses to stress
Temporal stem	-	From the amygdala to the lateral geniculate body	Learning, spatial, visual and verbal function
Brainstem fibers	Superior cerebellar peduncles	From the dentate nucleus to the thalamus, red nucleus, vestibular nuclei and reticular formation	Motor coordination and balance network
	Middle cerebellar peduncles	Cerebellum to the contralateral pontine nuclei of the cerebellum	Motor coordination and balance network
	Inferior cerebellar peduncles	Interconnections between cerebellum and medulla	Integration of proprioceptive sensory inputs with vestibular function.
	Medial lemniscus	Ascending sensory fibers to the thalamic ventroposterolateral nucleus	Sensitivity

Table 2: Resume of the main white matter fibers, their connections and the relative function [Wycoco et al., 2013].

1.6. Aging and white matter degeneration

It is known that ageing, in terms of changes observed across the course of the life of an otherwise healthy person, affects brain as all the other parts of the body [Liu et al., 2017]. Cerebral ageing is usually and variably associated with some decline in cognitive functions, in particular quantitative reasoning and perceptual speed [Caserta et al., 2009; Liu et al., 2017].

It has been also demonstrated that several degenerative changes occur also in the WM, at a micro and macroscopical level, in a complex pathophysiological scenario [Liu et al., 2017; Hase et al., 2018].

From a microscopic point of view, for example, it has been observed that axons of aged mice, when compared to the axons of younger mice, tend to have a bigger caliber and thicker myelin sheaths, and contains longer and thicker mitochondria with altered levels of mitochondrial shaping proteins that are associated with impaired production of adenosin triphosphate and increased generation of nitric oxide, protein nitration and lipid peroxidation [Stahon et al., 2016]. Other studies evidenced also that ageing is associated with splitting of myelin sheath, balloon formation, and a reduction of the integrity of the paranode (i.e. the structure anchors the myelin to the axolemma) [Sugiyama et al., 2002; Liu et al., 2017]. Other microscopic changes observed are impairments in OPC recruitment and differentiation [Kohama et al, 2012; Liu et al., 2017] and in microglia [Clemente et al., 2013; Liu et al., 2017] and astrocytes activation [Diniz et al., 2010; Liu et al., 2017].

Another actor that plays a pivotal role in brain aging is the cerebrovascular system [Yang et al., 2017]. In fact, it is note that the cerebrovascular system undergoes to complex vascular phenotypic changes, due to a series of multiple pathophysiological processes [Yang et al., 2017]. The first mechanism is the age-related arterial stiffness, that contributes to increase systolic pressure and to decrease diastolic pressure, leading to vascular remodeling and pro-atherogenic changes in the vascular wall [Ungvari et al., 2010; Yang et al., 2017]. The atherosclerotic process, due to the development of plaque in the vessel wall of the large vessels, and the arteriosclerosis process in small vessels due to the accumulation of toxic proteins within the walls of the small vessels lead to the

luminal narrowing of the cerebrovascular network and impairments in brain perfusion [Yang et al., 2017; Wang et al., 2019]. Another factor to be taken into account is the endothelial replicative senescence due to the arrest of the proliferation of mitotically active cells (in order to prevent cancer development), with the accumulation of damaged endothelial cells [Campisi, 2003; Yang et al., 2017], and the consequent microvascular rarefaction, observed in particular in the hippocampus in some rodents studies [Csizar et al., 2007; Yang et al., 2017]. Lastly, the oxidative stress induced by the age-related increase in reactive oxygen species can lead to mitochondrial dysfunction and can alter the physiological production of nitric oxide, a molecule that confers protective effects on the endothelium, including inhibition of platelet aggregation and of endothelial apoptosis [Ungvari et al., 2010; Springo et al., 2015; Yang et al., 2017].

The combination of all the complex above mentioned microscopical mechanisms can lead are at the base of the macroscopic aging-related changes of WM, that can be observed in vivo with several imaging modalities (in particular MRI). Firstly, it is known that WM volume gradually increases in the first 40 years, and tend to rapidly decrease from 60 years of age onwards [Liu et al., 2016; Liu et al., 2017]. The second important macroscopic feature observable on MRI is represented by the so called “white matter hyperintensities of presumed vascular origin” (WMH), also known as White Matter Lesions (WML) [Wardlaw et al., 2015]. These lesions can be easily detected on MRI, and they appear as small focal areas of the WM that appear hyperintense on T2-weighted (T2-W) sequences, in particular on FLuid Attenuated Inversion Recovery (FLAIR) sequence, and hypointense on T1-weighted (T1-W) sequences [Wardlaw et al., 2015]. Although the exact nature of these MRI lesions has not been clarified because of the few pathological studies conducted to determine their nature, it has been hypothesized their microvascular ischemic etiology due to the wide spectrum of pathological findings reported, including myelin rarefaction, tissue infarction, reactive gliosis, and axonal loss [Fazekas et al., 1993; Brown et al., 2002; Moran et al., 2012; Wardlaw et al., 2015]; further, a study by *Young et al.* [Young et al., 2008], revealed a loss of the integrity of the small vessel endothelium inside of these lesions, suggesting the vascular origin of these lesions.

According also to the above evidences, WMH are considered a part of the spectrum of the cerebral small vessel disease (CSVD), a condition associated with cognitive impairment commonly found in elderly population, characterized by the presence of lacunar ischemic lesions, microbleeds and brain atrophy [Wardlaw et al., 2013].

These lesions are typically located in the periventricular and deep WM, whereas the juxtacortical localization is less typical [Wardlaw et al., 2015]. Further, it is also known that the WMH tend to evolve: often they can increase in size, occasionally shrink, and they lead to atrophy of WM and overlying cortex [Gow et al., 2012; Wardlaw et al., 2015].

Lastly, it is known the fact that the presence of vascular risk factors such as hypertension, diabetes and smoking is associated with increasing in WMH number and load, whereas it has been evidenced an inverse correlation between physical activity is and WMH load [Wardlaw et al., 2015].

1.7. The analysis of white matter status on MRI

MRI is one of the main "in vivo" imaging modality used in clinical practice and in the neuroscience field for the study of both CNS and PNS. Regarding the study of WM status, this can be performed by using several techniques.

As we have seen above, the T1-W and T2-W are morphological sequences optimal for identifying the WMH [Wardlaw et al., 2015]. In particular, T1 weighted sequences are optimal for distinguishing Wm from GM structures (cortical GM and subcortical structures included basal ganglia, thalamus and subtentorial nuclei) [Riphagen et al., 2018]. In the last decades, the development of isotropic (3D) T1 and T2-sequences allowed to better identify and define the WM lesions thanks to their intrinsic higher spatial resolution when compared to the traditional anisotropic two dimensional (2D) sequences [Mascalchi et al., 2016; Wardlaw et al., 2015]. WM lesions in particular can be detected and quantified manually or by using semi-automated and fully automated software [Caligiuri et al., 2015].

The Diffusion Tensor Imaging (DTI) is another technique used for the analysis of WM anatomy and properties [O'Donnell et al., 2011; Jeurissen et al., 2019]. This technique derives from the Diffusion Weighted Imaging (DWI) technique, that allows to study the diffusion of water molecules by quantifying the diffusion coefficient of water molecules, expressed in mm^2/s [O'Donnell et al., 2011; Jeurissen et al., 2019]. The water molecules inside the WM fibers cannot freely move in all directions as it happens in a glass of pure water (isotropic diffusion), but their diffusion is limited by the presence of the cellular membranes and myelin sheaths (anisotropic diffusion) [O'Donnell et al., 2011; Jeurissen et al., 2019]. The DTI technique is based on the application of the magnetic field gradients in order to register the anisotropic diffusion signal of water molecules inside the WM fibers in various directions of the space (at least six), and by simultaneously canceling out the isotropic signal of stationary water [O'Donnell et al., 2011; Jeurissen et al., 2019]. Simplifying, the registered signal is proportional to the anisotropic diffusion of water molecules in a particular direction [O'Donnell et al., 2011].

The DTI technique assumes that each voxel of the matrix is characterized by a single predominant fiber orientation, and the WM fibers are reconstructed by elaborating the apparent diffusion coefficient (ADC) registered at different directions in the three dimensional space of every voxel on a predefined 3 x 3 matrix by using a Gaussian model [O'Donnell et al., 2011; Jeurissen et al., 2019]. This results in the extrapolation of three eigenvalues (λ_1, λ_2, λ_3), and of a single eigenvector for every voxel [O'Donnell et al., 2011; Jeurissen et al., 2019].

A Red-Green-Blue (RGB) color map is usually applied to eigenvectors to visually delineate the course of the fibers (conventionally, reddish for fibers that run along the latero-lateral direction, blueish along the cranio-caudal direction, and green along the antero-posterior direction) [O'Donnell et al., 2011; Jeurissen et al., 2019].

For what concerns eigenvalues, several quantitative parameters can be extrapolated from them, and among the most studied in research it is noteworthy to mention the Fractional Anisotropy (FA), the Mean Diffusivity (MD), the Axial Diffusivity (AD) and the Radial Diffusivity (RD) [Soares et al., 2013]. These values can be calculated for every single voxel, on a predefined region of interest (as for example along a specific WM tract) or at a global level [O'Donnell et al., 2011].

FA is the normalized standard deviation of the diffusivities, with values ranging from 0 (absolute isotropic diffusion) to 1 (absolute anisotropic diffusion in a single direction) [Basser et al., 1996; Assaf et al., 2008]. In 2017 *Chang et al.* [Chang et al., 2017] made an interest study that compared the results of ex-vivo high-resolution DTI sequences with two-photon laser microscopy of intact mice, demonstrating that FA values correlate with myelination degree of the WM fibers, with higher FA values indicating a better myelination status. Other animal studies indicated also that FA values are influenced by axon density [Zhang, 2010]. RD is calculated as the magnitude of water diffusion perpendicular to the eigenvector, and it has been demonstrated that this value strongly correlates with electrophysiological markers of demyelination [Winklewski et al., 2018], as demonstrated for example by Song et al. [Song et al., 2005], that evidenced a correlation between increasing RD values and degree of demyelination in corpus callosum of mouse brain affected by cuprizone treatment. MD

value is calculated by the mean of the three eigenvalues, and it corresponds to the molecular diffusion rate in each direction, and it is typically in damaged tissues as a result of increased isotropic diffusion [Soares et al., 2013; Winklewski et al., 2018]. AD evaluates the mean diffusion coefficient of water molecules that diffuse parallel to the eigenvector within the voxel of interest [Winklewski et al., 2018], and it tends to decrease in case of axonal injury [Mac Donald et al., 2007].

1.8. The correlation between MRI markers of white matter degeneration and the cognitive sphere

Two of the most studied MRI markers of WM status that have been found to be correlated with decline of cognitive function in physiological aging are the WMH and the FA, as evidenced in several studies [Grieve et al., 2007; Chutinet et al., 2014; Kloppenberg et al., 2014; Alber et al., 2019; Maillard et al., 2019; Gullet et al., 2020; Xing et al, 2021; Chen et al., 2021].

Regarding the WMH, it is known for example that they tend to increase with age [Zhuang et al., 2018], especially in midlife [d'Arbeloff et al., 2019]. Further, it is known that their prevalence tend to increase when cardiovascular risk factors are present, included hypertension, diabetes and smoking [Dufoil et al., 2001; Gons et al., 2011; Tamura et al., 2015; Wardlaw et al., 2015]. It is also known that the prevalence of WMH is associated with impairments in several higher neurological functions [Debette et al., 2010; Wardlaw et al., 2015; Salvadó et al., 2019]. For example, it is note that higher levels of WMH burden are associated with lower motor performances, and that physical activity can attenuate the effect of WMH on the motor function in healthy older adults [Fleischman et al., 2015]. Further, it is known an association between WMH and the risk of late onset depression [Hermann et al., 2008]. It has been also demonstrated that the effects of WMH on brain functions vary according to their localization [Debette et al., 2010].

Looking more specifically at the cognitive sphere, many studies have evidenced a correlation between WMH load and the development of dementia [Wardlaw et al., 2015; Chen et al., 2021]. For example, in a meta-analysis conducted by *Debette et al.* [Debette et al., 2010], that analyzed 22 studies, it has been confirmed that WMH load is associated with progressive cognitive decline and increased risk of dementia (2-fold) and stroke (3-fold) onset. Further, the Leukoaraiosis And DISability (LADIS) study confirmed that the progression of WMH, more than the baseline levels, is significantly correlated with neurocognitive impairment [The LADIS study group, 2011; Schmidt et al., 2015], and more recently it has been also demonstrated that a bigger WMH load is associated with impairments of specific regional cognitive performances deficit, in particular decreased

information processing speed and executive function [Sivakumar et al., 2017; Alber et al., 2019; Chen et al., 2021].

The location of WMH is another factor to be taken into account when approaching this topic [Chen et al., 2021]. In fact, it has been evidenced that cognitive impairment tends to be more pronounced in relation to the periventricular WMH load than to non-periventricualar WMH load [Tubi et al., 2020]. A study by *Marquine et al.* [Marquiine et al., 2010] demonstrated that WMH located in posterior areas are associated with reduced visual-constructional functions and those located in the frontal area areas are associated with reduction in processing speed, and more recently *Boutzoukas et al.* [Boutzoukas et al., 2021] demonstrated that the WMH located in the frontal WM is associated with impairments in executive functioning.

It is also known that periventricular (pvWMH), deep (dWMH) and juxtacortical WMH (jcWMH) have different functional and clinical correlates: pvWMH are associated with impaired cognitive function, especially in processing speed and executive function [Griffanti et al., 2018; Debette et al., 2010], dWMH are associated with impairments in basic activities of daily living [Kee Hyung Park et al., 2011], whereas the jcWMH are associated to multiform clinical symptoms, including headache, depression, anxiety, and insomnia [Shan et al., 2017].

Interestingly, it has been also found a correlation between WMH load and longitudinal hippocampal volume loss in cognitively normal adults [Fiford et al., 2017]. It is note that hippocampus is a fundamental structure of the human brain that plays a critical role in different tasks, including memory formation and spatial orientation [Bird et al., 2008]. Even if the exact mechanisms underlying hippocampal shrinkage have still not been clarified, it has been proposed that the axonal damage of the fibers within the WMH could eventually lead to hippocampal shrinkage as final result in Wallerian degeneration [von Bohlen und Halbach et al., 2002].

Regarding the WM microstructural properties, several studies confirmed a relationship between alterations in quantitative markers measurable with the DTI technique and cognitive impairment. . For example, in 2011, *Fjell et al.* [Fjell et al., 2011], in a study in which 270 participants performed

a speeded continuous performance task (Eriksen flanker task [Eriksen et al., 1974]) with two conditions (congruent, incongruent), demonstrated an inverse correlation between intraindividual standard deviation of the reaction time and FA, and a positive correlation with AD, MD and RD, independently from median reaction time, age and sex, suggesting that reduced white matter is related with cognitive instability. Another population-based study by *Vernooij et al.* [Vernooij et al., 2009] analyzed 860 people older than 60 years, and the authors found that the microstructural integrity of both WMH and of Normal Appearing WM (NAWM) measured with FA, AD, RD and MD, were associated with better cognitive performances, with a direct correlation between FA anisotropy values and information processing speed and motor speed. Further, the studies by *Bennett et al.* [Bennett et al., 2014] and by *Wassenaar et al.* [Wassenaar et al., 2019] confirmed that lower FA values reflects a loss of WM structural integrity because of lower WM directionality.

Going more deeply in the analysis of regional WM microstructure, a research by *Grieve et al.* [Grieve et al., 2007] analyzed the relationships between regional FA and a range of cognitive measures, finding that frontal, temporal and parietal FA values were inversely correlated to cognitive performances in executive maze and in attention-switching tasks. Finally, a more recent longitudinal study by *Coelho et al.* [Coelho et al., 2021] demonstrated that aging is associated with both microstructural changes of WM analyzed with the DTI technique and decline in neurocognitive performances.

1.9. Aging-related cognitive decline - the disconnection hypothesis

Although more studies are needed in order to confirmed the results of the above mentioned studies, it is reasonable to affirm that WMH and quantitative parameters of WM integrity measured with the DTI technique (FA in particular) can be considered potential interesting biomarker of WM degeneration in clinical practice, and their study can help researchers to better understand the mechanisms underlying the aging-related cognitive decline observed in healthy population.

In the last two decades, several authors purposed the so called "disconnection hypothesis" in the aging brain as at least a partial explanation of the cognitive decline observed in physiological aging [O'Sullivan et al., 2001; Ferreira et al., 2013; Antonenko et al., 2014; Bennett et al., 2014; Fjell et al., 2017; Madden et al., 2017; Coelho et al., 2021]. This theory is based on the concept that the aging-associated cognitive decline can be due to the degeneration of WM that lead to the disruption of the normal intercommunications between the cortical and subcortical cerebral regions [Coelho et al., 2021].

Evidences from some rs-fMRI studies focused on the analysis of WMH and FA suggest the validity of this theory.

For what concern WMH, it has been evidenced that the WMH, both in terms of global and local volume, interfere in brain networking by decreasing tract-specific functional connectivity, both directly and indirectly [Langen et al., 2017]. The study by *Reijmer et al.* [Reijmer et al., 2015] analyzed the impact of WMH load on the connectivity of M-FPN on a population of 125 clinically normal older adults (age between 65 and 87), finding a decoupling between structural and functional connectivity of the DMN and a correlation between this decoupling and worse executive functioning and memory performances. A more recent study by *Keřkovský, M. et al.* [Keřkovský, M. et al., 2019] analyzed a population of 60 young healthy subjects finding that both the number and the load of WMH were correlated with changes of functional connectivity between several brain regions, in particular of the cerebellum. It has been also evidenced that brain can activate compensatory mechanisms in order to try to overcome the connectivity impairments induced by WMH. For

example, the study by *De Marco et al.* [De Marco et al., 2017], performed with the ICA technique, found a positive association between WMH load and increased connectivity of the anterior M-FPN and the M-CIN, interpreting these results as a compensatory response to WMH development. This theory was confirmed by another publication by *Benson et al.* [Benson et al., 2018] that evidenced how higher global functional connectivity in the D-FPN and higher local functional connectivity between M-CIN and medial frontal cortex are able to mitigate the impact of WMH on executive in subjects with larger WMH volume.

Regarding the impact of FA on cerebral activity, an interesting example is the study performed by *Yang et al.* [Yang et al., 2016]. In this study the authors analyzed a population of 140 young and 109 older healthy subjects with the FCD technique, demonstrating that the older subjects showed widespread reductions in white matter integrity measured with FA and reduced FCD in the ON and PN, and increased FCD in M-FPN when compared to the young subjects, supporting the idea that the aging-associated WM degeneration leads to cognitive impairments but at the same time is associated with compensatory mechanisms in order to overcome them [Yang et al., 2016].

Despite there are some proofs in support of the “disconnected hypothesis”, still many aspects need still to be verified. However, at the same time, these evidences push us to improve our knowledges in the field for a better comprehension of the role of WM status on brain activity.

2. The PhD research project

2.1. Background and general design

According to the above evidences reported in the previous section, in particular to the so-called "disconnection hypothesis" [O'Sullivan et al., 2001; Ferreira et al., 2013; Antonenko et al., 2014; Bennett et al., 2014], our team designed a research project in order to analyze the effects of imaging markers of WM degeneration on rs-fMRI in a population of healthy subjects. We focused on two markers, the WMH load and the global FA (gFA). Three distinct studies were designed and conducted, two of them focused on the effects of WMH burden (WMHb) and one on the effects of gFA. Of the two studies focused on the analysis of WMHb, one analyzed the effects of total WMHb on the brain activity measured with the fALFF technique [Porcu et al. 2021a], and the other one on the effects of the regional WMHb on brain connectivity (measured with the ROI-based functional connectivity approach) and hippocampal volume [Porcu et al., 2020a]. The study focused on the gFA analyzed the effect of this marker on brain activity by exploiting the fALFF, and the effects on brain networking by exploiting ROI-based functional connectivity approach [Porcu et al. 2021a].

The ethical approval was not required because the study was performed exploiting the public dataset "Leipzig Study for Mind-Body-Emotion Interactions" (LEMON) [Babayan et al., 2019], and the research project did not receive any specific grant from funding agencies in the public, commercial, or non-profit sectors.

These three studies recognized three common methodological features.

The first one regards the population studies, that were extracted from the same dataset, the "Leipzig Study for Mind-Body-Emotion Interactions" (LEMON) dataset [Babayan et al., 2019]. This dataset is a freely public available dataset released in 2019 by the University of Leipzig, originally designed for the study of mind-body-emotion interactions [Babayan et al., 2019]. However, it is important to underline that the three studies of the PhD project differ one to each other in terms of population study composition because of the different exclusion criteria applied in the population selection procedure according to the information reported in the dataset and to the goal of the single study.

The second common aspect is the extrapolation of the markers of white matter degeneration through the analysis of MRI structural and DWI data, performed in the same modalities for all the subjects analyzed.

The third common feature is represented by the preprocessing and processing methods adopted for the analysis of the rs-fMRI data.

Before talking about the details of every single study (discussion included), these three common aspects will be analyzed in the following sections.

2.2. The LEMON dataset

The dataset consists of 227 subjects recruited on a voluntary based in the period between September 2013 and September 2015 [Babayan et al., 2019]. Two different subgroups can be identified in this population of 227 subjects: the young age group (20-35 years old) that consisted of 153 subjects (108 males and 45 females; median age = 24 years; mean age = 25.1 years; standard deviation = 3.1), and the older age group (59-77 years old) that consisted of 74 subjects (37 males and 37 females; median age = 67 years; mean age = 67.6 years; standard deviation = 4.7) [Babayan et al., 2019]. The age of the subjects included in the dataset was reported as a 5 years age range; for this reason, we grouped the age of the subjects in 16 progressive categories (category 1 = 0-5 years, category 2 = 5-10 years, category 3 = 10-15 years, and so on).

Every subject underwent on a series of medical investigation and neuropsychological tests. Regarding the medical investigations, all the subjects performed an anthropometry examination, blood and urine examination, hair sample examination, double blood pressure measure, electroencephalographic and MRI examination. The MRI scan was acquired on the same scanner, a 3 Tesla MAGNETOM Verio (Siemens Healthcare GmbH, Erlangen, Germany) with a 32-channel head coil [Babayan et al., 2019]. The MRI protocol was the same form all the subjects included in the dataset, and it included: 1) a T1-W Magnetization Prepared 2 Rapid Acquisition Gradient Echoes (T1-W MP2RAGE) sequence; 2) a T2-W isotropic sequence; 3) a functional T2*-W gradient echo EPI (T2*-W GRE-EPI), acquired on resting state, for the functional imaging [Babayan et al., 2019]. Further, for the first 112 subjects it was performed a 60 diffusion-encoding gradient directions DWI sequence and an anisotropic 2D-FLAIR sequence, whereas for the other 115 patients it was performed an updated 60 diffusion-encoding gradient directions DWI sequence with the same parameters of the precious version but with a faster calibration procedure, and an isotropic 3D SPACE sequence with FLAIR preparation (3D-FLAIR) [Babayan et al., 2019]. The details of the sequences are reported in Table 3.

MRI sequences parameters of the LEMON dataset	
Sequence	***Parameters***
Structural T1-weighted isotropic Magnetization Prepared 2 Rapid Acquisition Gradient Echoes sequence (T1-W MP2RAGE)	Acquisition orientation = sagittal; slices = 176; TR = 5000 ms; TE = 2.92 ms; TI 1 = 700 ms; TI 2 = 2500 ms; FA 1 = 4°; FA 2 = 5°; pre-scan normalization; echo spacing = 6.9 ms; bandwidth = 240 Hz/pixel; FOV=256 mm; voxel size = 1 mm; isotropic; slice order = interleaved; duration = 8 min 22 s.
T2-W isotropic sequence	Acquisition orientation = sagittal; slices = 176; TR = 3200 ms; TE = 409 ms; FA = variable; pre-scan normalization; echo spacing = 3.42 ms; bandwidth = 751 Hz/pixel; FOV = 256 mm; voxel size = 1 mm isotropic; duration = 4 min 43 s.
Resting-state functional T2*-W gradient echo EPI sequence (T2*-W GRE-EPI)	Acquisition orientation = axial; phase encoding = A ≫ P; voxel size = 2.3 mm, isotropic; FOV = 202 mm; imaging matrix = 88 × 88; 64 slices with 2.3 mm thickness; TR = 1400 ms; TE = 30 ms; flip angle = 69°; echo spacing = 0.67 ms; bandwidth=1776 Hz/pixel; partial fourier 7/8; no pre-scan normalization; multiband acceleration factor = 4; 657 volumes; slice order = interleaved; duration = 15 min 30 s.
60 diffusion-encoding gradient directions DWI sequence (first 112 participants)	88 axial slices; voxel size = 1.7 mm isotropic; 60 diffusion-encoding gradient directions, b-value of 1000 s/mm2; 7 non-diffusion-weighted b0 distributed in the sequence; TR = 7000 ms; TE = 80 ms; FA = 90°; bandwidth = 1502 Hz/ pixel; echo spacing = 0.78 ms, FOV = 220 mm, voxel dimension = 1.7 mm isotropic, imaging matrix = 128 × 128, 60 diffusion-encoding gradient directions, b-value = 1000 s/mm2; 7 b0 images, multiband acceleration factor 2, phase encoding A ≫ P, duration = 9 min 27 s.
Updated 60 diffusion-encoding gradient directions DWI sequence (last 115 subjects)	88 axial slices; voxel size = 1.7 mm isotropic; 60 diffusion-encoding gradient directions, b-value of 1000 s/mm2; 7 non-diffusion-weighted b0 distributed in the sequence; TR = 7000 ms; TE = 80 ms; FA = 90°; bandwidth = 1502 Hz/ pixel; echo spacing = 0.78 ms, FOV = 220 mm, voxel dimension = 1.7 mm isotropic, imaging matrix = 128 × 128, 60 diffusion-encoding gradient directions, b-value = 1000 s/mm2; 7 b0 images, multiband acceleration factor 2, phase encoding A ≫ P, duration = 8 min 38 s.
2D FLAIR (first 112 participants)	Acquisition orientation = axial; one 2D volume with 28 slices; TR = 10000 ms; TE = 90 ms; TI = 2500 ms; FA = 180°; pre-scan normalization; echo spacing = 9.98 ms; bandwidth = 199 Hz/pixel; FOV = 220 mm; voxel size = 0.9 × 0.9 × 4.0 mm^3; slice order = interleaved, duration = 4 min 42 s.
3D SPACE sequence with FLAIR preparation (3D-FLAIR) (last 115 subjects)	Acquisition orientation = sagittal; one 3D volume with 192 slices; TR = 5000 ms; TE = 395 ms; TI =1800 ms; FA = variable; pre-scan normalization; echo spacing = 3.36 ms; bandwidth = 781 Hz/pixel; FOV = 250 mm; voxel size = 1 mm; isotropic; duration = 7 min 2 s.

Table 3: Sequences included in the MRI protocol [Babayan et al., 2019].

All the patients performed also a battery of neuropsychological and neurocognitive tests for the evaluation of different aspects of mood and cognition. Among the neurocognitive tests, the subjects performed the Trail Making Test subtest A (TMT-A) and B (TMT-B) [Reitan et al., 1988; Reitan, 1992]. These tests evaluate several cognitive domains, including processing speed, cognitive sequencing, cognitive flexibility, and visual-motor skills [Corrigan et al, 1987; Reitan et al., 1988; Reitan, 1992; Bowie et al, 2006; Vazzana et al., 2010]; in particular, TMT-A is used for estimating the visuomotor speed, and TMT-B for the executive function. For both TMT-A and TMT-B were reported the time it took to connect numbers (TMT-A time) and numbers and letters (TMT-B time), and the performance scores of brain functions (PSBF) for both TMT-A (PSBF TMT-A) and TMT-B (PSBF TMT-B) [Reitan, 1992]: a) grade 1: perfectly normal (0-26 seconds for TMT-A; 0-65 seconds

for TMT-B); b) grade 2: normal (27-39 seconds for TMT-A; 66-85 seconds for TMT-B); c) grade 3: mild/moderately impaired (40-51 seconds for TMT-A; 86-120 seconds for TMT-B); d) grade 4: moderately/severely impaired (> 51 seconds for TMT-A; > 120 seconds for TMT-B). Further, for every subject, we calculated the difference between TMT-B time and TMT-A time (TMT-B minus A), considered as a measure of cognitive flexibility relatively independent from manual dexterity [Corrigan et al., 1987; Vazzana et al., 2010].

Up to now the main details of the LEMON dataset have been reported because they are indispensable for understanding the three studies conducted in the PhD project; for more details about the LEMON dataset, the reader is invited to consult the LEMON dataset publication [Babayan et al., 2019].

2.3. The extrapolation of the markers of white matter degeneration through the analysis of MRI structural and DWI data

The extrapolation of the white matter markers of degeneration (WMHb and gFA respectively) was conducted through the use of specific software.

The calculation of WMHb was performed by using the lesionBrain online tool [Coupé et al, 2018], in analogy to other studies [Porcu et al., 2020b; Porcu et al., 2020c]. This automated software, whose architecture is based on shallow neural networks, adopts a three-stage strategy that includes: multimodal patch-based segmentation, regularization of probability map and error correction [Coupé et al, 2018]. The pipeline consists of three main phases [Coupé et al, 2018]:

- Preprocessing for the normalization of the image intensity and for registration of the images into the Montreal Neurological Institute (MNI) space [Collins et al., 1994];
- Structural and WMH segmentation;
- WMH classification according to their localization.

For each subject, the T1-W MP2RAGE and 2D FLAIR (for the first 112 subjects) or the 3D FLAIR (for the other 115 subjects) sequences were processed using the default pipeline to obtain the total WM absolute volume (tWMv) and the total WMH absolute volume (tWMHv), both expressed in cm^3. For every subject was extracted the tWMHb according to the formula:

$$tWMHb = \frac{tWMHv}{tWMv}$$

and the results were expressed in percentage (%). By using the same approach, it was calculated the regional WMHb according to the localization of the WMH [Coupé et al, 2018; Porcu et al., 2020b; Porcu et al., 2020c]. In particular, it was extracted:

- The burden of the pvWMH (pvWMHb) for those WMH detected within three voxels (i.e., 3 mm in the MNI space) from the lateral ventricles, by dividing the absolute volume of pvWMH (pvWMHv) to the tWMv;

- The burden of the jcWMH (jcWMHb) for those WMH detected within three voxels from the grey matter, by dividing the absolute volume of jcWMH (jcWMHv) to the tWMv;
- The burden of the infratentorial WMH (itWMHb) for those WMH detected below the junction of brain stem and cerebellum, by dividing the absolute volume of itWMH (itWMHv) to the tWMv;
- The burden of the remaining WMH, classified as dWMH dWMH, by dividing the absolute volume of dWMH (dWMHv) to the tWMv.

Also in this case, the results were expressed in percentage (%). An example of WMH identification and quantification is reported in Figure 1.

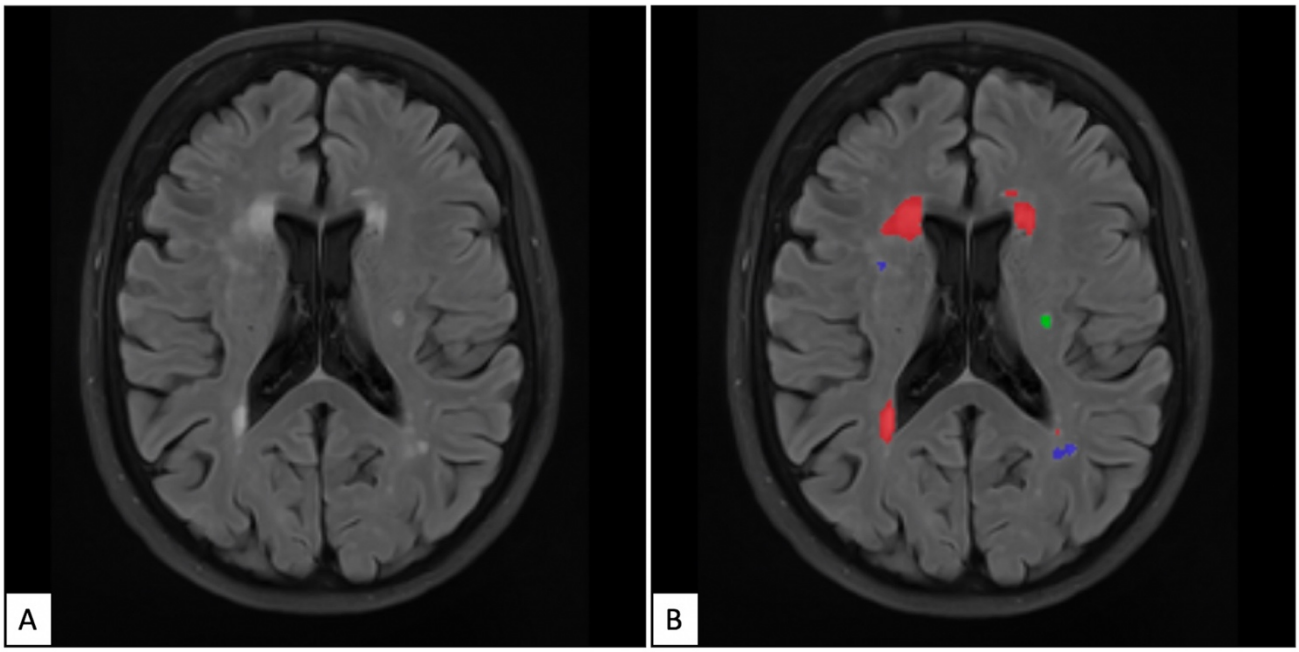

Figure 1: Example of WMH segmentation with lesionBrain [Coupé et al, 2018]. A) Original image; B) Segmented image: red areas = pvWMHs; green area: dWMH; blue area = jcWMH. [Porcu et al., 2020a].

We also extrapolated the hippocampal volumetric data from structural T1-W MP2RAGE and T2-W isotropic sequences by using the HIPS online tool [Romero et al., 2017]. HIPS is a patch-based segmentation automated tool that exploits the sole T1-weighted images (monospectral modality) or both the T1-W and T2-weighted images (multispectral modality) for the segmentation of the

hippocampus and of its subfields [Romero et al., 2017]. The pipeline consists of [Romero et al., 2017]:

- Preprocessing for the normalization of the intensity of the images and for their registration into the MNI space [Collins et al., 1994];
- Hippocampus segmentation associated with a systematic error corrector method based on a patch-ensemble of neural networks.

Starting from the T1-W MP2RAGE and T2-W isotropic sequences we exploited the multispectral modality of HIPS with the Kulaga-Yoskovitz protocol [Kulaga-Yoskovitz et al., 2015] for extrapolating the total hippocampal relative volume (tHRV), i.e. the sum of the absolute volumes of right and left hippocampus divided by the absolute intracranial volume, expressed in percentage (%). An example of hippocampal volume quantification is reported in Figure 2.

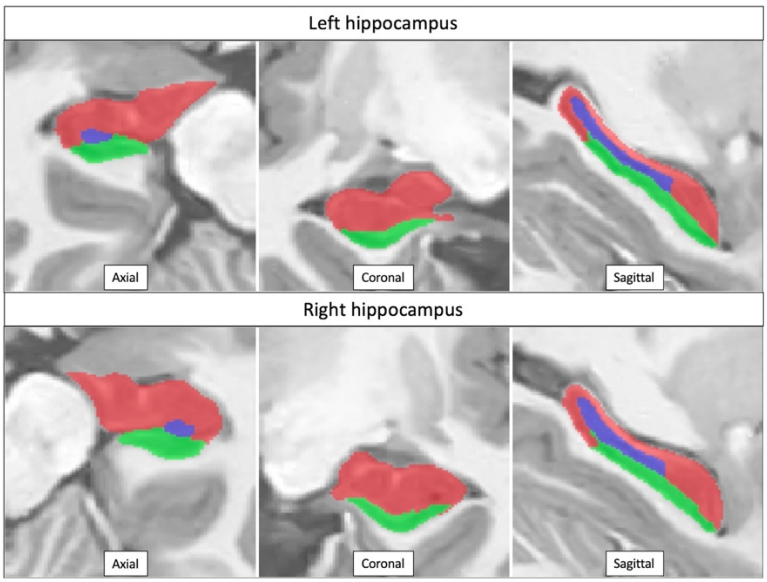

Figure 2: Example of hippocampus segmentation by HIPS (multispectral modality, Kulaga-Yoskovitz method) [Romer oet al., 2017; Kulaga-Yoskovitz et al., 2015]. Red area = cornus ammonis parts 1-3; Blue area = cornus ammonis part 4 – dentate gyrus; Green area = Subiculum. [Porcu et al., 2020a].

The accuracy of the above mentioned volumetric analyses was blindly verified by two expert Neuroradiologists (Luca Saba and Michele Porcu, 14 and 9 years of experience in the use of MRI for clinical research respectively), and the subjects whose analyses were judged inadequate by at least one of the Neuroradiologists were excluded from the studies.

Regarding the analysis of DWI sequences, it was performed using DSI Studio (version 2020_012, http://dsi-studio.labsolver.org/). The b-table was checked by an automatic quality control routine to ensure its accuracy [Schilling et al., 2019]. Subjects were excluded from the study if there was: a) incomplete or low quality/defective scans (DWI count < 67; image dimension ≠ 128 x 128 x 88; image resolution ≠ 1.71875 x 1.71875 x 1.7 mm; max b-value ≠ 1005); b) presence of ≥ 1 bad slice because of signal dropout; c) sequences with neighboring DWI correlation value < 0.80.

The DWI sequences were reconstructed by exploiting the DTI model-based method in order to obtain the gFA value within the individual space for every participant. The diffusion tensor was calculated, and a deterministic fiber tracking algorithm [Yeh et al., 2013] was used with augmented tracking strategies [Yeh, 2020] to improve reproducibility. The seeding region comprised the whole brain. The anisotropy threshold was randomly selected, and the change threshold was 20% [Wade et al., 2021]. The angular threshold was randomly selected from 15° to 90°. The step size was randomly selected from 0.5 voxels to 1.5 voxels. Tracks with lengths shorter than 25.7812 or longer than 257.812 mm were discarded, and a total of 100000 seeds were placed [Bergamino et al., 2020]. An example of DTI elaboration for calculation of gFA is reported in Figure 3.

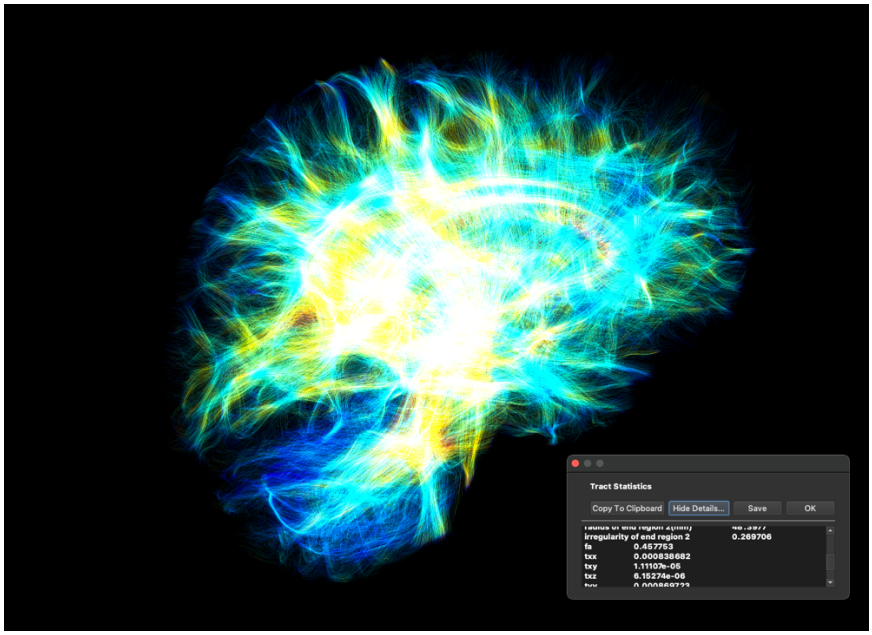

Figure 3: Example of DTI elaboration for gFA calculation with DSI studio (version 2020_012, http://dsi-studio.labsolver.org/).

2.4. Preprocessing and processing of the rs-fMRI data

As above reported, the three studies derived of the PhD project share a common rs-fMRI data preprocessing and processing, and it was made through the Matlab platform vR2020b (Mathworks, Inc., California, USA) by using the CONN-fMRI fc toolbox v20b [Whitfield-Gabrieli et al., 2012], based on the SPM 12 software package (Wellcome Department of Imaging Neuroscience, London, UK; http://www.fil.ion.ucl.ac.uk/spm/).

Similarly to previous studies [Porcu et al., 2019a; Porcu et al., 2019b; Porcu et al., 2020b], structural T1-W MP2RAGE and functional T2*-W GRE-EPI sequences were pre-processed adopting CONN's default pipeline for volume-based analysis following these steps:

- Functional realignment and unwarping;
- Functional slice-timing correction;
- Functional outlier detection adopting liberal settings (97^{th} percentile in the normative sample in functional outlier detection system: global-signal z-value threshold = 5; subject-motion threshold = 0.9 mm);
- Functional and structural direct segmentation of GM, WM and cerebrospinal fluid, followed by the normalization to Montreal Neurological Institute (MNI) [Collins et al., 1994] by using the default tissue probability maps (target resolution = 2 mm);
- Functional smoothing, using 8 mm full width half maximum Gaussian kernel filter.

The first 10 volumes of the SE-EPI sequence were discarded from analysis to reduce the fluctuation of the MRI signal in the initial stage of scanning [Porcu et al., 2019a]. Subjects with at least one of these features identified in the quality control following the preprocessing phase were excluded from the analysis: a) a number of invalid scans > 10% of the total amount; b) maximum global-signal z-value change > 9 std; c) maximum subject motion > 2 mm.

In order to minimize the residual non-neural variability of functional data, we applied the default principal component analysis (PCA) based denoising pipeline, called "aCompCor" [Nieto-Castanon, 2020], consisting of linear regression of potential confounding effects, including BOLD signals

registered in CSF and WM [Porcu et al., 2019a, 2020b], estimated subject-motion parameters and identified outlier scans as per the “scrubbing” procedure [Power et al, 2014; Nieto-Castanon, 2020]. Further, we applied a temporal band-pass filtering (0.008 to 0.09 Hz) to reduce noise effects and low-frequency drift [Porcu et al., 2019a; Porcu et al., 2020b; Nieto-Castanon, 2020].

The CONN’s default atlas was used for the mapping of the cerebral regions of interest (ROI): the Harvard-Oxford atlas [Desikan et al., 2006] for cortical and subcortical regions, and the Automated Anatomical Labelling (AAL) atlas [Tzourio-Mazoyer et al., 2002] for cerebellar regions.

2.5. Study 1 - The association between white matter hyperintensities, cognition and regional neural activity in healthy subjects

This study was published in 2021 on "*European Journal of Neuroscience*" [Porcu et al. 2021a]. The other authors of this paper were Luigi Cocco (Università di Cagliari - Italy), Josep Puig (Unveristy Hospital of Girona - Spain), Lorenzo Mannelli (SDN Napoli – Italy), Qi Yang (University Hospital of Xwanhu – China), Jasjt S Suri (Atheropoint^{TM}, Roseville, CA - USA) Giovanni Defazio and Luca Saba (Università di Cagliari - Italy).

According to the hypothesis that WMH alter the cognitive functions by inducing a reduction of regional neural activity, we conducted a cross-sectional study analysing the association between tWMHb and cognitive impairment measured with the TMT-A and TMT-B. Secondly, we analysed the impact of tWMHb on brain activity with the fALFF [Zou et al., 2008; Lv et al., 2018; Porcu et al., 2020d]. This approach was chosen because of its simplicity and high temporal stability [Küblböck et al., 2014; Lv et al., 2018], and because this type of analysis is more specific to grey matter activity when compared to the ALFF approach, thanks to its relative independence from non-specific signal components of the cerebrospinal fluid (CSF) [Zou et al., 2008].

2.5.1. Study population

We applied the following exclusion criteria to the LEMON dataset in order to make the study population as much homogeneous as possible: a) subjects who underwent 2D FLAIR sequence; b) left-handed and/or ambidextrous subjects; c) subjects with urine test positive for the presence of psychoactive substances; d) subjects with a diagnosis of past or current psychiatric disease; e) subjects whose volumetric analysis of WMHs burden was judged not correct by at least one of the Neuroradiologists. Once applied these exclusion criteria the final study population consisted of 75 subjects, that consisted of 58 males and 17 females; (median age category value = 6; minimum age category = 5; maximum age category = 15) (Table 4).

	Exclusion criteria	Number of subjects
Total dataset population	-	227
Subjects excluded according to the demographic data*	Subjects that performed a 2D FLAIR sequence	113
	Left-handed and ambidextrous subjects	25
	Subjects with urine test positive for the presence of drugs	12
	Subjects with psychiatric disease diagnosed in the anamnestic phase.	40
Subjects excluded in the volumetric analysis	Subjects whose volumetric analysis of WMHs burden was judged not correct by at least one of the Neuroradiologists	0
Final study population	-	75
**One or more exclusion criteria can be present at the same time in one subject.*		

Table 4: Final study population following the application of the exclusion criteria.

2.5.2. Statistical analysis: relationship between demographic, cognitive and volumetric data

Kolmogorov-Smirnov normality test (with Lilliefors correction) was performed for evaluating the normal/not normal distribution of the following variables (data were considered normally distributed for p-value > 0.05): age of the subjects (grouped in 16 progressive categories as above mentioned), tWMHb, TMT-A time, PSBF TMT-A, TMT-B time, PSBF TMT-B, and TMT-B minus A.

These tests revealed that only one variable was normally distributed (see below), so we performed one-tailed Spearman's correlation tests for analyzing the relationships between the seven above mentioned variables. The correlation's coefficient (ρ) was calculated choosing a Bonferroni corrected p-value for multiple comparisons = 0.008 as statistical threshold for identifying statistically significant correlations. The statistical analyses were made by using the SPSS 24.0 statistical package (SPSS Inc., Chicago, IL).

2.5.3. Statistical analysis: rs-fMRI

We analysed the processed rs-fMRI data (see above) with the fALFF mehod by computing for each voxel the relative amplitude (root mean square ratio) of BOLD signal fluctuations in the frequency band of interest (previously chosen in the denoising process - 0.008 to 0.09 Hz) compared with the entire detectable frequency range [Zou et al, 2008].

Three mass univariate second-level regression analyses (Subanalysis 1, 2, and 3), generated on the bases of the rs-fMRI processed data, were used to measure the effect of tWMHb on fALFF, including in the model age and sex as confounding factors due to the fact that WMHb tend to increase with physiological aging [Habes et al., 2016; Zhuang et al., 2018; d'Arbeloff et al., 2019], and it is higher in females than in males [Sachdev et al., 2009]. The three subanalyses differed one to each other because of the different statistical method applied for cluster-level inferences:

- Subanalysis 1: parametric statistics based on Gaussian Random Field theory (GRFT), adopting a cluster level uncorrected p-value (p-unc) < 0.001 for height threshold and a p-value corrected for False Discovery Rate (p-FDR) < 0.05 [Worsley et al., 1996; Nieto-Castanon, 2020].

- Subanalysis 2: nonparametric statistics based on randomization/permutation, performing 1000 permutation iterations of the original data, and adopting a p-unc < 0.001 for height threshold and p-FDR < 0.05 for cluster level threshold [Bullmore et al., 1999; Nieto-Castanon, 2020;].

- Subanalysis 3: nonparametric statistics based on Threshold Free Cluster Enhancement (TFCE), using 1000 permutation iterations of the original data and adopting a peak family wise corrected p-value (p-FWE) < 0.05 for voxel threshold [Smith et al., 2009; Nieto-Castanon, 2020].

2.5.4. Results: neuropsychological evaluation and volumetric analysis

The mean tWMHb value, derived from the volumetric analysis, was 0.121% (minimum value = 0%; maximum value = 1.590%). Regarding the distribution of WMH, the mean jcWMHb was 0.004% (minimum value = 0%; maximum value = 0.115%), the mean dWMHb value was 0.006% (minimum value = 0%; maximum value = 0.103%), and the mean pvWMHb value was 0.101% (minimum value = 0%; maximum value = 1.526%). No itWMH were detected.

Regarding the TMT-A and TMT-B tests, the mean TMT-A time was 31.26 s (minimum value = 12.97 s; maximum value = 71.81 s), and the mean TMT-B time was 66.95 s (minimum value = 30.72 s; maximum value = 154 s). According to the PSBF TMT-A, 34 people resulted perfectly normal, 25 people were classified as normal, 11 people showed mild/moderately impaired performances, and 5 people showed moderately/severe impaired results. For what concern the PSBF TMT-B, 45 people resulted perfectly normal, 14 people were classified as normal, 13 people showed mild/moderately impaired performances, and 3 people showed moderately/severe impaired results. TMT-B minus A mean value was 35.69 s (minimum value = -0.78 s; maximum value = 100 s).

The resume of the demographic data, the results of TMT-A and TMT-B tests, and the WMHb volumetric data are reported in Table 5.

Gender composition	**Age (subjects per grade)**	**Mean TMT-A time (s)**	**Subjects per PSBF TMT-A**	**Mean TMT-B time (s)**	**Subjects per PSBF TMT-B**	**Mean TMT-B minus A (s)**	**Mean tWMHb (%)**	**Mean jcWMHb (%)**	**Mean dWMHb (%)**	**Mean pvWMHb (%)**
58 males 17 females	Category 5 (20-25): 24 Category 6 (25-30): 26 Category 7 (30-35): 3 Category 12 (55-60): 2 Category 13 (60-65): 7 Category 14 (65-70): 8 Category 15 (70-75): 6	31.26 (Minimum value = 12.97; Maximum value = 71.81)	Grade 1 (perfectly normal – 0-26 s): 34 Grade 2 (normal – 27-39 s): 25 Grade 3 (mild/moderately impaired – 40-51 s): 11 Grade 4 (moderately/severely impaired - > 51 s): 5	66.95 (Minimum value = 30.72; Maximum value = 154)	Grade 1 (perfectly normal – 0-65 s): 45 Grade 2 (normal – 66-85 s): 14 Grade 3 (mild/moderately impaired – 86-120 s): 13 Grade 4 (moderately/severely impaired - >120 s): 3	35.69 (Minimum value = -0.78 ; Maximum value = 100)	0.121 (Minimum value = 0; Maximum value = 1.590)	0.004 (Minimum value = 0; Maximum value = 0.115)	0.006 (Minimum value = 0; Maximum value = 0.103)	0.101 (Minimum value = 0; Maximum value = 1.526)

Table 5: Resume of demographic, cognitive and WMHb volumetric data. TMT-A time = time it took to connect numbers, expressed in seconds; PSBF-TMT-A = performance scores of brain functions of TMT-A. TMT-B time = time it took to connect numbers and letters, expressed in seconds; PSBF-TMT-B = performance scores of brain functions of TMT-B; TMT-B minus A = TMT-B time minus TMT-A time; tWMHb = total white matter hyperintensities burden, expressed in percentage; jcWMHb: juxtacortical white matter hyperintensities burden, expressed in percentage; dWMHb = deep white matter hyperintensities burden, expressed in percentage; pvWMHb = periventricular white matter hyperintensities burden, expressed in percentage.

The Kolmogorov-Smirnov normality test (with Lilliefors correction) revealed that only TMT-B minus A was normally distributed (Table 6).

Kolmogorov-Smirnov (with Lilliefors correction)			
	Statistic	df	p-value
Age	0.362	75	< 0.001
tWMHb	0.356	75	< 0.001
TMT-A time	0.160	75	< 0.001
PSBF TMT-A	0.269	75	< 0.001
TMT-B time	0.143	75	0.001
PSBF TMT-B	0.364	75	< 0.001

TMT-B minus A	0.089	75	0.200*
*Normally distribuited data			

Table 6: Results of the Kolmogorov-Smirnov test of normality (with Lilliefors correction). df = degree of freedom; tWMHb = total white matter hyperintensities burden. TMT-A time = time it took to connect numbers; PSBF TMT-A = performance scores of brain functions of TMT-A; TMT-B time = time it took to connect numbers and letters; PSBF TMT-B = performance scores of brain functions of TMT-B; TMT-B minus A = TMT-B time minus TMT-A time.

All the Spearman's correlation tests identified statistically significant positive correlation between all the other variables: in particular, tWMHs resulted to be positively correlated with age ($\rho = 0.555$; p-value < 0.0001), TMT-A time ($\rho = 0.413$; p-value < 0.0001), PSBF TMT-A ($\rho = 0.388$; p-value < 0.0001), TMT-B time ($\rho = 0.472$; p-value < 0.0001); PSBF TMT-B ($\rho = 0.476$; p-value < 0.0001) and TMT-B minus A ($\rho = 0.435$; p-value < 0.0001). All the results are reported in Table 7.

Spearman's correlation analyses							
		Age	TMT-A time	PSBF TMT-A	TMT-B time	PSBF TMT-B	TMT-B minus A
tWMHb	ρ	0.555	0.413	0.388	0.472	0.476	0.435
	Sig. (1-tailed)	<0.001	<0.001	<0.001	<0.001	<0.001	<0.001
	N	75	75	75	75	75	75
Age	ρ	-	0.531	0.514	0.545	0.649	0.484
	Sig. (1-tailed)	-	<0.001	<0.001	<0.001	<0.001	<0.001
	N	-	75	75	75	75	75
TMT-A time	ρ	-	-	0.931	0.636	0.682	0.319
	Sig. (1-tailed)	-	-	<0.001	<0.001	<0.001	<0.001
	N	-	-	75	75	75	75
PSBF TMT-A	ρ	-	-	-	0.623	0.711	0.359
	Sig. (1-tailed)	-	-	-	<0.001	<0.001	0.001
	N	-	-	-	75	75	75
TMT-B time	ρ	-	-	-	-	0.879	0.912
	Sig. (1-tailed)	-	-	-	-	<0.001	<0.001
	N	-	-	-	-	75	75
PSBF TMT-B	ρ	-	-	-	-	-	0.796
	Sig. (1-tailed)	-	-	-	-	-	<0.001
	N	-	-	-	-	-	75

Table 7: Spearman's correlation analyses that evaluated the relationships between the tWMHb, the age of the patients (according to the category it belongs to), and the results of the TMT-A and TMT-B subtests. ρ = correlation's coefficient; N = number of samples; tWMHb = total white matter hyperintensities burden; TMT-A time = time it took to connect numbers; PSBF TMT-A = performance scores of brain functions of TMT-A; TMT-B time = time it took to connect numbers and letters; PSBF TMT-B = performance scores of brain functions of TMT-B; TMT-B minus A = TMT-B time minus TMT-A time.

2.5.5. Results: rs.fMRI analyses

The fALFF analysis identified several areas of decreased regional neural activity related to tWMHb, whereas no areas of increased regional neural activity were found. Results were slightly different according to the statistical method used. Subanalysis 1, based on GRFT, identified 4894 voxels organized in 14 distinct clusters that showed reduced fALFF (Table 8).

Subanalysis 1 – GRFT cluster-level inferences							
Cluster number	**Cluster (x,y,z according to MNI space)**	**Size (Number of voxels)**	**Size p-FWE**	**Size p-FDR**	**Size p-unc**	**Peak p-FWE**	**Peak p-unc**
1	-04 -72 +58	964	<0.000001	<0.000001	<0.000001	0.06846	0.000001
2	+54 +34 +06	911	<0.000001	<0.000001	<0.000001	0.000073	<0.000001
3	-42 -60 -52	577	<0.000001	<0.000001	<0.000001	0.10381	0.000001
4	+28 -76 -36	570	<0.000001	<0.000001	<0.000001	0.346363	0.000004
5	+06 +48 +14	503	<0.000001	<0.000001	<0.000001	0.157774	0.000001
6	-52 +34 -08	345	0.000007	0.000004	<0.000001	0.110508	0.000001
7	-24 +42 +44	208	0.00056	0.000266	0.000016	0.358623	0.000004
8	-62 -36 +46	140	0.007209	0.002785	0.000209	0.023211	<0.000001
9	+04 +32 +38	139	0.007505	0.002785	0.000218	0.248823	0.000003
10	-54 -66 +06	129	0.01128	0.003775	0.000328	0.120071	0.000001
11	-20 -70 -52	108	0.027411	0.008408	0.000804	0.271996	0.000003
12	+34 -80 +30	90	0.060892	0.017421	0.001818	0.330537	0.000004
13	+36 -50 -30	83	0.083805	0.021828	0.002533	0.625475	0.000011
14	+16 +50 +36	82	0.08775	0.021828	0.002657	0.247981	0.000003
Voxels that showed statistically significant reduced fALFF (10 biggest ROI)*							
• 798 voxels covering 10% of atlas.FP r (Frontal Pole Right) • 509 voxels covering 11% of atlas.sLOC r (Lateral Occipital Cortex, superior division Right) • 423 voxels covering 20% of atlas.Cereb2 r (Cerebelum Crus2 Right) • 401 voxels covering 6% of atlas.FP l (Frontal Pole Left) • 374 voxels covering 19% of atlas.Cereb2 l (Cerebelum Crus2 Left) • 370 voxels covering 7% of atlas.Precuneous (Precuneous Cortex) • 210 voxels covering 38% of atlas.IFG tri r (Inferior Frontal Gyrus, pars triangularis Right) • 181 voxels covering 13% of atlas.PaCiG r (Paracingulate Gyrus Right) • 146 voxels covering 6% of atlas.Cereb1 r (Cerebelum Crus1 Right) • 140 voxels covering 5% of atlas.MidFG r (Middle Frontal Gyrus Right)							
*Total suprathreshold voxels = 4849							

Table 8: Results of subnalysis 1 based on Gaussian random field theory - clusters of reduced fALFF. GRFT = Gaussian random field theory; MNI = Montreal neurological institute; p-FWE = p-value corrected for Family Wise Error; p-unc = uncorrected p-value; ROI = Region of interest.

Subanalysis 2, based on permutation/randomization, identified 18020 voxels with reduced fALFF organized in 6 distinct clusters (Table 9).

Subanalysis 2 – permutation/randomization analysis									
Cluster number	**Cluster (x,y,z according to MNI space)**	**Size (Number of voxels)**	**size p-FWE**	**size p-FDR**	**size p-unc**	**mass**	**mass p-FWE**	**mass p-FDR**	**mass p-unc**
1	+54 +34 +06	8547	0.004000	0.004267	0.000025	95032.99	0.003000	0.003763	0.000022
2	-04 -72 +58	3983	0.009000	0.005205	0.000061	43792.84	0.009000	0.004529	0.000058
3	+28 -76 -36	2068	0.021000	0.005890	0.000134	23607.51	0.014000	0.004529	0.000096
4	-42 -60 -52	2044	0.021000	0.005890	0.000137	23045.24	0.016000	0.004529	0.000105
5	-54 -66 +06	886	0.088000	0.025205	0.000733	9184.60	0.085000	0.024118	0.000701
6	-62 -36 +46	492	0.185000	0.056309	0.001964	5679.92	0.146000	0.041186	0.001437
Voxels that showed statistically significant reduced fALFF (10 biggest ROI)*									
• 2181 voxels covering 27% of atlas.FP r (Frontal Pole Right) • 1442 voxels covering 21% of atlas.FP l (Frontal Pole Left) • 1358 voxels covering 28% of atlas.sLOC r (Lateral Occipital Cortex, superior division Right) • 1062 voxels covering 19% of atlas.Precuneous (Precuneus Cortex) • 905 voxels covering 47% of atlas.Cereb2 l (Cerebelum Crus2 Left) • 838 voxels covering 39% of atlas.Cereb2 r (Cerebelum Crus2 Right) • 614 voxels covering 24% of atlas.Cereb1 r (Cerebelum Crus1 Right) • 594 voxels covering 22% of atlas.MidFG r (Middle Frontal Gyrus Right) • 570 voxels covering 42% of atlas.PaCiG r (Paracingulate Gyrus Right) • 563 voxels covering 11% of atlas.sLOC l (Lateral Occipital Cortex, superior division Left)									
*Total suprathreshold voxels = 18020									

Table 9: Results of subnalysis 2 based on permutation/randomization - clusters of reduced fALFF.; MNI = Montreal neurological institute; mass = the sum of the T-squared across all voxels within each cluster; p-FWE = p-value corrected for Family Wise Error; p-FDR = p-value corrected for false discovery rate; p-unc = uncorrected p-value; ROI = Region of interest.

Subanalysis 3, based on TFCE, identified 23752 voxels with reduced fALFF organized in 21 distinct clusters (Table 10).

Subanalysis 3 – TFCE							
Cluster number	**Cluster (x,y,z according to MNI space)**	**Size (Number of voxels)**	**Peaks**	**TFCE**	**Peak p-FWE**	**Peak p-FDR**	**Peak p-unc**
1	+56 +34 +06	12184	377	2422.58	<0.000001	<0.000001	<0.000001
2	-02 -74 +56	4785	121	1637.71	0.003000	0.009779	0.000113
3	-44 -66 -46	2202	61	1530.87	0.006000	0.009779	0.000236
4	+28 -76 -38	2009	61	1441.41	0.007000	0.009779	0.000383
5	-62 -44 +40	536	11	1314.41	0.011000	0.010660	0.000742
6	-54 -66 +02	945	33	1249.69	0.017000	0.011069	0.001005
7	+58 -60 -12	122	1	1033.30	0.028000	0.011560	0.002078
8	+10 +14 -06	209	5	1023.02	0.032000	0.011560	0.002140
9	-08 -60 +10	95	1	1010.01	0.033000	0.011621	0.002236
10	+56 -54 +20	147	5	991.62	0.039000	0.011861	0.002384
11	-30 -88 +14	91	1	980.61	0.040000	0.011929	0.002464
12	+38 -36 -32	56	3	974.10	0.042000	0.012072	0.002525
13	+02 +04 -36	30	1	973.67	0.042000	0.012072	0.002532
14	-64 -18 -08	57	7	973.50	0.043000	0.012072	0.002532

15	+64 +04 +24	81	5	968.94	0.044000	0.012132	0.002585
16	+64 -42 -06	42	1	964.51	0.045000	0.012132	0.002629
17	+64 -18 +34	49	1	954.91	0.050000	0.012293	0.002727
18	-36 -48 -34	18	1	953.46	0.050000	0.012345	0.002747
19	-10 +08 +00	30	1	953.44	0.050000	0.012345	0.002747
20	-52 -70 -20	56	1	952.91	0.050000	0.012345	0.002754
21	-42 -28 +48	8	1	952.75	0.050000	0.012345	0.002754
Voxels that showed statistically significant reduced fALFF (10 biggest ROI)*							
• 2760 voxels covering 34% of atlas.FP r (Frontal Pole Right) • 1906 voxels covering 28% of atlas.FP l (Frontal Pole Left) • 1608 voxels covering 33% of atlas.sLOC r (Lateral Occipital Cortex, superior division Right) • 1323 voxels covering 24% of atlas.Precuneous (Precuneus Cortex) • 957 voxels covering 50% of atlas.Cereb2 l (Cerebelum Crus2 Left) • 837 voxels covering 39% of atlas.Cereb2 r (Cerebelum Crus2 Right) • 813 voxels covering 30% of atlas.MidFG r (Middle Frontal Gyrus Right) • 736 voxels covering 15% of atlas.sLOC l (Lateral Occipital Cortex, superior division Left) • 698 voxels covering 51% of atlas.PaCiG r (Paracingulate Gyrus Right) • 614 voxels covering 24% of atlas.Cereb1 r (Cerebelum Crus1 Right)							
*Total suprathreshold voxels = 23752							

Table 10: Results of subnalysis 3 based on threshold free cluster enhancement - clusters of reduced fALFF. TFCE = threshold free cluster enhancement; MNI = Montreal neurological institute; p-FWE = p-value corrected for Family Wise Error; p-FDR = p-value corrected for false discovery rate; p-unc = uncorrected p-value; ROI = Region of interest.

In particular, all the three subanalyses shared similar results regarding the decreasing activity of the precuneus, prefrontal cortex (PFC) and cerebellar Crus I/II. The results of the analysis are shown in Figure 4 and 5.

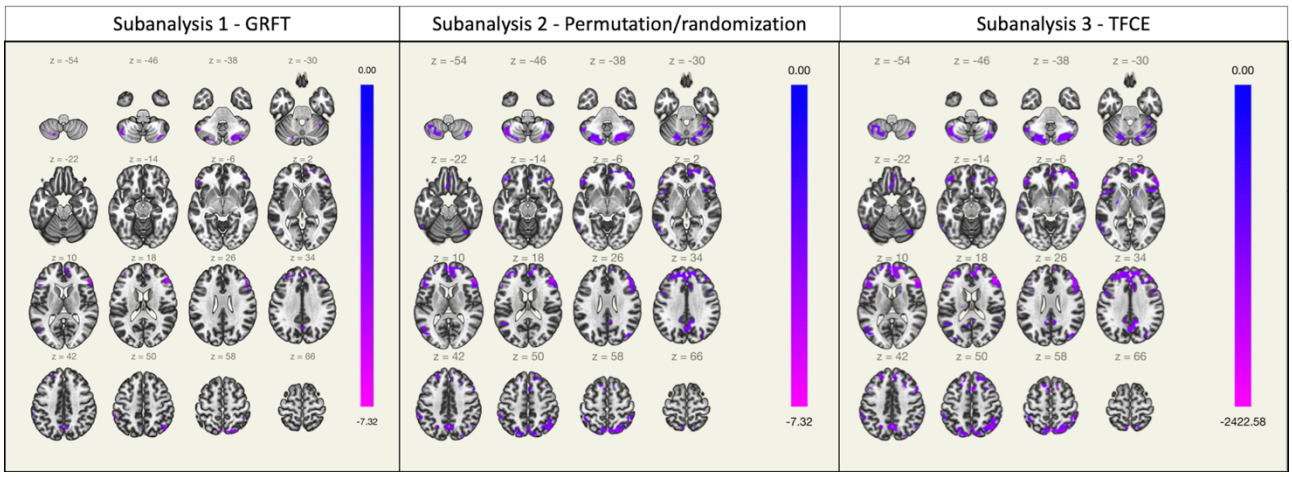

Figure 4 Results of fALFF analysis according to the statistical method used; only clusters of reduced fALFF activity were identified (blueish/purplish colored). fALFF = fractional amplitude of low frequency fluctuation; GRFT = Gaussian random field theory; TFCE = threshold free cluster enhancement. [Porcu et al., 2020a].

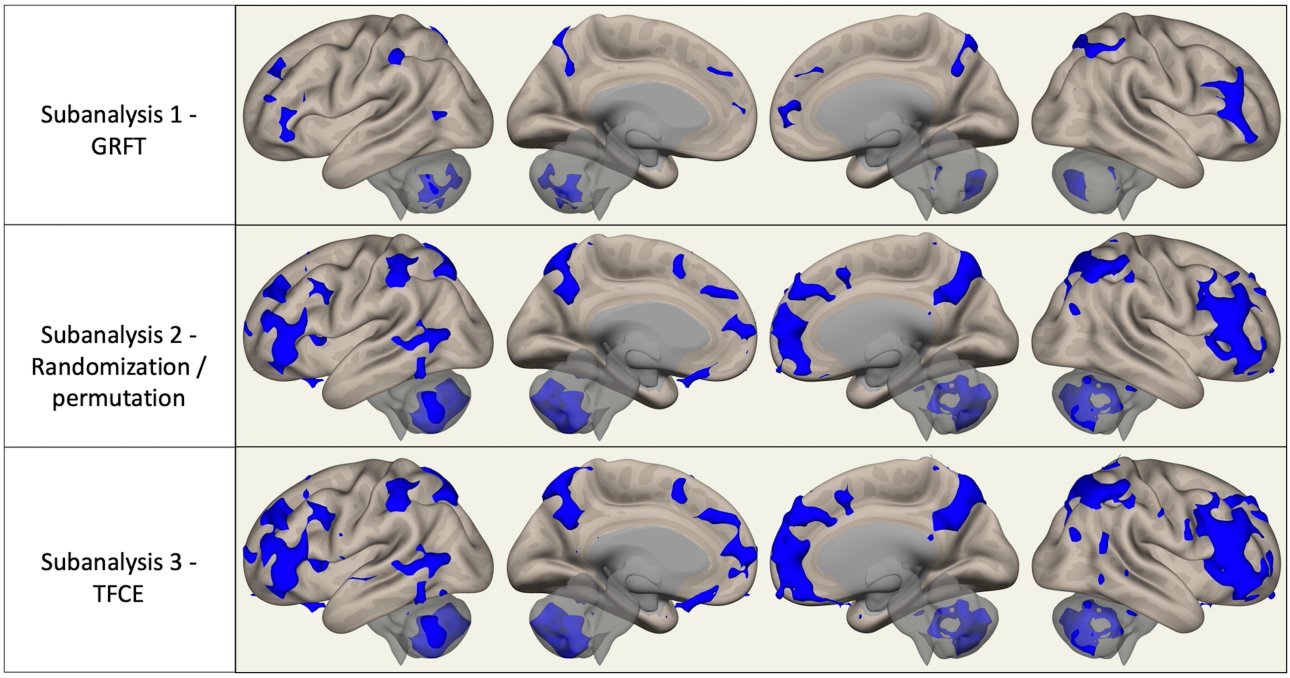

Figure 5: 3-dimensional view of the results of fALFF analysis according to the statistical method used; only clusters of reduced fALFF activity were identified (blue areas). fALFF = fractional amplitude of low frequency fluctuation; GRFT = Gaussian random field theory; TFCE = threshold free cluster enhancement. [Porcu et al., 2021a].

2.5.6. Discussion

In this research, we tested the hypothesis that WMH (in terms of tWMHb) are able to alter the cognitive function in healthy subjects by inducing a reduction of the function of several cerebral regions, according to the theory that the disruption of the fibres included in the WMH could alter the normal functioning of the respective linked cortical structures [Schmidt et al., 2005; Mok et al., 2011; Ding et al., 2015].

Firstly, we verified the correlations between age, tWMH, and the scores of TMT-A and B subtests in our study population. Although several neurocognitive tests were performed in the LEMON dataset [Babayan et al., 2019], we chose to use the TMT subtests as an indicator of the cognitive status because they are widely used in research and clinical practice as tool for detecting neuropsychological impairment, and they are able to assess several aspects of neurocognition (in particular processing speed, cognitive sequencing, cognitive flexibility and visual-motor skills) [Bowie & Harvey, 2006]. Despite the fact that 5 people showed moderately/severely impaired results in the PSBF TMT-A, and 3 people showed moderately/severely impaired results in the PSBF TMT-B, we did not exclude these

subjects from the final population study because the results of these tests alone are not sufficient for the diagnosis of dementia [Hugo et al., 2014], besides the fact that no diagnosis of dementia was reported for these subjects in the LEMON dataset [Babayan et al., 2019]. Statistically significant positive correlation were found for all the tests, in particular between age and WMHb, as well as the other positive correlations between tWMHs and TMT-A, PSBF TMT-A, TMT-B, PSBF TMT-B, and TMT B minus A. These results were in line with what found in previous studies [Wright et al., 2008; Prins et al., 2015; Chavda et al., 2019; MacPherson et al., 2017].

Subsequently, we performed the fALFF analysis for investigating the effects of tWMHb on regional neural activity. According to the lack of a unique standardized method of analysis of rs-fMRI data, we decided to make multiple subanalyses applying different statistic approaches in order to limit potential biases derived from the analytical flexibility of rs-fMR data [Botvinik-Nezer et al., 2020]. In particular, we made three different subanalyses; all of them revealed that tWMHb influence the brain activity of different cerebral areas, even if the results were slightly different. In fact, the absolute number of voxels that showed altered activity in relation to WMHb of subanalysis 1 was smaller when compared to the other two; further, the number, organization and composition of the clusters of voxels was different. However, all the three subanalyses shared a common aspect: they showed reduced regional activity of several same cerebral regions and no areas of increased regional activity in relation to the increase of WMHb.

By looking globally at the results, we tried to make a sum of these findings and we observed that three main cerebral areas that showed reduced regional activity in relation to the increase of WMHb were the precuneus, PFC, and cerebellar Crus I/II. Studies from literature demonstrated that the dysfunction of these areas is involved in the impairment of several cognitive functions. For example, precuneus is a pivotal region of the M-PFN, involved in several cognitive process, included highly integrated tasks and visuo-spatial imagery [Kim et al., 2011], and recently *Wang Z et al.* [Wang et al., 2020] demonstrated an association between WMH load and dysfunction of M-PFN in patients with mild cognitive impairment. PFC is another cerebral regions that play a pivotal role in executive

functions control, as evidenced by several lesion studies [Yuan et al., 2014]. It is note from literature the association between WMH and dysfunction of PFC: in fact, a tasking fMRI study by *Nordhal C et al.* [Nordhal et al., 2006] demonstrated that both global WMH volume and WMH volume in the dorsolateral frontal regions are associated with decreased PFC function, and the results of our investigation, despite the different techniques of analysis, are in line with these observations. Lastly, despite to the best of our knowledge no studies analysed the relationships between WMH and the cerebellar activity, it is not surprising that the reduction of the cerebellar regional neural activity observed in relation to the increasing tWMHb could contribute neurocognitive impairment altering the activity of the cerebro-cerebellar networks. Indeed, it is well known that lesions of the neocerebellum in humans can cause severe impairments in executive functions [Schmahmann et al., 1998]. Further, recent anatomical and fMRI studies demonstrated that cerebellum is involved in a wide spectrum of cognitive functions, and that the neocerebellum plays a pivotal role in executive function control [Jacobi et al., 2021]. For example, the rs-fMRI study conducted by *Habas C et al.* [Habas et al., 2009] with the Independent Component Analysis (ICA) method confirmed that cerebellar lobules Crus I/II (that belong to the neocerebellar cortex) participate in the right and left executive controls networks; this evidence has been also confirmed in a more recently tasking fMRI study by *Balster JH et al.* [Balster et al., 2013], demonstrating that the cerebellum contributes to cognitive control independently from motor control by elaborating inputs from PFC in the prefrontal-projecting cerebellar lobules Crus I/II,

Finally, looking at the distribution of the WMH, we observed that the majority of WMH were located in the periventricular region, and these data are in line with those found from literature [Nyquist et al., 2015]. This data suggests that pvWMH might play a role in influencing the cerebral regional activity that leads to cognitive impairment, according also to the robust evidence that pvWMH have a stronger significant negative impact on cognitive abilities when compared to jcWMH and dWMH [Bolandzadeh et al., 2012]. However, the analysis of the effects of the location of WMH on regional neural activity was beyond the purpose of this study.

2.5.7. Limits

We recognize at least two major limits of this study. The first limit is the small study population, which resulted also heterogeneous in age and gender composition. However, we chose to apply strict criteria in order to limit biases derived by medical conditions such as known neurological diseases or drug use; further, we included age and sex as confounding factors in the regression model of all the three subanalyses of the rs-fMRI data in order to overcome the limitations of the heterogeneity of the study population. The second limit regards the fact that we tried to interpret the effects of tWMHb on the sole cognitive sphere: our first goal was to evaluate the pure statistical effect of WMHb on brain activity rs-fMR, and it is reasonable to speculate that these effects could influence other neuropsychological aspects such as mood and behaviour, or other higher cerebral functions such as for example motion and visual perception; future studies could clarify these aspects.

2.6. Study 2 - Effects of white matter hyperintensities on brain connectivity and hippocampal volume in healthy subjects according to their localization

This study was published in 2020 on "*Brain connectivity*" [Porcu et al. 2020a]. The other authors of this paper were Annunziata Operamolla, Elisa Scapin, Paolo Garofalo, Francesco Destro, Alessandro Caneglias (Università di Cagliari - Italy), Jasjt S Suri (Atheropoint^{TM}, Roseville, CA - USA), Andrea Falini (Università San Raffaele, Milano – Italy), Giovanni Defazio, Francesco Marrosu and Luca Saba (Università di Cagliari - Italy).

Starting from the evidences exposed in the previous sections, we designed a cross-sectional study in order to investigate whether the localization of supratentorial WMH load (jcWMH, dWMH, and pvWMH) plays a role in hippocampal shrinkage in HS and if it has also an impact on the global cerebral functional connectivity, assuming the involvement of the hippocampal regions. An exploratory cross-sectional study was designed for investigating the relationships between supratentorial hippocampal volume (in terms of tHRV) and WMHb of each zone of the white matter (jcWMHb, dWMHb and pvWMHb); subsequently, we analysed the influence of the jcWMHb, dWMHb and pvWMHb on global brain networking by making a resting-state fMRI analysis. The graph theoretical approach was applied to resting state functional integration analysis for the interpretation of the results [Bullmore et al., 2009; Barabási et al., 2011; Bassett et al, 2017; Liao et al., 2017; Bassett et al., 2018].

2.6.1. Study population

We applied the following exclusion criteria to the LEMON dataset [Babayan et al., 2019] in order to make the study population as much homogeneous as possible: a) subjects that had only performed a 2D FLAIR instead of the 3D FLAIR; b) left-handed and ambidextrous subjects; c) subjects with urine test positive for the presence of drugs or that did not undergo the test; d) smokers, occasional smokers and subjects without this information; e) subjects with psychiatric disease diagnosed in the anamnestic phase or with no data relative to the presence/absence of psychiatric

disease; f) subjects with alcohol dependence and subjects without alcohol information; g) patients whose WMH segmentation was judged not correct form at least of the two expert Neuroradiologists.

Once applied these exclusion criteria the final study population consisted of 38 subjects, that consisted of 29 males and 9 females; (median age category value = 6; minimum age category = 5; maximum age category = 15). The mean tWMHb value was 0.963% (lower value = 0%; upper value = 6.392%), the mean pvWMHb value was 0.152% (lower value = 0%; upper value = 1.230%), the mean jcWMHb value was 0.800% (lower value = 0%; upper value = 5.420%), the mean dWMHb value was 0.012% (lower value = 0%; upper value = 0.021%), and the mean tHRV value was 0.494% (lower value = 0.395%; upper value = 0.617%).

The complete study population data, included the results of the volumetric analysis of WMH and hippocampus, are reported in Table 11.

Study population								
Subject ID	**Gender**	**Age**	**Age (grade)**	**tWMHb (%)**	**pvWMHb (%)**	**jcWMHb (%)**	**dWMH b(%)**	**tHRV (%)**
sub-010005	male	25-30	6	0.003	0.003	0.000	0.001	0.483
sub-010093	female	70-75	15	0.690	0.625	0.048	0.017	0.450
sub-010126	female	20-25	5	0.000	0.000	0.000	0.000	0.507
sub-010137	female	25-30	6	0.000	0.000	0.000	0.000	0.481
sub-010138	male	25-30	6	0.000	0.000	0.000	0.000	0.530
sub-010146	female	65-70	14	0.295	0.011	0.275	0.009	0.576
sub-010157	female	20-25	5	0.297	0.016	0.267	0.013	0.430
sub-010163	female	25-30	6	1.066	0.196	0.864	0.006	0.555
sub-010176	male	25-30	6	1.333	0.158	1.155	0.020	0.461
sub-010191	male	25-30	6	0.678	0.038	0.610	0.031	0.460
sub-010194	male	25-30	6	0.000	0.000	0.000	0.000	0.395
sub-010195	male	20-25	5	0.018	0.000	0.006	0.011	0.411
sub-010200	male	20-25	5	0.000	0.000	0.000	0.000	0.492
sub-010203	male	25-30	6	0.003	0.000	0.000	0.003	0.493
sub-010213	male	25-30	6	0.000	0.000	0.000	0.000	0.497
sub-010220	male	30-35	7	0.564	0.001	0.562	0.000	0.489
sub-010225	male	20-25	5	2.760	0.813	1.908	0.038	0.463
sub-010226	male	25-30	6	0.012	0.000	0.000	0.012	0.450
sub-010227	male	20-25	5	0.007	0.000	0.006	0.001	0.482
sub-010228	male	20-25	5	3.464	0.027	3.416	0.021	0.498
sub-010229	male	30-35	7	0.996	0.011	0.975	0.011	0.502
sub-010239	male	60-65	13	1.710	0.485	1.217	0.008	0.532

sub-010256	female	25-30	6	1.071	0.000	1.071	0.000	0.553
sub-010267	male	70-75	15	4.155	1.230	2.885	0.041	0.429
sub-010275	female	55-60	12	0.497	0.006	0.484	0.007	0.539
sub-010279	female	55-60	12	0.475	0.030	0.440	0.006	0.440
sub-010283	male	70-75	15	0.728	0.451	0.262	0.015	0.575
sub-010284	male	70-75	15	1.500	0.045	1.454	0.001	0.507
sub-010285	male	65-70	14	0.018	0.005	0.000	0.012	0.481
sub-010286	male	65-70	14	2.225	0.400	1.821	0.004	0.506
sub-010287	male	65-70	14	6.392	0.952	5.420	0.021	0.514
sub-010289	male	60-65	13	3.237	0.254	2.885	0.098	0.455
sub-010290	male	60-65	13	0.860	0.007	0.850	0.003	0.527
sub-010302	male	25-30	6	1.537	0.000	1.514	0.023	0.487
sub-010303	male	20-25	5	0.010	0.000	0.000	0.010	0.492
sub-010304	male	20-25	5	0.001	0.000	0.000	0.001	0.617
sub-010310	male	20-25	5	0.000	0.000	0.000	0.000	0.516
sub-010316	male	30-35	7	0.007	0.000	0.006	0.001	0.499
Mean values	-	-	-	0.963	0.152	0.800	0.012	0.494

Table 11: Demographic data and data derived from volumetric analysis of WMH and hippocampus. Subject ID= subject identifier; tWMH = total white matter hyperintensities burden; pvWMH = periventricular white matter hyperintensities burden; jcWMH = jutacortical white matter hyperintensities burden; dWMH = deep white matter hyperintensities burden; tHRV = total hippocampal relative volume. The Subject corresponds to the one reported in the LEMON dataset [Babayan et al., 2019].

2.6.2. Statistical analysis: relationship between demographic and volumetric data

The statistical analysis about the realtionships between demographic and volumetric data was conducted using the SPSS 24.0 statistical package (SPSS Inc., Chicago, IL). We performed a Kolmogorov-Smirnov test applying the Lillefors significance correction, assuming a p-value = 0.200 as a statistical threshold, in order to verify the normal/nonnormal distribution of the following parameters: age of the subjects (expressed in grades), tWMH, pvWMH, dWMH, jcWMH and tHRV. This test revealed that only tHRV values followed a normal distribution (see below) and for this reason we choose to perform one-tailed Spearman's correlation analysis for testing the correlations between the above-mentioned variables. The correlation coefficient (ρ) was calculated for every single relationship, and p-value < 0.05 was used as statistical threshold to identify a statistically significant correlations. In accordance to one of the aims of the study (evaluation of the relationships between supratentorial hippocampal volume and WMH load according to localization of the lesions) a Bonferroni corrected p-value = 0.017 was also taken into account as a statistical threshold for the

following three correlations: tHRV – jcWMH, tHRV – dWMH and tHRV - pvWMH ($\alpha_{corrected}$ = 0.05/3 = 0.017).

2.6.3. Statistical analysis: rs-fMRI

A second-level graph-analysis was made by exploiting the processed rs-fMRI data (see above). Individual correlation maps of the whole brain were created by the mean resting-state BOLD time course of every single ROI, obtaining the correlation coefficients with the BOLD time-course between ROI [Whitfield-Gabrieli et al., 2012; Porcu et al., 2019a; Porcu et al., 2019b]. Correlations were generated by using the general linear model and bivariate correlation analysis weighted for hemodynamic response function: higher Z-scores indicated positive correlations, indicating increased connectivity between ROIS as a reflection of increased synchronicity between them; lower Z-scores indicated negative correlations, indicating decreased connectivity between ROIs as a reflection of decreased synchronicity between them [Whitfield-Gabrieli & Nieto-Castanon, 2012; Porcu et al., 2019a]. Fisher's transformation was then applied to all Z-scores, and correlation coefficients were converted into standard scores [Whitfield-Gabrieli & Nieto-Castanon, 2012; Porcu et al., 2019a]. The group rs-fc ROI-to-ROI analyses were made including age, pvWMH, dWMH, and jcWMH as second level covariates. Three multiple regression analyses were then performed: pvWMH was the dependent variable for the first analysis (Analysis 1), jcWMH for the second one (Analysis 2), and dWMH for the third one (Analysis 3). Collinearity diagnostics were performed prior the rs-fc analyses for evaluating the presence of multicollinearity among independent variables by checking the variance inflation factor (VIF): multicollinearity was considered absent when all the independent variables showed VIF = 1, mild when all the independent variables showed VIF < 4, and severe if at least one independent variable showed VIF > 4 [Hair et al., 2010].

The graph theoretical analysis [Achard et al., 2007], was made with the CONN's integrated tool, considering the ROIs as nodes and the suprathreshold connections as edges of the network [Nieto-Castanon, 2020]. The following values were calculated for every ROI of the network [Nieto-

Castanon, 2020]: a) degree, b) average path length, c) clustering coefficient, d) global efficiency, e) local efficiency, and f) betweenness centrality. For the calculation, a two-sided p-value corrected for False Discovery Rate (p-FDR) < 0.05 as statistic threshold for identifying statistically significant correlations between ROIs, and a two-sided cost value = 0.15 as adjacency matrix threshold for network edges were adopted [Alexander-Bloch et al., 2013; Porcu et al., 2019b; Dalong et al., 2020].

2.6.4. Results: relationship between demographic and volumetric data

The Kolmogorov-Smirnov test revealed that only the tHRV scores showed normal distribution (Table 12).

Tests of Normality – Kolmogorov-Smirnov test with Lillefors significance correction			
	Kolmogorov-Smirnov		
	Statistic	df	p-value
Age (grade)	0.313	38	0
tWMHb	0.247	38	0
pvWMHb	0.376	38	0
jcWMHb	0.251	38	0
dWMHb	0.258	38	0
tHRV	0.1	38	0.200*
*This is a lower bound of the true significance.			

Table 12: Results of Kolmogorov-Smirnov test with Lillefors significance correction. df = degree of freedom; tWMH = total white matter hyperintensities burden; pvWMH = periventricular white matter hyperintensities burden; jcWMH = juxtacortical white matter hyperintensities burden; dWMH = deep white matter hyperintensities burden; tHRV = total hippocampal relative volume.

The following Spearman's correlation tests identified 10 statistically significant correlations ($p < 0.05$), nine positive and one negative (Table 13).

One-tailed Spearman's correlation						
		tWMHb	pvWMHb**	jcWMHb**	dWMHb**	tHRV**
Age (grade)	ρ	0.474*	0.592*	0.389*	0.269	0.133
	p-value	0.001	0	0.008	0.051	0.213
	Number of subjects	38	38	38	38	38
tWMHb	ρ	-	0.795*	0.957*	0.728*	0.014
	p-value		0	0	0	0.467
	Number of subjects		38	38	38	38
pvWMHb**	ρ	-	-	0.736*	0.658*	-0.027

	p-value			0	0	0.435
	Number of subjects			38	38	38
scWMHb**	ρ	-	-	-	0.614*	0.046
	p-value				0	0.391
	Number of subjects				38	38
dWMHb**	ρ	-	-	-	-	-0.331*
	p-value					0.021
	Number of subjects					38
*Statistically significant result (p-value < 0.05) **No statistically significant results for Bonferroni corrected p-value (p-value < 0.017)						

Table 13: Spearman's correlations. r = Spearman's correlation coefficient; tWMHb = total white matter hyperintensities burden; pvWMHb = periventricular white matter hyperintensities burden; jcWMHb = juxtacortical white matter hyperintensities burden; dWMHb = deep white matter hyperintensities burden; tHRV = total hippocampal relative volume.

One statistically significant negative correlation was found between dWMHb and tHRV (ρ = 0.331, p-value = 0.042 – Figure 6).

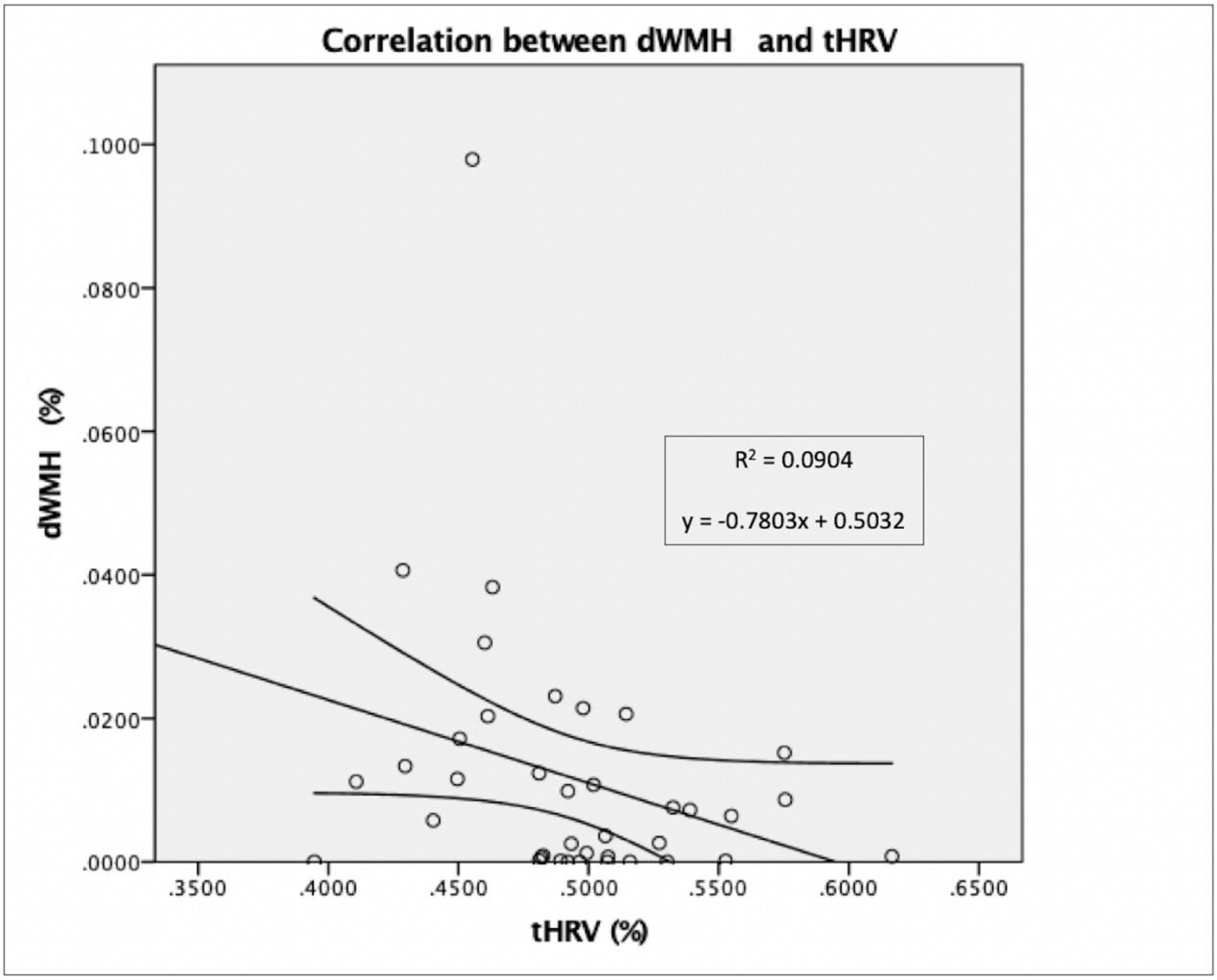

Figure 6: Negative correlation between dMWHb and tHRV. R2 = 0.0904; equation: y = -0.7803x + 0.5032.

No statistically significant positive or negative correlations were found between age and dWMHb, age and tHRV, tWMHb and tHRV, pvWMHb and tHRV, and between jcWMHb and tHRV, When the Bonferroni corrected p-value = 0.017 was taken into account as statistical threshold for the correlations between tHRV – jcWMHb, tHRV – dWMHb and tHRV – pvWMHb, no statistically significant findings were found.

2.6.5. Results: rs-fMRI analyses

The alignment of structural and functional data was considered correct for every subject included in the analyses by both the Neuroradiologists.

The independent variables showed VIF < 2 in all the analyses, indicating mild multicollinearity (Table 14).

Results of collinearity diagnostics				
Analysis	Dependent variable	Independent variables	Tolerance	VIF
Analysis 1	pvWMHb	Age (grade)	0.864	1.157
		dWMH	0.697	1.435
		jcWMH	0.649	1.54
Analysis 2	jcWMHb	Age (grade)	0.738	1.356
		dWMH	0.803	1.245
		pvWMH	0.636	1.572
Analysis 3	dWMHb	Age (grade)	0.737	1.357
		jcWMH	0.592	1.688
		pvWMH	0.503	1.987

Table 14: Results of collinearity diagnostics. VIF = Variance inflation factor; pvWMH = periventricular white matter hyperintensities burden; jcWMH = juxtacortical white matter hyperintensities burden; dWMH = deep white matter hyperintensities burden.

Analysis 1 (effects of pvWMHb) and 2 (effects of jcWMHb) did not reveal any statistically significant results. Analysis 3, focalised on the effects of dWMHb, revealed several statistically significant results. The properties of several ROIs of the network resulted influenced by dWMHb:

a) Global efficiency resulted reduced in the left posterior division of the parahippocapal gyrus (pPaHC L – beta value = -4.36; T-value = -6.41; p-FDR = 0.000033), left

hippocampus (Hippocampus L – beta value = -2.84; T-value = -5.47; p-FDR = 0.000277) and right hippocampus (Hippocampus R – beta value = -2.53; T-value = -5.05; p-FDR = 0.000649).

b) Average path length resulted increased in Hippocampus L (beta value = 21.54; T-value = 8.46; p-FDR < 0.000001) and Hippocampus R (beta value = 14.32; T-value = 6.21; p-FDR = 0.000035).

c) Local efficiency resulted reduced in Hippocampus R (beta value = -6.73; T-value = -6.44; p-FDR = 0.000036) and left putamen (Putamen L - beta value = -6.9; T-value = -4.11; p-FDR = 0.0016099).

d) Betweenness centrality resulted increased in the right amygdala (Amygdala R - beta value = 0.4; T-value = 4.42; p-FDR = 0.007308) and in cerebellum 3 left (Cereb3 L - beta value = 0.24; T-value = 4.39; p-FDR = 0.007308).

No ROIs were influenced in terms of degree and clustering coefficient. The results of analysis 3 are reported in Table 15 and Figure 7.

Analysis 3 - Effects of dWMHb						
Global efficiency						
ROI	Coordinates on the MNI space (x,y,z - mm)	beta	T	dof	p-unc	p-FDR
network	-	0.05	0.25	34	0.803085	-
pPaHC L	(-22, -32, -14)	-4.36	-6.41	34	0	0.000033
Hippocampus L	(-25, -23, -14)	-2.84	-5.47	34	0.000004	0.000277
Hippocampus R	(26, -21, -14)	-2.53	-5.05	34	0.000015	0.000649
Average path length						
ROI	Coordinates on the MNI space (x,y,z - mm)	beta	T	dof	p-unc	p-FDR
network	-	-0.3	-0.31	33	0.759814	-
Hippocampus L	(-25, -23, -14)	21.54	8.46	33	< 0.000001	< 0.000001
Hippocampus R	(26, -21, -14)	14.32	6.21	33	0.000001	0.000035
Local efficiency						
ROI	Coordinates on the MNI space (x,y,z - mm)	beta	T	dof	p-unc	p-FDR
network		0.02	0.09	33	0.926864	-
Hippocampus R	(26, -21, -14)	-6.73	-6.44	33	0	0.000036

Putamen L	(-25, 0, 0)	-6.9	-4.11	33	0.000244	0.016099
Betweenness centrality						
ROI	Coordinates on the MNI space (x,y,z - mm)	beta	T	dof	p-unc	p-FDR
network	-	0	-0.34	33	0.73728	-
Amygdala R	(23, 4, 18)	0.4	4.42	33	0.000101	0.007308
Cereb3 L	(-9, -37, -19)	0.24	4.39	33	0.000111	0.007308

Table 15: Results of the graph analysis 3. MNI = Montreal Neurological Institute; beta = beta value; T = T-value; dof = degree of freedom; p-unc = p uncorrected; p-FDR = p corrected for False Discovery Rate; pPaHC L = posterior division of the left parahippocampal gyrus; Hippocampus L = left hippocampus; Hippocampus R = light hippocampus; Putamen L = Left Putamen; Amygdala R = right amygdala; Cereb3 L = cerebelum 3 left.

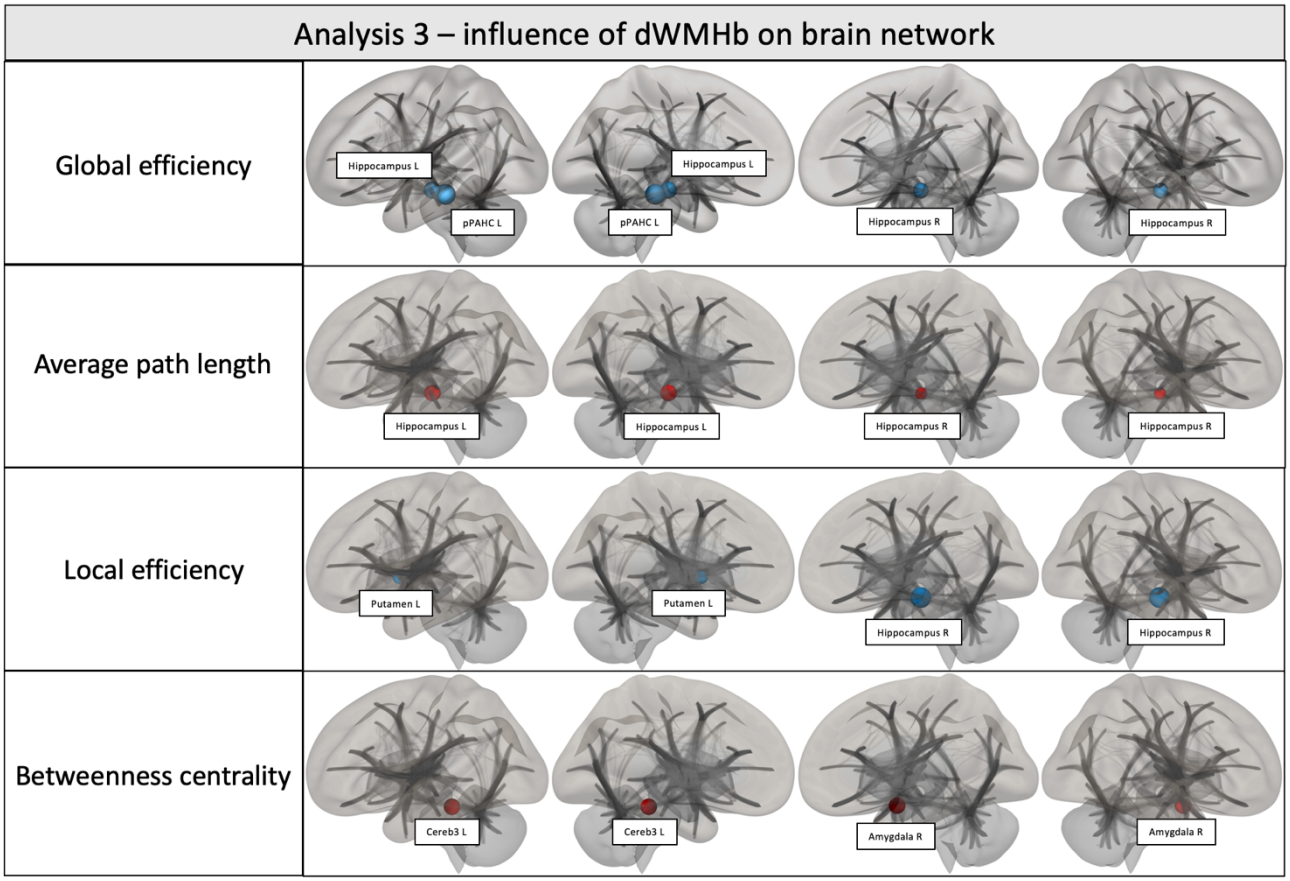

Figure 7: Analysis 3 – effects of dWMHb on brain network. pPaHC L = posterior division of the left parahippocampal gyrus; Hippocampus L = left hippocampus; Hippocampus R = light hippocampus; Putamen L = Left Putamen; Amygdala R = right amygdala; Cereb3 L = cerebelum 3 left. [Porcu et al., 2020a].

2.6.6. Discussion

The relationship between WMH and age [Sachdev et al., 2007] has been described in several previously published papers, whereas the correlation between WMH load and hippocampal shrinkage was recently demonstrated by *Fiford et al.* [Fiford et al., 2017]. In addition, some resting-state functional connectivity MRI studies already investigated the influence of WMHb on brain

connectivity in HS [Benson et al., 2018; De Marco et al., 2017; Reijmer et al., 2015]. In the current study, the results showed how the distribution of WMH influences both the hippocampal volume and the architecture of brain networks in HS.

The morphometric analysis confirms that tWMHb tends to increase with aging [Sachdev et al., 2007]. However, although tWMHb is positively correlated to pvWMHb and jcWMHb, no statistically significant correlations were found between tWMHb and dWMHb and between age and dWMHb. According to these findings, we hypothesize that the expression of dWMH follows an independent pathway compared to pvWMH and jcWMH due to the different suggested etiopathogenesis of these lesions [Gouw et al., 2011]. For example, it has been hypothesized that pvWMH recognized in chronic hemodynamic abnormalities the more likely development mechanism, whereas dWMH seems to be more likely related to ischemic changes due to atherosclerosis or micro-embolic events [Kim et al, 2008]. Moreover, previous studies found an association between dWMS and cardiovascular risk factors: *Strassburger TL et al.* [Strassburger TL et al, 1997] showed that subjects with hypertension showed increased dWMHb (but not pvWMHb) when compared to age-matched normotensive individuals. More recently it was shown that dWMH and pvWMH have different progression rates with aging, and that the progression of dWMH is associated with cardiovascular mortality [Sabayan et al., 2015]. The same study, interestingly, evidenced that the progression of pxWMH was associated with non-cardiovascular mortality [Sabayan et al., 2015]. The impact of scWMH on hippocampal volume loss would be less evident due to the involvement of short association fibers (U-fibers); similarly, the impact of pvWMH on hippocampal shrinkage would be minimal due to the low number of long-association fibers directed to the limbic region, although the periventricular fiber system consists of important crossroad areas [Judas et al., 2005]. Another interesting finding derived from these correlation analyses is related to the fact that only dWMH load resulted to be inversely correlated to tHRV. We know from neuroanatomic studies that the long association fibers of the brain pass mainly through the deep WM, and that lesions of these nerve bundles alter the connection between cortical areas engaged in different cognitive fields

[Schmahmann et al., 2008]. According to this, we assume that dWMH could prevent the regular interconnection between cortical areas, in particular the fibers of cortico-limbic system, leading to hippocampal volume loss as the final result of Wallerian degeneration [von Bohlen und Halbach et al., 2002]. A recent diffusion tensor imaging (DTI) study by *Reginold W et al.* [Reginold et al., 2018], which evidenced the alteration of diffusion properties of the WM tracts surrounding WMH along with WM pathways crossing the WMH, represents another evidence in support of this hypothesis.

The resting state functional connectivity analysis revealed that dWMHb represents the most relevant element which influences the weight of brain networks, whereas no significant results were found in analysis 1 (focused on the pure effects of pvWMHb) and analysis 2 (focused on the effects of jcWMHb). In particular, increased values of dWMHb were associated with increased average path length and reduced global efficiency in both the hippocampi. These data suggest that dWMH influences the activity of both hippocampi by reducing the centrality of these ROIs within the cerebral network or, in other words, reducing the degree of global connectedness of both the hippocampi within the network [Nieto-Castanon, 2020]. Hippcocampus R showed also reduced local efficiency, indicating a reduction of the ability of this ROI to transfer information at the local level. Reduced local efficiency was also found in the Putamen L, whereas the pPaHC L resulted reduced in global efficiency. Finally, the Amygdala R and the Cereb3 L showed increased betweenness centrality, indicating increased centrality of these structures within the network.

Although to the best of our knowledge the present study is the first to address these features in HS, it is worthwhile to interpret more holistically our data according to other investigations led in previous subjects. It is pertinent to recall that the most relevant hippocampal efferent return to the subicular complex and to the most inner part of the entorhinal cortex from where the information are routed back to the several parts of the neocortex, giving rise to a complex choreography of a recurrent multiplexed loop [Buzsáki, 1996; Buzsáki et al., 2003]; based on these considerations it becomes intuitive that even small interruption in this circuitry of recurrent pathways, which integrate the process of sophisticated retrieval of episodic memory and spatial maps, can easily induce crucial

disruptions. Indeed, it has been evidenced that WMH correlate with cognitive decline [Brickman, et al., 2009] and of particular interest is the observation that those located in the parietal lobe can predict impending severe cognitive decline in spite of normal hippocampal volumes [Brickman et al., 2012].

Together, the results of our explorative research allow us to speculate that the dWMH induces hippocampal atrophy through direct or indirect damage of the long association fibres of the deep WM, in particular the fibers of cortico-limbic system. The hippocampal structural changes are accompanied by alteration of the activity of hippocampus revealed by graph analysis, These complex alterations would induce a decreased ability to transfer information both at the global level (as well as at the local level of the Hippocampus R) by impairing the functions of spatial and memory retrieval [Abrahams et al., 1997] since these lesions disrupt the correct structural and biochemical hippocampal operations along the entire sleep-waking cycle [Marrosu et al., 1995].

It is also interesting to note that the dWMH load influences the activity of other several cerebral regions. We observed reduction of global efficiency in pPaHC (involved in many cognitive processes, including episodic memory and visuospatial processing [Aminoff et al., 2013]), reduced local efficiency of the Putamen L (involved in the articulatory process [Abutalebi et al., 2013]), and the increased betweenness centrality of Amygdala R (a structure implied in instructed and experienced-based fear [Braem et al., 2017]) and Cereb3 L (cerebellar region whose alterations are correlated with ataxia [Schmahmann, 2019]).

2.6.7. Limits

In this study, we have identified several limits. The first one is related to the sample count represented by the relatively low number of patients, even if the study was designed as exploratory: we applied strict exclusion criteria in order to minimize potential biases related to the presence of conditions such as drug consumption and alcohol dependence. Another significant limitation of the analysis, somewhat related to the above mentioned, is the potential bias related to the gender disproportion in the study population (9 females and 29 males), considering the fact that it is noted

that WMH is more common in women than in men [Sachdev et al., 2009]; this parameter should have to be taken into account in a future confirmative study.

For what concerns the correlation's analyses, another important limitation is related to the fact that no statistically significant results were found in the correlations between tHRV and jcWMHb, dWMHb, and pvWMHb when the Bonferroni corrected p-value was taken into account. In our opinion, the exploratory nature of the study can justify the choice of considering as statistically significant the result of the correlation between tHRV and dWMHb avoiding applying a multiple comparison correction. Further, the p-value obtained in this analysis (p-value = 0.021) slightly exceeds the Bonferroni corrected p-value adopted as the statistical threshold (p-value = 0.017); in our opinion, this data is noteworthy because it can be interpreted as a strong clue that this correlation would result statistically significant in future confirmative studies with bigger study populations, although this theory is purely speculative.

Besides the low sample size, the presence of a mild degree of multicollinearity between the independent variables in all the resting state functional connectivity analyses represents another limit of the study. Further, the low VIF values observed let us reasonably affirm that these values were not severe enough to determine significant biases.

Finally, a possible limit is represented by the absence of correlation with clinical data: indeed, even though several cognitive and behavioural data have been collected in the dataset, we focused our attention on the "pure" anatomical elements according to the fact that all the subjects included in the population study were considered as in healthy conditions. Again, further longitudinal study with statistically eloquent cohort of subjects will help to better evaluate whether studies lead with the WMH approach may impact our knowledge on the cognitive decline or other related conditions (e.g. several neurodegenerative diseases).

2.7. Study 3 - Global fractional anisotropy: effect on resting-state neural activity and brain networking in healthy participants

This study was published in 2021 on "*Neuroscience*" [Porcu et al. 2021b]. The other authors of this paper were Luigi Cocco (Università di Cagliari - Italy), Sirio Cocozza, Giuseppe Pontillo (Università Federico II, Napoli - Italy), Giovanni Defazio (Università di Cagliari - Italy), Jasjt S Suri (Atheropoint^{TM}, Roseville, CA - USA), Arturo Brunetti (Università Federico II, Napoli – Italy), and Luca Saba (Università di Cagliari - Italy).

In addition to the other evidences above mentioned, a recent study by *Garcia-Lazaro et al.*, [Garcia-Lazaro et al., 2016] demonstrated that gFA is a good parameter for discriminating young from older participants in healthy population; further, the authors of this study suggested that age-related changes in FA should be evaluated by using a global rather than a regional approach due to the fact that the global approach allows a comprehensive evaluation of the state of WM integrity and not only a partial measurement (as is the case when a regional-based approach is used) [Garcia-Lazaro et al., 2016]. According to this study and to the fact that aging-related reduced integrity of specific WM tracts is associated with decreased functional connectivity in several hubs, particularly in the default mode network (DMN) [Yang et al., 2016; Teipel et al., 2010], we conducted a cross-sectional study to explore the effects of gFA value as a quantative marker of global white matter integrity on the functional activity of the whole brain at resting-state.

2.7.1. Study population

We applied the following exclusion criteria to the LEMON dataset [Babayan et al., 2019] in order to make the study population as much homogeneous as possible:

a) Left-handers participants
b) Diagnosis of previous or current psychiatric disease, including alcohol and drug addiction, and participants with urine test positive for the presence of drugs
c) Smoker participants

d) Subjects whose DWI scans resulted incomplete or low quality/defective, i.e. that showed at least one of these features (see above):

    1. DWI count < 67; image dimension ≠ 128 x 128 x 88; image resolution ≠ 1.71875 x 1.71875 x 1.7 mm; max b-value ≠ 1005
    2. Presence of ≥ 1 bad slice because of signal dropout
    3. Sequences with neighboring DWI correlation value < 0.80.

e) Subjects with at least one of these features identified in the quality control following the preprocessing phase:

    1. a number of invalid scans > 10% of the total amount
    2. maximum global-signal z-value change > 9 std
    3. maximum subject motion > 2 mm

Once applied these exclusion criteria, the final population study consisted of 79 participants (Table 16).

Population study selection		
	Exclusion criteria	Number of subjects
Total dataset population	-	227
Participants excluded according to the clinical data*	Non-right handed participants	25
	Diagnosis of past or current psychiatric disease, including alcohol and drug addiction, and participants with urine test positive for the presence of drugs	76
	Smoker participants	36
Participants excluded following the DWI sequences analysis*	Incomplete or defective scans	1
	Presence of ≥ 1 bad slices because of signal dropout	7
	Sequences with neighboring DWI correlation value < 0.80	2
Participants excluded following the quality control of the preprocessing phase of the fMRI analysis*	Number of invalid scans > 10% of the total amount	2
	Maximum global-signal z-value change > 9 std	19
	Maximum subject motion > 2 mm	4
Final study population	-	79
**One or more exclusion criteria can be present at the same time in one subject.*		

Table 16: Details of the study population selection process. std = standard deviations.

2.7.2. Statistical analysis: relationship between demographic data and gFA value

The evaluation of the relationships between gFA values and age, and the comparison of the mean distribution values of gFA between males and females were made by using the SPSS 24.0 statistical package (SPSS Inc., Chicago, IL).

Firstly, we identified the outliers with the interquartile range rule using a multiplier of 3.0 according to *Hoaglin et al.* [Hoaglin et al., 2018] on both age and gFA values obtained from the DWI analysis.

Secondly, we performed a Kolmogorov-Smirnov normality test (with Lilliefors correction) in order to evaluate the normal/ abnormal distribution of age and gFA values, assuming a $p = 0.2$ as lower bound of the true significance. This test revealed that only the gFA variable was normally distributed (see below), so we performed a two-tailed Spearman's correlation test for analyzing the relationships between age and gFA. The correlation's coefficient (ρ) was calculated choosing a $p < 0.05$ as the statistical threshold for refusing the null hypothesis.

By looking at the abnormal composition of the population in terms of age categories through the inspection of the skweness and kurtosis measures and standard errors, and the visual inspection of its histogram [Cramer et al., 2004; Doane et al., 2011], we divided the population into two distinct subgroups (see below): a) a young subgroup (age categories: 5-7), and b) an elderly subgroup (age categories: 12-16).

Lastly, we performed a nonparametric Levene's test for equality of variance for evaluating the variance of gFA in males and females values of the whole population, young group, and elderly group assuming a $p < 0.05$ for rejecting the null hypothesis. According to the fact that the null hypothesis was rejected in all these cases (see below), we performed a Mann-Whitney U test for evaluating the presence of statistically significant differences in gFA mean ranks values between males and females in the whole population, young group and elderly group, by assuming a $p < 0.05$ to reject the null hypothesis.

2.7.3. Statistical analysis: rs-fMRI

Similarly to a previously published paper [Porcu et al., 2020d], we conducted three different rs-fMRI analyses on the processed rs-fMRI data to study the effects of gFA values: the first (Analysis A) aimed at evaluating the regional neural activity by exploiting the fALFF method [Zou et al., 2008; Lv et al., 2018]; the second (Analysis B) and the third (Analysis C) aimed at evaluating the functional connectivity throughout the whole brain by exploiting ROI-to-ROI approach [Lv et al., 2018; Porcu et al., 2019a].

Analysis A was made with the fALFF method by calculating for each voxel the relative amplitude (root mean square ratio) of BOLD signal fluctuations in the frequency band of interest (0.008 to 0.09 Hz, as previously set in the denoising process) compared with the entire detectable frequency range [Zou et al., 2008; Lv et al., 2018; Porcu et al., 2019a]. A mass univariate regression analysis was then performed by using the gFA values as a second-level covariate, adopting nonparametric statistics based on Threshold Free Cluster Enhancement (TFCE), using 1000 permutation iterations of the original data, choosing a peak family-wise corrected p (p-FWE) < 0.05 for voxel statistical threshold and a cluster size > 100 voxels for cluster statistical threshold [Smith et al., 2009; Nieto-Castanon, 2020].

Regarding the seed-based analyses (analyses B and C), individual correlation maps of the whole brain were made using the mean resting-state BOLD time course of each ROI, followed by the computation of the correlation coefficients of the BOLD time-course among predefined ROIs [Whitfield-Gabrieli et al., 2012; Porcu et al., 2019a,; Porcu et al., 2020d]. Correlations were computed by using the General Linear Model (GLM), applying a bivariate correlation analysis weighted for Haemodynamic Response Function (HRF) [Whitfield-Gabrieli et al., 2012; Porcu et al., 2019a,; Porcu et al., 2020d]: higher Z-scores indicated positive correlations as a reflection of the increased synchronicity between ROIs and vice-versa [Whitfield-Gabrieli et al., 2012; Porcu et al., 2019a,; Porcu et al., 2020d]. Fisher's transformation was applied to all Z-scores, and the correlation coefficients were converted into standard scores [Whitfield-Gabrieli et al., 2012; Porcu et al., 2019a,;

Porcu et al., 2020d; Porcu et al., 2021c]. In analogy to analysis A, a linear regression analysis was performed to measure the effects of gFA values on functional connectivity among the ROIs. For analysis B, the TFCE nonparametric statistics for cluster-level inferences identification was applied, using 1000 permutation iterations of the original data, adopting p-FWE < 0.05 for connection threshold [Smith et al., 2009; Nieto-Castanon, 2020]. For analysis C, we applied the graph-theoretical approach in order to identify statistically significant changes of several properties of the ROIs of the network [Bullmore et al., 2009; Nieto-Castanon, 2020]: global efficiency, local efficiency, average path length, degree, cost, betweenness centrality, and clustering coefficient. In analogy to *Porcu et al.* [Porcu et al., 2020c] we applied a conventional two-sided p-value corrected for false discovery rate (p-FDR) < 0.05 for identifying statistically significant correlations between ROIs of the network, and a two-sided cost value = 0.15 as adjacency matrix threshold for network edges.

2.7.4. Results: relationship between demographic and volumetric data

The population study consisted of 46 males and 33 females, with overall median value of age categories = 6 (25-30 years). Mean gFA value was of 0.461 (minimum value = 0.392; maximum value = 0.489), and no outliers were detected (see below) (Table 17).

Final study population							
Number of participants and gender composition	*Composition of the group by age categories*	*Median age categoy value*	*Skewness (age category)*	*Kurtosis (age category)*	*Mean gFA value*	*Skewness (gFA value)*	*Kurtosis (gFA value)*
Males = 33 Females = 46 Total = 79	Age category 5 (20-25) = 32 Age cateogry 6 (25-30) = 21 Age category 7 (30-35) = 3 Age category 12 (55-60) = 2 Age category 13 (60-65) = 6 Age category 14 (65-70) = 6 Age category 15 (70-75) = 7 Age category 16 (75-80) = 2	6	0.962 (standard error = 0.271)	-0.918 (standard error = 0.535)	0.4619 (range = 0.3928 – 0.4899; standard deviation = 0.0169)	-0.921 (standard error = 0.271)	2.411 (standard error = 0.535)

Table 17: Details of the final study population. gFA = global fractional anisotropy.

Kolmogorov-Smirnov normality test (with Lilliefors correction) revealed that the gFA values were normally distributed (p-value = 0.062) whereas the age resulted abnormally distributed (p-value

= 0.360); Therefore, we performed a Spearman's correlation analysis, that revealed a statistically significant moderate inverse correlation between gFA and age (ρ = -0.343; p-value = 0.002).

The whole population study present a bimodal distribution (Figure 8).

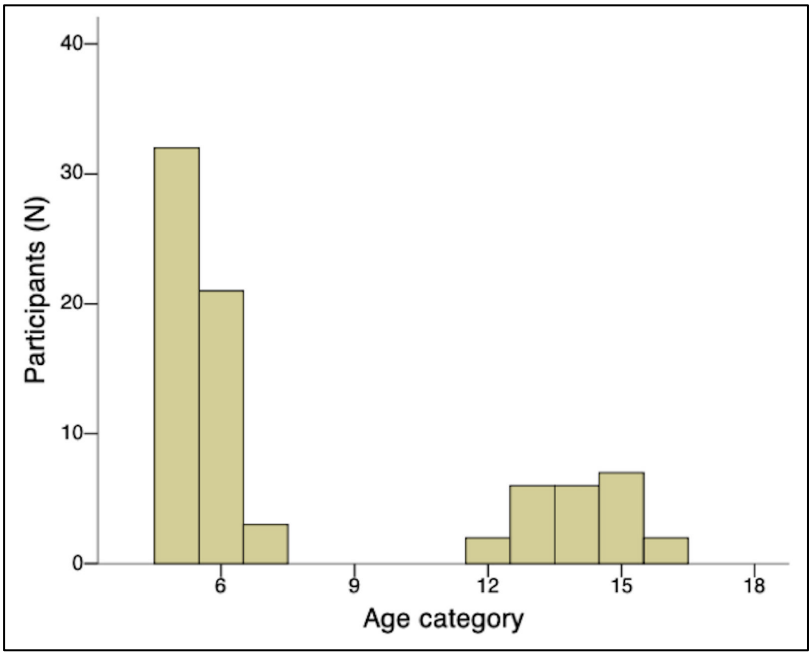

Figure 8: Distribution of the participants of the whole population study according to their age category. It is possible to note the bimodal distribution of the population. [Porcu et al., 2021b].

We further divided the whole population in two subgroups: the young subgroup (total population = 56 participants; gender composition = 36 males and 20 females; age categories = 5-7; median age category value = 6) and the elderly subgroup (total population = 23 participants; gender composition = 10 males and 13 females; age categories = 12-16; median age category value = 14).

The nonparametric Levene's test for equality of variance did not demonstrate a statistically significant different variance in gFA distribution between males and females in the whole population (p = 0.216), in the young subgroup (p = 0.107), and in the elderly subgroup (p = 0.839); the subsequent Mann-Whitney U tests did not show statistically significant differences in gFA mean ranks values between males and females in the whole population (p = 0.229), in the young subgroup (p = 0.798) and in the elderly subgroup (p = 0.951).

2.7.5. Results: rs-fMRI

Analysis A (fALFF analysis with TFCE statistics) identified a single cluster of voxels of increased regional neural activity related to gFA; this cluster consisted of 94117 voxels and 1167 (peak p-FWE < 0.00001; peak p-unc < 0.00001; peak p-FDR < 0.00001), and it covered the brain almost ubiquitously in both in cortical and subcortical regions. No other clusters were identified, in particular, we did not detect any cluster of reduced regional neural activity. The statistical data are reported in Table 18, the results are graphically shown in Figure 9.

Analysis A (fALFF analysis - TFCE statistics)						
Cluster (x,y,z)	*Cluster size (number of voxels)*	*peaks*	*TFCE*	*peak p-FWE*	*peak p-FDR*	*peak p-unc*
+58 +20 + 02	94117	1167	3577.68	< 0.00001	< 0.00001	< 0.00001
Voxels identified and relative brain areas						
• 5792 voxels (6%) covering 72% of atlas.FP r (Frontal Pole Right) • 3561 voxels (4%) covering 51% of atlas.FP l (Frontal Pole Left) • 2600 voxels (3%) covering 46% of atlas.Precuneous (Precuneous Cortex) • 2494 voxels (3%) covering 57% of atlas.PreCG l (Precentral Gyrus Left) • 2211 voxels (2%) covering 46% of atlas.sLOC r (Lateral Occipital Cortex, superior division Right) • 2208 voxels (2%) covering 52% of atlas.PreCG r (Precentral Gyrus Right) • 2204 voxels (2%) covering 88% of atlas.OP r (Occipital Pole Right) • 1969 voxels (2%) covering 75% of atlas.OP l (Occipital Pole Left) • 1802 voxels (2%) covering 69% of atlas.AC (Cingulate Gyrus, anterior division) • 1794 voxels (2%) covering 49% of atlas.PostCG l (Postcentral Gyrus Left) • 1783 voxels (2%) covering 36% of atlas.sLOC l (Lateral Occipital Cortex, superior division Left) • 1754 voxels (2%) covering 54% of atlas.PostCG r (Postcentral Gyrus Right) • 1651 voxels (2%) covering 62% of atlas.SFG r (Superior Frontal Gyrus Right) • 1419 voxels (2%) covering 52% of atlas.MidFG r (Middle Frontal Gyrus Right) • 1252 voxels (1%) covering 44% of atlas.SFG l (Superior Frontal Gyrus Left) • 1172 voxels (1%) covering 86% of atlas.PaCiG r (Paracingulate Gyrus Right) • 1091 voxels (1%) covering 57% of atlas.Cereb2 l (Cerebelum Crus2 Left) • 1087 voxels (1%) covering 48% of atlas.Cereb8 r (Cerebelum 8 Right) • 1060 voxels (1%) covering 44% of atlas.PC (Cingulate Gyrus, posterior division) • 1059 voxels (1%) covering 52% of atlas.iLOC l (Lateral Occipital Cortex, inferior division Left) • 1054 voxels (1%) covering 52% of atlas.iLOC r (Lateral Occipital Cortex, inferior division Right) • 1008 voxels (1%) covering 47% of atlas.Cereb2 r (Cerebelum Crus2 Right) • 52092 voxels (55%) covering other brain areas						

Table 18: Results of analysis A (fALFF with TFCE statistics). fALFF = fractional amplitude of low frequency fluctuations; TFCE = ; threshold free cluster enhancement; p-FWE = family wise error corrected p-value; p-FDR = p-value corrected for false discovery rate; p-unc = p-value uncorrected.

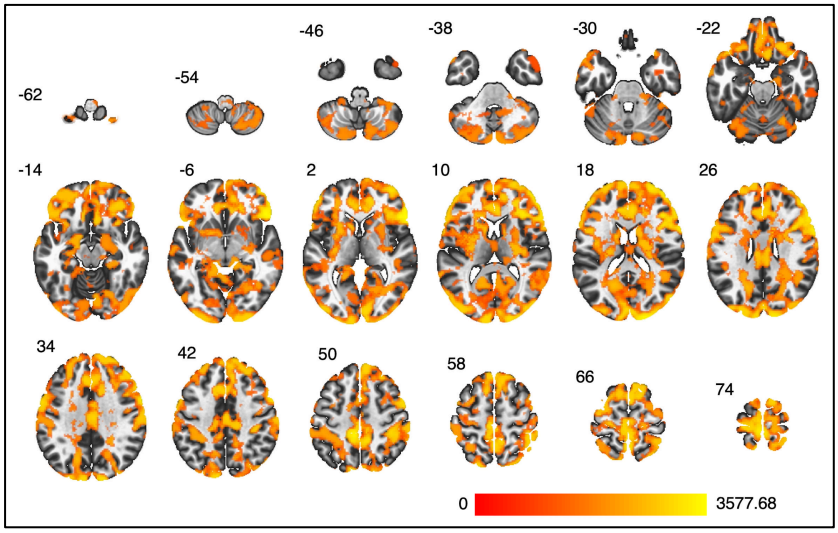

Figure 9: Results of analysis A (fALFF – TFCE statistics); results are showed on axial view with TFCE colorimetric scale. [Porcu et al., 2021b].

Analysis B (seed-based analysis with TFCE statistics) identified 7 clusters of increased connectivity related to gFA (TFCE comprised between 79.06 and 183.17; degrees of freedom = 77), in particular the regions of the limbic system (hippocampal cortex and amygdala of both sides), the basal ganglia, the cerebellum (cerebellar lobules 4, 5 and 6), the cuneal cortex and several areas of the temporal and occipital cortex. No clusters of reduced connectivity were found. The biggest cluster consisted of 56 connections. The statistical data are reported in Table 19, and the resuming connectogram is reported in Figure 10.

Analysis B (Seed-based analysis – TFCE statistics)					
Analysis Unit	*Number of connections*	*Statistic*	*p-unc*	*p-FDR*	*p-FWE*
Cluster 1/7	56	TFCE = 183.17	< 0.00001	< 0.00001	< 0.00001
Cluster 2/7	2	TFCE = 88.43	0.000124	0.025200	0.026000
Cluster 3/7	2	TFCE = 87.46	0.000134	0.025200	0.030000
Cluster 4/7	7	TFCE = 83.17	0.000185	0.025200	0.040000
Cluster 5/7	1	TFCE = 82.48	0.000189	0.025200	0.041000
Cluster 6/7	7	TFCE = 79.56	0.000228	0.025200	0.046000
Cluster 7/7	2	TFCE = 79.06	0.000240	0.025200	0.050000

Table 19: Results of analysis B (Seed-based analysis -TFCE statistics). ROI-to-ROI = region of interest to region of interest; TFCE = threshold free cluster enhancement; p-FWE = family wise error corrected p-value; p-FDR = p-value corrected for false discovery rate; p-unc = p-value uncorrected.

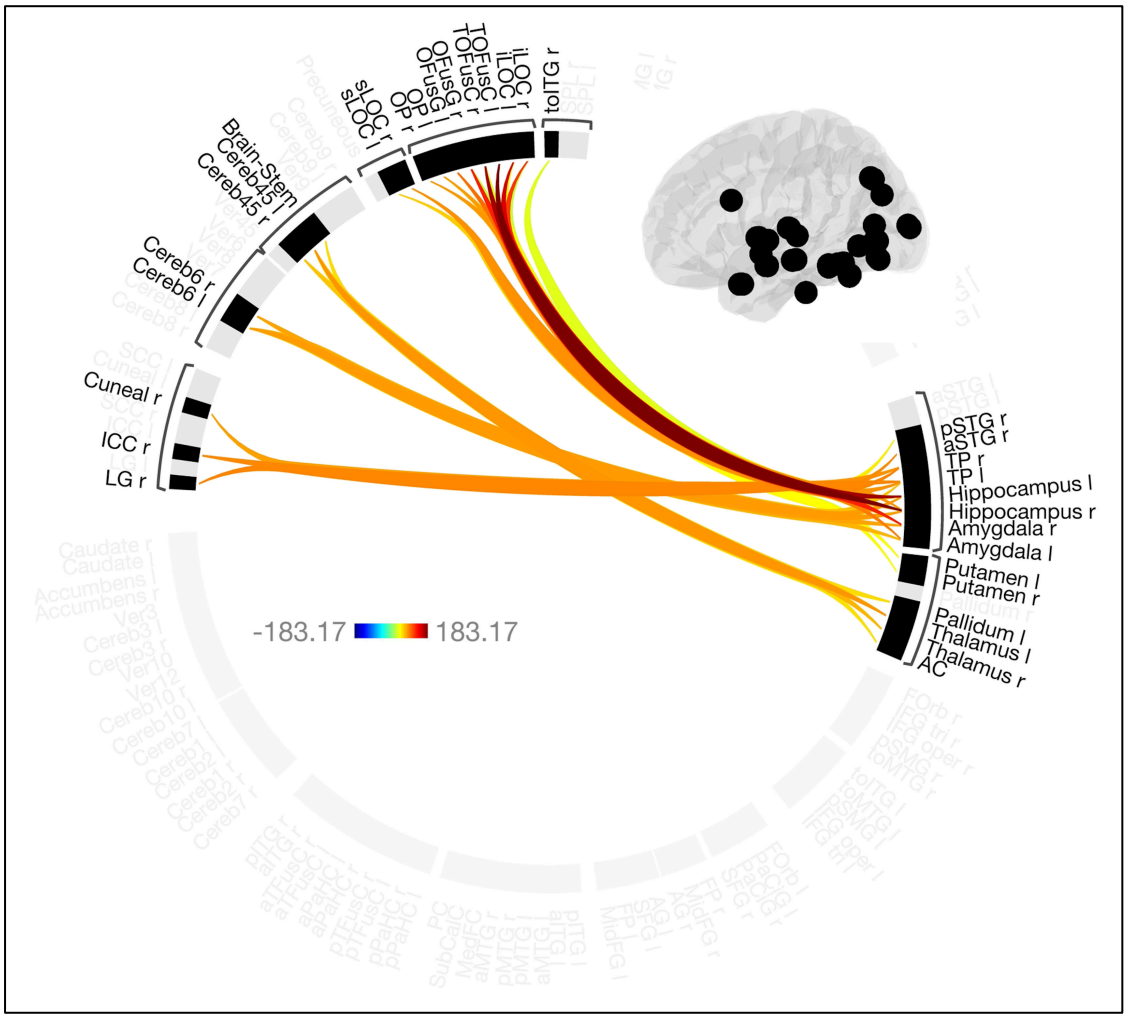

Figure 10: Resuming connectogram of the results of Analysis B (ROI-to-ROI analysis – TFCE) with TFCE colorimetric scale (upper right corner). l = left; r = right; LG = Lingual gyrus; ICC= Intracalcarine cortex; Cereb45 = Cerebellar lobules 4 and 5; Cereb6 = Cerebellar lobule 6;; sLOC = Lateral occipital cortex, superior division; OP = Occipital cortex; OFusG = Occipital fusiform gyrus; TOFusC = Temporal occipital fusiform cortex; iLOC = Lateral occipital cortex, inferior division; toITG = Inferior Temporal Gyrus, temporooccipital part; pSTG = Superior temporal gyrus, posterior division; aSTG = Superior temporal gyrus, anterior division; TP = Temporal pole; AC = Cingulate gyrus, anterior division. [Porcu et al., 2021b].

Analysis C (graph analysis) revealed various statistically significant changes of several properties of the ROIs of the network in relation to gFA values (p-FDR < 0.05; degrees of freedom = 77). In particular, global efficiency resulted increase in 9 ROIs (posterior division of right and left parahippocampal gyrus, a posterior division of right and left temporal fusiform cortex, both the amygdalae, vermis 6, and cerebellar 4th and 5th lobules). The clustering coefficient was reduced in the anterior division of the right superior temporal gyrus. Finally, betweenness centrality resulted reduced in vermis 1 and 2. Regarding degree and cost, we observed reduced values of these two properties in

the left frontal pole and right superior parietal lobule and increased values in both the amygdale and in the posterior division of the right parahippocampal cortex. No statistically significant changes in the average path length were found. The results are reported in Table 20 and in Figure 11.

Analysis C (Graph analysis – TFCE statistics)						
Global efficiency						
ROI	*Coordinates in MNI space x, y, z (mm)*	*beta*	*T*	*dof*	*p-unc*	*p-FDR*
Network	-	0.39	2.57	77	0.012207	-
pPaHC l (Parahippocampal gyrus, posterior division left)	-22, -32, -17	1.96	4.32	77	0.000047	0.002704
pPaHC r (Parahippocampal gyrus, posterior division right)	23, -31, -17	2.04	4.27	77	0.000055	0.002704
Ver6 (Vermis 6)	1, -66, -16	2.30	4.22	77	0.000066	0.002704
Amygdala l	-23, -5. -18	1.74	4.16	77	0.000082	0.002704
Amygdala r	23, -4, -18	1.71	3.54	77	0.000679	0.017931
Cereb45 l (Cereb 4 5 left)	-14, -44, -17	2.36	3.48	77	0.000841	0.018497
aITG l (Inferior temporal gyrus, anterior division left)	-48, -5, -39	2.17	3.38	77	0.001158	0.021837
pTFusC r (Temporal fusiform cortex, posterior division right)	36, -24, -28	1.16	3.23	77	0.001830	0.028805
pTFusC l (Temporal fusiform cortex, posterior division left)	-36, -30, -25	1.41	3.21	77	0.001964	0.028805
Local efficiency						
ROI	*Coordinates in MNI space x,y,z (mm)*	*beta*	*T*	*dof*	*p-unc*	*p-FDR*
Network	-	-0.09	-0.53	77	0.596947	-
aSTG r (Superior temporal gyrus, anterior division right)	58, -1, -10	-2.37	-4.14	77	0.000089	0.011713
Betweenness Centrality						
ROI	*Coordinates in MNI space x,y,z (mm)*	*beta*	*T*	*dof*	*p-unc*	*p-FDR*
Network	-	0.00	0.62	77	0.536241	-
Ver12 (Vermis 1 2)	*1, -39, -20*	-0.05	-4.14	77	0.000089	0.011710
Average path length						
ROI	*Coordinates in MNI space x,y,z (mm)*	*beta*	*T*	*dof*	*p-unc*	*p-FDR*
Network	-	-0,43	-0,88	77	0,383990	-
Clustering coefficient						
ROI	*Coordinates in MNI space x,y,z (mm)*	*beta*	*T*	*dof*	*p-unc*	*p-FDR*
Network	-	-0.42	-1.58	77	0.117738	-
aSTG r (Superior temporal gyrus, anterior division right)	*58, -1, -10*	-3.98	-4.79	77	0.000008	0.001061
Degree						

ROI	*Coordinates in MNI space x,y,z (mm)*	*beta*	*T*	*dof*	*p-unc*	*p-FDR*
Network	-	0.00	-0.11	77	0.915683	-
pPaHC r (Parahippocampal gyrus, posterior division right)	23, -31, -17	163.10	3.67	77	0.000439	0.036586
Amygdala l	-23, -5. -18	208.49	3.54	77	0.000687	0.036586
Amygdala r	23, -4, -18	214.31	3.48	77	0.000832	0.036586
SPL r (Superior parietal lobule right)	29, -48, 59	-201.02	-3.31	77	0.001400	0.037362
FP l (Frontal pole left)	-25, 53, 8	-188.81	-3.31	77	0.001415	0.037362
Cost						
ROI	*Coordinates in MNI space x,y,z (mm)*	*beta*	*T*	*dof*	*p-unc*	*p-FDR*
Network	-	0.00	-0.11	77	0.915504	-
pPaHC r (Parahippocampal gyrus, posterior division right)	23, -31, -17	1.25	3.67	77	0.000439	0.036586
Amygdala l	-23, -5. -18	1.59	3.54	77	0.000687	0.036586
Amygdala r	23, -4, -18	1.64	3.48	77	0.000832	0.036586
SPL r (Superior parietal lobule right)	29, -48, 59	-1.53	-3.31	77	0.001400	0.037362
FP l (Frontal pole left)	-25, 53, 8	-1.44	-3.31	77	0.001415	0.037362

Table 20: Results of analysis C (Graph analysis). ROI = region of interest; ROI-to-ROI = region of interest to region of interest; T = T-score; dof = degree of freedom; p-unc = p-value uncorrected; p-FDR = p-value corrected for false discovery rate.

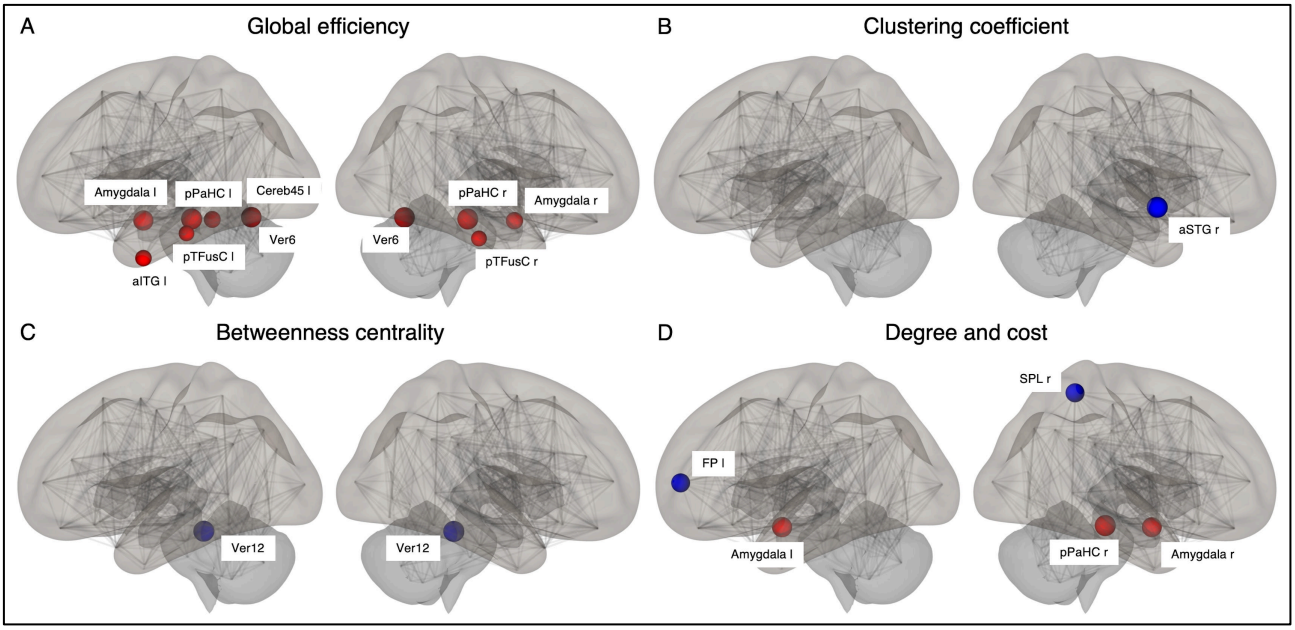

Figure 11: Results of analysis C (Graph analysis): a) global efficiency; b) clustering coefficient; c) betweenness centrality; d) degree and cost. l = left; r = right; pPaHC = Parahippocampal gyrus, posterior division; Cereb45 = Cerebellar lobules 4 and 5; Ver6 = Vermis 6; pTFusC = Temporal fusiform cortex, posterior divison; aITG = Inferior temporal gyrus, anterior division; aSTG = Superior temporal gyrus, anterior division; Ver12 = Vermis 1 and 2; FP = Frontal pole; SPL = Superior parietal lobule. [Porcu et al., 2021b].

2.7.6. Discussion

In the current study, we aimed to evaluate how gFA influences brain activity and brain networks of the whole brain in healthy participants of different ages. We applied strict exclusion criteria in order to avoid biases related by confounding factors, such as smoking or psychiatric diseases.

The first step of the study was focused on the evaluation of the relationships between gFA values, sex, and age. Despite the limited number of participants included in the analyses and the heterogeneity of the study population in terms of age and gender composition, we found no statistical significant differences in mean gFA between males and females, both at a global level and in the young and elderly subgroups. Although several studies identified sex-related regional differences in FA values in various WM tracts [van Hemmen J et al., 2017], our findings at a global level are in line with other studies. *Hsu et al.* [Hsu et al., 2008] demonstrated no differences in gFA between males and females. However, we found an inverse correlation between age and gFA. This finding is in agreement with the literature [Hsu et al., 2008; Wassenaar et al., 2019]. The inverse correlation was not absolute but moderate can be related with other factors besides aging, that are associated with the degree of myelination [Wassenaar et al., 2019], such as the body mass index [Bennett et al., 2017].

Regarding the fMRI analysis, it is noted from the literature that the fMRI field of research suffers of an intrinsic limit of reproducibility due to the great analytical approach variability, as well demonstrated for example by the recent research conducted by *Botvinik-Nezer R et al.* [Botvinik-Nezer R et al., 2020]. Every technique of fMRI analysis has its pros and cons, and a single standard method of analysis has still not been identified [Lv et al., 2018]. The choice of the analytical approach for this research was driven in particular by its exploratory nature; for this reason, we opted for an approachable to give information about brain activity and networking that could be easy to be computed and interpreted. In particular, we adopted a functional segregation approach for the analysis of the activity of specific cerebral region by using the fALFF technique, and a functional segregation approach for the analysis of the relationships between the cerebral regions by using the ROI-to-ROI technique with an a priori definition of the ROI [Lv et al., 2018]. The advantage of the fALFF

approach lies in its simplicity of analysis in absence of an underlying hypothesis [Lv et al., 2018] and its specificity for grey matter activity [Zou et al., 2008]. Looking at the functional integration approach, it is note that the ROI-to-ROI approach requires a priori definition of the ROI, and that the results of the analysis depend on the selection of the seeds, making it vulnerable to biases [Lv et al., 2018]. A data-driven approach like the independent component analysis (ICA) does not suffer from the limitations derived by the a priori definition of the ROI, but it has other important disadvantages such as the fact that ICA presents network one by one and it is unable to show interconnections between different brain networks [Bertolero et al., 2015; Lv et al., 2018]; for this reason, we finally opted for the ROI-to-ROI technique, exploiting atlases already extensively used in research for the definition of the ROI [Tzourio-Mazoyer et al., 2002; Desikan et al., 2006]

The results of Analysis A (fALFF) evidenced that the neural activity was increased in patients with higher gFA, included different areas of the M-FPN, the primary sensor and motor regions, and several areas of the cerebellum. A possible interpretation of these findings is that a better degree of global myelination may improve the transmission of the neural impulse throughout the brain, resulting in a diffuse activation of brain areas. This is seen for example in areas of the M-FPN (in particular of precuneus, both the frontal poles). M-FPN is one of the most studied brain networks, and notes its role in cognition and self-generated thoughts [Axelrod et al., 2017]; our findings are in line with those of two previous combined DTI-fMRI studies [Teipel et al., 2010; Yang et al., 2016]. They demonstrated that loss of WM integrity is associated with a reduction of the activity of several hubs of M-FPN. The increased activation of primary motor and sensory areas in the precentral and postcentral gyrus has been reported previously, suggesting that higher gFA values lead to better transmission of information to and from these regions [Warbrick et al., 2017].

In the seed-based analyses, several areas showed increased activation synchronicity across the whole brain, involving particular areas of the limbic system (both the hippocampi and amygdala), the basal ganglia, the cuneal cortex and several areas of the temporal and occipital cortex. Further, no statistically significant patterns of decreased synchronicity were found. Additionally, gFA values

influenced the properties of several nodes of the network; the majority of these findings involved structures of the limbic areas. In fact, increased global efficiency correlated with increased gFA values in the amygdalae, posterior division of the parahippocampal cortex of both sides, and in cerebellum (left fourth and fifth lobules and vermis 6), as well as in the temporal lobes (the posterior division of the temporal fusiform cortex of both hemispheres and the anterior division of the left inferior temporal gyrus). Both the amygdalae and the right posterior division of parahippocampal cortex also showed increased degree and cost in relation to increased values of gFA, whereas the left frontal pole and the right superior parietal lobule (areas not comprised in the limbic system) showed reduced cost and degree. Finally, the increase of gFA was associated with a reduction of the clustering coefficient of the anterior division of the right superior temporal gyrus, and reduced betweenness centrality of the cerebellar vermis 1 and 2.

Although a precise interpretation of the findings is hard due to the complex interactions that exist between the different areas of the brain, these findings evidence how the gFA may influence the activity of the limbic system and its relationships with the other cerebral and cerebellar areas. The limbic system is a complex anatomical and functional structure implied in the process of sensory inputs from the internal and external environment for determining motor autonomic, emotional and cognitive responses for self-preservation and survival through memory and motivation [McLachlan, 2009]. Due to these properties, the limbic system interact with different areas of the brain, included the temporal cortex (important in particular for visual memory, verbal function, and hearing [Patel et al., 2020]) and occipital cortex (important in particular for visual function [Rehman et al., 2020]). Further, it is noteworthy to observe how the activity of several cerebellar areas are influenced by gFA, as seen for as well as the interactions of the cerebellum with the structures of the limbic system; however, this is not surprisingly according to the recent definition of the cerebellum-hippocampal network, a polysynaptic network involved in spatial and temporal processing [Weaver, 2005; Yu et al., 2015].

We speculate that impairments of the normal functioning of the limbic system could at least partly explain the neurological impairments observed in aging, according to the fact the limbic system structures are among the more sensible to the WM damage than in healthy participants. The degeneration of WM, characterized also by reduction of myelination of the WM, could disrupt the intrinsic functioning of the limbic system and of the interactions between the limbic system and the surrounding structure of the brain. This hypothesis is also sustained by the absence of negative correlations found in both Analyses A and B, suggesting that WM integrity is crucial in preserving the neural activity of intercommunication of the different cerebral regions.

2.7.7. Limits

This study has limitations merit to comment. The sample size is small, despite we opted to significantly reduce the number in order to limit biases resulting from several serious confounding factors; further, we did not correlate these findings with cognitive status and education. However, our study was designed as exploratory, and it was focused on structural and functional data. The analysis of the effects of gFA values on the neurocognitive sphere was beyond the goal of our investigation. The results of our research, of course, will need to be confirmed within future studies with bigger populations, but at the same time they could be useful food for thoughts for further analyses of the complex relationships between white matter integrity and higher neurological functions.

3. General considerations and conclusion

The findings of our studies could help to better understand how the aging-associated degenerative changes of the white matter affect brain activity and cognitive performances.

Regarding the first study [Porcu et al. 2021a] we demonstrated that the increase in tWMHb is associated with impairments in neurocognitive function and a reduction of the neural activity of several cortical supratentorial and infratentorial areas, cerebellum included. The validity of our results is mainly sustained by the strict exclusion criteria applied for the study population selection, by the fact that age and sex were included as confounding factors in the study model, and by the fact that similar results were obtained by using three different statistical analysis methods. Of course, the small population study remain the main limit of our study.

Regarding the second study [Porcu et al. 2020a], we demonstrated that the location of WMH differently affects cerebral networking. In particular we demonstrated a statistically significant inverse correlation between dWMHb and tHRV, and we further demonstrated that dWMHb significantly alter the network properties of several areas limbic structures, hippocampus included. On the contrary, no statistically significant effects found for what concern jcWMH and pvWMH. According to these results, we speculate that brain is able to compensate the effects of jcWMH pvWMH, whereas these compensatory mechanisms are not able to compensate the effects of dWMH, deeply altering the network architecture of the limbic system. However, the very small population study (38 subjects) and the absence of a correlation analysis with the neurocognitive tests represent the major limits of this study.

In the third study [Porcu et al. 2021b] we analyzed the effect of a quantitative parameter of WMH degeneration, the gFA, on both the neural activity and brain networking. We opted for gFA because it is relatively easy to calculate and because it gives information on the microstructural status of WM, in particular about the myelination status of WM. We found that higher gFA values, indicating better myelination status, is associated with increased activity of several cerebral areas; by looking at the distribution of these areas, it is interesting to observe a substantial overlap between these areas and those found in the first study [Porcu et al. 2021a]. Further, we observed that a better

myelination status is associated with higher connectivity between several cerebral areas, in particular within the limbic system, and when the graph theory was applied to the results several nodes of the limbic system showed better global efficiency values as reflection of a better ability of these nodes to exchange information at a global level. Also in this case, in analogy to the second study [Porcu et al. 2020a], the small number of subjects included in the study population and the absence of a correlation analysis with the neurocognitive tests represent the major limits of this study.

By trying to give an holistic interpretation of the results of our studies, it is interesting to note that they tend to confirm the so called "disconnection hypothesis" [O'Sullivan et al., 2001; Salat, 2011; Bennett et al., 2014; Filley et al., 2016]. In our opinion, the most interesting data in this sense is the substantial overlap of the results of the first [Porcu et al. 2021a] and the third study [Porcu et al. 2021b] regarding the effects of WMH and gFA on regional neural activity measured with the fALFF technique, despite the fact that these studies differed in terms of study population according to the different exclusion criteria adopted. In our opinion this result can be considered as a proof about the validity of our studies and it clearly proves that WM degeneration is associated with a generalized reduction of neural activity of the brain. Secondly, it is reasonable to speculate that this finding represents another proof that demonstrates that WMH and gFA are strictly interconnected one to each other and that these two markers represent different expressions of the same degenerative process of the WM. For what concern the effects on brain networking, the results are less easily interpretable, due to the heterogeneity of analysis; however, it is clear that the localization of WMH influences differently brain networking, and that WM degeneration mainly affect the activity of the limbic system, with reflections also in the volume of anatomic structures, such as the hippocampus.

Of course it is important to underline that the studies realized in the PhD project were designed as explorative and not confirmative, although they were based on clear evidences derived from literature. Even if further studies with bigger study populations will help to better clarified the validity of our findings, these results can represent a useful starting point for better understand other aspects of the effects of WM degeneration on brain circuits in healthy aging, such as for example the

compensatory mechanisms activated by brain in order as a response to WM degeneration, and the contribution of WM degeneration in other pathological conditions, included degenerative conditions such as Alzheimer disease and vascular dementia.

4. Literature

- Abbott, N. J., Patabendige, A. A., Dolman, D. E., Yusof, S. R., & Begley, D. J. (2010). Structure and function of the blood-brain barrier. Neurobiology of disease, 37(1), 13–25. https://doi.org/10.1016/j.nbd.2009.07.030
- Abrahams, S., Pickering, A., Polkey, C. E., & Morris, R. G. (1997). Spatial memory deficits in patients with unilateral damage to the right hippocampal formation. Neuropsychologia, 35(1), 11–24. https://doi.org/10.1016/s0028-3932(96)00051-6
- Abutalebi, J., Della Rosa, P. A., Gonzaga, A. K., Keim, R., Costa, A., & Perani, D. (2013). The role of the left putamen in multilingual language production. Brain and language, 125(3), 307–315. https://doi.org/10.1016/j.bandl.2012.03.009
- Achard, S., & Bullmore, E. (2007). Efficiency and cost of economical brain functional networks. PLoS computational biology, 3(2), e17. https://doi.org/10.1371/journal.pcbi.0030017
- Alber, J., Alladi, S., Bae, H. J., Barton, D. A., Beckett, L. A., Bell, J. M., Berman, S. E., Biessels, G. J., Black, S. E., Bos, I., Bowman, G. L., Brai, E., Brickman, A. M., Callahan, B. L., Corriveau, R. A., Fossati, S., Gottesman, R. F., Gustafson, D. R., Hachinski, V., Hayden, K. M., … Hainsworth, A. H. (2019). White matter hyperintensities in vascular contributions to cognitive impairment and dementia (VCID): Knowledge gaps and opportunities. Alzheimer's & dementia (New York, N. Y.), 5, 107–117. https://doi.org/10.1016/j.trci.2019.02.001
- Alexander-Bloch, A., Giedd, J. N., & Bullmore, E. (2013). Imaging structural co-variance between human brain regions. Nature reviews. Neuroscience, 14(5), 322–336. https://doi.org/10.1038/nrn3465
- Aminoff, E. M., Kveraga, K., & Bar, M. (2013). The role of the parahippocampal cortex in cognition. Trends in cognitive sciences, 17(8), 379–390. https://doi.org/10.1016/j.tics.2013.06.009
- Antonenko, D., & Flöel, A. (2014). Healthy aging by staying selectively connected: a mini-review. Gerontology, 60(1), 3–9. https://doi.org/10.1159/000354376
- Assaf, Y., & Pasternak, O. (2008). Diffusion tensor imaging (DTI)-based white matter mapping in brain research: a review. Journal of molecular neuroscience : MN, 34(1), 51–61. https://doi.org/10.1007/s12031-007-0029-0
- Axelrod V, Rees G, Bar M (2017) The default network and the combination of cognitive processes that mediate self-generated thought. Nat Hum Behav 1:896-910. https://doi.org/10.1038/s41562-017-0244-9
- Babayan, A., Erbey, M., Kumral, D., Reinelt, J. D., Reiter, A., Röbbig, J., Schaare, H. L., Uhlig, M., Anwander, A., Bazin, P. L., Horstmann, A., Lampe, L., Nikulin, V. V., Okon-Singer, H., Preusser, S., Pampel, A., Rohr, C. S., Sacher, J., Thöne-Otto, A., Trapp, S., … Villringer, A. (2019). A mind-brain-body dataset of MRI, EEG, cognition, emotion, and peripheral physiology in young and old adults. Scientific data, 6, 180308. https://doi.org/10.1038/sdata.2018.308
- Balsters, J. H., Whelan, C. D., Robertson, I. H., & Ramnani, N. (2013). Cerebellum and cognition: evidence for the encoding of higher order rules. Cerebral cortex (New York, N.Y. : 1991), 23(6), 1433–1443. https://doi.org/10.1093/cercor/bhs127
- Barabási, A. L., Gulbahce, N., & Loscalzo, J. (2011). Network medicine: a network-based approach to human disease. Nature reviews. Genetics, 12(1), 56–68. https://doi.org/10.1038/nrg2918
- Basser, P. J., & Pierpaoli, C. (1996). Microstructural and physiological features of tissues elucidated by quantitative-diffusion-tensor MRI. Journal of magnetic resonance. Series B, 111(3), 209–219. https://doi.org/10.1006/jmrb.1996.0086
- Bassett, D. S., & Sporns, O. (2017). Network neuroscience. Nature neuroscience, 20(3), 353–364. https://doi.org/10.1038/nn.4502
- Bassett, D. S., Zurn, P., & Gold, J. I. (2018). On the nature and use of models in network neuroscience. Nature reviews. Neuroscience, 19(9), 566–578. https://doi.org/10.1038/s41583-018-0038-8
- Bauer, C. E., Zachariou, V., Seago, E., & Gold, B. T. (2021). White Matter Hyperintensity Volume and Location: Associations With WM Microstructure, Brain Iron, and Cerebral Perfusion. Frontiers in aging neuroscience, 13, 617947. https://doi.org/10.3389/fnagi.2021.617947
- Benagiano, V., Rizzi, A., Lorusso, L., Flace, P., Saccia, M., Cagiano, R., Ribatti, D., Roncali, L., & Ambrosi, G. (2018). The functional anatomy of the cerebrocerebellar circuit: A review and new concepts. The Journal of comparative neurology, 526(5), 769–789. https://doi.org/10.1002/cne.24361
- Bennett, I. J., & Madden, D. J. (2014). Disconnected aging: cerebral white matter integrity and age-related differences in cognition. Neuroscience, 276, 187–205. https://doi.org/10.1016/j.neuroscience.2013.11.026
- Bennett IJ, Greenia DE, Maillard P, Sajjadi SA, DeCarli C, Corrada MM, Kawas CH (2017) Age-related white matter integrity differences in oldest-old without dementia. Neurobiol Aging 56:108-114. https://doi.org/10.1016/j.neurobiolaging.2017.04.013
- Benson, G., Hildebrandt, A., Lange, C., Schwarz, C., Köbe, T., Sommer, W., Flöel, A., & Wirth, M. (2018). Functional connectivity in cognitive control networks mitigates the impact of white matter lesions in the elderly. Alzheimer's research & therapy, 10(1), 109. https://doi.org/10.1186/s13195-018-0434-3
- Bergamino M, Keeling EG, Mishra VR, Stokes AM, Walsh RR (2020) Assessing White Matter Pathology in Early-Stage Parkinson Disease Using Diffusion MRI: A Systematic Review. Front Neurol 11:314. https://doi.org/10.3389/fneur.2020.00314
- Bertolero, M. A., Yeo, B. T., & D'Esposito, M. (2015). The modular and integrative functional architecture of the human brain. Proceedings of the National Academy of Sciences of the United States of America, 112(49), E6798–E6807. https://doi.org/10.1073/pnas.1510619112
- Biswal, B., Yetkin, F. Z., Haughton, V. M., & Hyde, J. S. (1995). Functional connectivity in the motor cortex of resting human brain using echo-planar MRI. Magnetic resonance in medicine, 34(4), 537–541. https://doi.org/10.1002/mrm.1910340409
- Bird, C. M., & Burgess, N. (2008). The hippocampus and memory: insights from spatial processing. Nature reviews. Neuroscience, 9(3), 182–194. https://doi.org/10.1038/nrn2335
- Bolandzadeh, N., Davis, J. C., Tam, R., Handy, T. C., & Liu-Ambrose, T. (2012). The association between cognitive function and white matter lesion location in older adults: a systematic review. BMC neurology, 12, 126. https://doi.org/10.1186/1471-2377-12-126
- Boutzoukas, E. M., O'Shea, A., Albizu, A., Evangelista, N. D., Hausman, H. K., Kraft, J. N., Van Etten, E. J., Bharadwaj, P. K., Smith, S. G., Song, H., Porges, E. C., Hishaw, A., DeKosky, S. T., Wu, S. S., Marsiske, M., Alexander, G. E., Cohen, R., & Woods, A. J. (2021). Frontal White Matter Hyperintensities and Executive Functioning Performance in Older Adults. Frontiers in aging neuroscience, 13, 672535. https://doi.org/10.3389/fnagi.2021.672535
- Botvinik-Nezer, R., Holzmeister, F., Camerer, C. F., Dreber, A., Huber, J., Johannesson, M., Kirchler, M., Iwanir, R., Mumford, J. A., Adcock, R. A., Avesani, P., Baczkowski, B. M., Bajracharya, A., Bakst, L., Ball, S., Barilari, M., Bault, N., Beaton, D.,

Beitner, J., Benoit, R. G., … Schonberg, T. (2020). Variability in the analysis of a single neuroimaging dataset by many teams. Nature, 582(7810), 84–88. https://doi.org/10.1038/s41586-020-2314-9

- Bowie, C. R., & Harvey, P. D. (2006). Administration and interpretation of the Trail Making Test. Nature protocols, 1(5), 2277–2281. https://doi.org/10.1038/nprot.2006.390
- Braem, S., De Houwer, J., Demanet, J., Yuen, K., Kalisch, R., & Brass, M. (2017). Pattern Analyses Reveal Separate Experience-Based Fear Memories in the Human Right Amygdala. The Journal of neuroscience : the official journal of the Society for Neuroscience, 37(34), 8116–8130. https://doi.org/10.1523/JNEUROSCI.0908-17.2017
- Brickman, A. M., Muraskin, J., & Zimmerman, M. E. (2009). Structural neuroimaging in Altheimer's disease: do white matter hyperintensities matter?. Dialogues in clinical neuroscience, 11(2), 181–190.
- Brickman, A. M., Provenzano, F. A., Muraskin, J., Manly, J. J., Blum, S., Apa, Z., Stern, Y., Brown, T. R., Luchsinger, J. A., & Mayeux, R. (2012). Regional white matter hyperintensity volume, not hippocampal atrophy, predicts incident Alzheimer disease in the community. Archives of neurology, 69(12), 1621–1627. https://doi.org/10.1001/archneurol.2012.1527
- Brown, W. R., Moody, D. M., Challa, V. R., Thore, C. R., & Anstrom, J. A. (2002). Venous collagenosis and arteriolar tortuosity in leukoaraiosis. Journal of the neurological sciences, 203-204, 159–163. https://doi.org/10.1016/s0022-510x(02)00283-6
- Bullmore, E. T., Suckling, J., Overmeyer, S., Rabe-Hesketh, S., Taylor, E., & Brammer, M. J. (1999). Global, voxel, and cluster tests, by theory and permutation, for a difference between two groups of structural MR images of the brain. IEEE transactions on medical imaging, 18(1), 32–42. https://doi.org/10.1109/42.750253
- Bullmore, E., & Sporns, O. (2009). Complex brain networks: graph theoretical analysis of structural and functional systems. Nature reviews. Neuroscience, 10(3), 186–198. https://doi.org/10.1038/nrn2575
- Buzsáki G. (1996). The hippocampo-neocortical dialogue. Cerebral cortex (New York, N.Y. : 1991), 6(2), 81–92. https://doi.org/10.1093/cercor/6.2.81
- Buzsáki, G., Buhl, D. L., Harris, K. D., Csicsvari, J., Czéh, B., & Morozov, A. (2003). Hippocampal network patterns of activity in the mouse. Neuroscience, 116(1), 201–211. https://doi.org/10.1016/s0306-4522(02)00669-3
- Caligiuri, M. E., Perrotta, P., Augimeri, A., Rocca, F., Quattrone, A., & Cherubini, A. (2015). Automatic Detection of White Matter Hyperintensities in Healthy Aging and Pathology Using Magnetic Resonance Imaging: A Review. Neuroinformatics, 13(3), 261–276. https://doi.org/10.1007/s12021-015-9260-y
- Campisi J. (2003). Cellular senescence and apoptosis: how cellular responses might influence aging phenotypes. Experimental gerontology, 38(1-2), 5–11. https://doi.org/10.1016/s0531-5565(02)00152-3
- Caserta, M. T., Bannon, Y., Fernandez, F., Giunta, B., Schoenberg, M. R., & Tan, J. (2009). Normal brain aging clinical, immunological, neuropsychological, and neuroimaging features. International review of neurobiology, 84, 1–19. https://doi.org/10.1016/S0074-7742(09)00401-2
- Chang, E. H., Argyelan, M., Aggarwal, M., Chandon, T. S., Karlsgodt, K. H., Mori, S., & Malhotra, A. K. (2017). The role of myelination in measures of white matter integrity: Combination of diffusion tensor imaging and two-photon microscopy of CLARITY intact brains. NeuroImage, 147, 253–261. https://doi.org/10.1016/j.neuroimage.2016.11.068
- Chavda, R., Cao, J. S., & Benge, J. F. (2019). Neuropsychological impact of white matter hyperintensities in older adults without dementia. Applied neuropsychology. Adult, 1–9. Advance online publication. https://doi.org/10.1080/23279095.2019.1633536
- Chen, Y., Wang, X., Guan, L., & Wang, Y. (2021). Role of White Matter Hyperintensities and Related Risk Factors in Vascular Cognitive Impairment: A Review. Biomolecules, 11(8), 1102. https://doi.org/10.3390/biom11081102
- Chutinet, A., & Rost, N. S. (2014). White matter disease as a biomarker for long-term cerebrovascular disease and dementia. Current treatment options in cardiovascular medicine, 16(3), 292. https://doi.org/10.1007/s11936-013-0292-z
- Clemente, D., Ortega, M. C., Melero-Jerez, C., & de Castro, F. (2013). The effect of glia-glia interactions on oligodendrocyte precursor cell biology during development and in demyelinating diseases. Frontiers in cellular neuroscience, 7, 268. https://doi.org/10.3389/fncel.2013.00268
- Coelho, A., Fernandes, H. M., Magalhães, R., Moreira, P. S., Marques, P., Soares, J. M., Amorim, L., Portugal-Nunes, C., Castanho, T., Santos, N. C., & Sousa, N. (2021). Signatures of white-matter microstructure degradation during aging and its association with cognitive status. Scientific reports, 11(1), 4517. https://doi.org/10.1038/s41598-021-83983-7
- Cole, D. M., Smith, S. M., & Beckmann, C. F. (2010). Advances and pitfalls in the analysis and interpretation of resting-state FMRI data. Frontiers in systems neuroscience, 4, 8. https://doi.org/10.3389/fnsys.2010.00008
- Collins, D. L., Neelin, P., Peters, T. M., & Evans, A. C. (1994). Automatic 3D intersubject registration of MR volumetric data in standardized Talairach space. Journal of computer assisted tomography, 18(2), 192–205.
- Corbetta, M., & Shulman, G. L. (2002). Control of goal-directed and stimulus-driven attention in the brain. Nature reviews. Neuroscience, 3(3), 201–215. https://doi.org/10.1038/nrn755
- Corrigan, J. D., & Hinkeldey, N. S. (1987). Relationships between parts A and B of the Trail Making Test. Journal of clinical psychology, 43(4), 402–409. https://doi.org/10.1002/1097-4679(198707)43:4<402::aid-jclp2270430411>3.0.co;2-e
- Coupé P, Tourdias T, Linck P, Romero JE, Manjón JV. LesionBrain: An Online Tool for White Matter Lesion Segmentation. Patched-Based Techniques in Medical Imaging - 4th International Workshop, Patch-MI 2018, Held in Conjunction with MICCAI 2018, Granada, Spain, September 20, 2018, Proceedings; September 2018. https://doi.org/10.1007/978-3-030-00500-9_11
- Cramer D, Howitt DL (2004) The SAGE Dictionary of Statistics: A Practical Resource for Students in Social Sciences. London: SAGE Publications Ltd. https://doi.org/10.4135/9780857020123
- Csiszar, A., Labinskyy, N., Orosz, Z., Xiangmin, Z., Buffenstein, R., & Ungvari, Z. (2007). Vascular aging in the longest-living rodent, the naked mole rat. American journal of physiology. Heart and circulatory physiology, 293(2), H919–H927. https://doi.org/10.1152/ajpheart.01287.2006
- d'Arbeloff, T., Elliott, M. L., Knodt, A. R., Melzer, T. R., Keenan, R., Ireland, D., Ramrakha, S., Poulton, R., Anderson, T., Caspi, A., Moffitt, T. E., & Hariri, A. R. (2019). White matter hyperintensities are common in midlife and already associated with cognitive decline. Brain communications, 1(1), fcz041. https://doi.org/10.1093/braincomms/fcz041

- Dalong, G., Jiyuan, L., Ying, Z., Lei, Z., Yanhong, H., & Yongcong, S. (2020). Transcranial direct current stimulation reconstructs diminished thalamocortical connectivity during prolonged resting wakefulness: a resting-state fMRI pilot study. Brain imaging and behavior, 14(1), 278–288. https://doi.org/10.1007/s11682-018-9979-9
- Damoiseaux, J. S., Rombouts, S. A., Barkhof, F., Scheltens, P., Stam, C. J., Smith, S. M., & Beckmann, C. F. (2006). Consistent resting-state networks across healthy subjects. Proceedings of the National Academy of Sciences of the United States of America, 103(37), 13848–13853. https://doi.org/10.1073/pnas.0601417103
- Dance A. (2015). Neuroscience: Connectomes make the map. Nature, 526(7571), 147–149. https://doi.org/10.1038/526147a
- De Luca, M., Beckmann, C. F., De Stefano, N., Matthews, P. M., & Smith, S. M. (2006). fMRI resting state networks define distinct modes of long-distance interactions in the human brain. NeuroImage, 29(4), 1359–1367. https://doi.org/10.1016/j.neuroimage.2005.08.035
- De Marco, M., Manca, R., Mitolo, M., & Venneri, A. (2017). White Matter Hyperintensity Load Modulates Brain Morphometry and Brain Connectivity in Healthy Adults: A Neuroplastic Mechanism?. Neural plasticity, 2017, 4050536. https://doi.org/10.1155/2017/4050536
- Debette, S., & Markus, H. S. (2010). The clinical importance of white matter hyperintensities on brain magnetic resonance imaging: systematic review and meta-analysis. BMJ (Clinical research ed.), 341, c3666. https://doi.org/10.1136/bmj.c3666
- Desikan, R. S., Ségonne, F., Fischl, B., Quinn, B. T., Dickerson, B. C., Blacker, D., Buckner, R. L., Dale, A. M., Maguire, R. P., Hyman, B. T., Albert, M. S., & Killiany, R. J. (2006). An automated labeling system for subdividing the human cerebral cortex on MRI scans into gyral based regions of interest. NeuroImage, 31(3), 968–980. https://doi.org/10.1016/j.neuroimage.2006.01.021
- Ding, X., Wu, J., Zhou, Z., & Zheng, J. (2015). Specific locations within the white matter and cortex are involved in the cognitive impairments associated with periventricular white matter lesions (PWMLs). Behavioural brain research, 289, 9–18. https://doi.org/10.1016/j.bbr.2015.04.021
- Diniz, D. G., Foro, C. A., Rego, C. M., Gloria, D. A., de Oliveira, F. R., Paes, J. M., de Sousa, A. A., Tokuhashi, T. P., Trindade, L. S., Turiel, M. C., Vasconcelos, E. G., Torres, J. B., Cunnigham, C., Perry, V. H., Vasconcelos, P. F., & Diniz, C. W. (2010). Environmental impoverishment and aging alter object recognition, spatial learning, and dentate gyrus astrocytes. The European journal of neuroscience, 32(3), 509–519. https://doi.org/10.1111/j.1460-9568.2010.07296.x
- Doane D, Seward LE (2011) Measuring Skewness: A Forgotten Statistic? Journal of Statistics Education, 19
- Dufouil, C., de Kersaint-Gilly, A., Besançon, V., Levy, C., Auffray, E., Brunnereau, L., Alpérovitch, A., & Tzourio, C. (2001). Longitudinal study of blood pressure and white matter hyperintensities: the EVA MRI Cohort. Neurology, 56(7), 921–926. https://doi.org/10.1212/wnl.56.7.921
- Eriksen, B.A., Eriksen, C.W. (1974) Effects of noise letters upon the identification of a target letter in a nonsearch task. Perception & Psychophysics 16, 143–149. https://doi.org/10.3758/BF03203267
- Fazekas, F., Kleinert, R., Offenbacher, H., Schmidt, R., Kleinert, G., Payer, F., Radner, H., & Lechner, H. (1993). Pathologic correlates of incidental MRI white matter signal hyperintensities. Neurology, 43(9), 1683–1689. https://doi.org/10.1212/wnl.43.9.1683
- Ferreira, L. K., & Busatto, G. F. (2013). Resting-state functional connectivity in normal brain aging. Neuroscience and biobehavioral reviews, 37(3), 384–400. https://doi.org/10.1016/j.neubiorev.2013.01.017
- Fiford, C. M., Manning, E. N., Bartlett, J. W., Cash, D. M., Malone, I. B., Ridgway, G. R., Lehmann, M., Leung, K. K., Sudre, C. H., Ourselin, S., Biessels, G. J., Carmichael, O. T., Fox, N. C., Cardoso, M. J., Barnes, J., & Alzheimer's Disease Neuroimaging Initiative (2017). White matter hyperintensities are associated with disproportionate progressive hippocampal atrophy. Hippocampus, 27(3), 249–262. https://doi.org/10.1002/hipo.22690
- Filley, C. M., & Fields, R. D. (2016). White matter and cognition: making the connection. Journal of neurophysiology, 116(5), 2093–2104. https://doi.org/10.1152/jn.00221.2016
- Fjell, A. M., Westlye, L. T., Amlien, I. K., & Walhovd, K. B. (2011). Reduced white matter integrity is related to cognitive instability. The Journal of neuroscience : the official journal of the Society for Neuroscience, 31(49), 18060–18072. https://doi.org/10.1523/JNEUROSCI.4735-11.2011
- Fjell, A. M., Sneve, M. H., Grydeland, H., Storsve, A. B., & Walhovd, K. B. (2017). The Disconnected Brain and Executive Function Decline in Aging. Cerebral cortex (New York, N.Y. : 1991), 27(3), 2303–2317. https://doi.org/10.1093/cercor/bhw082
- Fleischman, D. A., Yang, J., Arfanakis, K., Arvanitakis, Z., Leurgans, S. E., Turner, A. D., Barnes, L. L., Bennett, D. A., & Buchman, A. S. (2015). Physical activity, motor function, and white matter hyperintensity burden in healthy older adults. Neurology, 84(13), 1294–1300. https://doi.org/10.1212/WNL.0000000000001417
- Fox, M. D., Corbetta, M., Snyder, A. Z., Vincent, J. L., & Raichle, M. E. (2006). Spontaneous neuronal activity distinguishes human dorsal and ventral attention systems. Proceedings of the National Academy of Sciences of the United States of America, 103(26), 10046–10051. https://doi.org/10.1073/pnas.0604187103
- Garman R. H. (2011). Histology of the central nervous system. Toxicologic pathology, 39(1), 22–35. https://doi.org/10.1177/0192623310389621
- Garcia-Lazaro HG, Becerra-Laparra I, Cortez-Conradis D, Roldan-Valadez E (2016) Global fractional anisotropy and mean diffusivity together with segmented brain volumes assemble a predictive discriminant model for young and elderly healthy brains: a pilot study at 3T. Funct Neurol 31(1):39-46. https://doi.org/10.11138/fneur/2016.31.1.039
- Gons, R. A., van Norden, A. G., de Laat, K. F., van Oudheusden, L. J., van Uden, I. W., Zwiers, M. P., Norris, D. G., & de Leeuw, F. E. (2011). Cigarette smoking is associated with reduced microstructural integrity of cerebral white matter. Brain : a journal of neurology, 134(Pt 7), 2116–2124. https://doi.org/10.1093/brain/awr145
- Gow, A. J., Bastin, M. E., Muñoz Maniega, S., Valdés Hernández, M. C., Morris, Z., Murray, C., Royle, N. A., Starr, J. M., Deary, I. J., & Wardlaw, J. M. (2012). Neuroprotective lifestyles and the aging brain: activity, atrophy, and white matter integrity. Neurology, 79(17), 1802–1808. https://doi.org/10.1212/WNL.0b013e3182703fd2
- Grieve, S. M., Williams, L. M., Paul, R. H., Clark, C. R., & Gordon, E. (2007). Cognitive aging, executive function, and fractional anisotropy: a diffusion tensor MR imaging study. AJNR. American journal of neuroradiology, 28(2), 226–235.

- Gullett, J. M., O'Shea, A., Lamb, D. G., Porges, E. C., O'Shea, D. M., Pasternak, O., Cohen, R. A., & Woods, A. J. (2020). The association of white matter free water with cognition in older adults. NeuroImage, 219, 117040. https://doi.org/10.1016/j.neuroimage.2020.117040
- Griffanti, L., Jenkinson, M., Suri, S., Zsoldos, E., Mahmood, A., Filippini, N., Sexton, C. E., Topiwala, A., Allan, C., Kivimäki, M., Singh-Manoux, A., Ebmeier, K. P., Mackay, C. E., & Zamboni, G. (2018). Classification and characterization of periventricular and deep white matter hyperintensities on MRI: A study in older adults. NeuroImage, 170, 174–181. https://doi.org/10.1016/j.neuroimage.2017.03.024
- Habas, C., Kamdar, N., Nguyen, D., Prater, K., Beckmann, C. F., Menon, V., & Greicius, M. D. (2009). Distinct cerebellar contributions to intrinsic connectivity networks. The Journal of neuroscience : the official journal of the Society for Neuroscience, 29(26), 8586–8594. https://doi.org/10.1523/JNEUROSCI.1868-09.2009
- Habes, M., Erus, G., Toledo, J. B., Zhang, T., Bryan, N., Launer, L. J., Rosseel, Y., Janowitz, D., Doshi, J., Van der Auwera, S., von Sarnowski, B., Hegenscheid, K., Hosten, N., Homuth, G., Völzke, H., Schminke, U., Hoffmann, W., Grabe, H. J., & Davatzikos, C. (2016). White matter hyperintensities and imaging patterns of brain aging in the general population. Brain : a journal of neurology, 139(Pt 4), 1164–1179. https://doi.org/10.1093/brain/aww008
- Hase, Y., Horsburgh, K., Ihara, M., & Kalaria, R. N. (2018). White matter degeneration in vascular and other ageing-related dementias. Journal of neurochemistry, 144(5), 617–633. https://doi.org/10.1111/jnc.14271
- Hainsworth, A. H., Oommen, A. T., & Bridges, L. R. (2015). Endothelial cells and human cerebral small vessel disease. Brain pathology (Zurich, Switzerland), 25(1), 44–50. https://doi.org/10.1111/bpa.12224
- Hair, J.F., Black, W.C., Babin, B.J., Anderson, R.E., Tatham, R.L. (2010), Multivariate Data Analysis. 7th ed. New York: Pearson.
- Haxby, J. V., Horwitz, B., Ungerleider, L. G., Maisog, J. M., Pietrini, P., & Grady, C. L. (1994). The functional organization of human extrastriate cortex: a PET-rCBF study of selective attention to faces and locations. The Journal of neuroscience : the official journal of the Society for Neuroscience, 14(11 Pt 1), 6336–6353. https://doi.org/10.1523/JNEUROSCI.14-11-06336.1994
- Herrmann, L. L., Le Masurier, M., & Ebmeier, K. P. (2008). White matter hyperintensities in late life depression: a systematic review. Journal of neurology, neurosurgery, and psychiatry, 79(6), 619–624. https://doi.org/10.1136/jnnp.2007.124651
- Hoaglin DC, Iglewicz B (1987) Fine-Tuning Some Resistant Rules for Outlier Labeling. J AM STAT ASSOC 82:400, 1147-1149. https://doi.org/10.1080/01621459.1987.10478551
- Hsu JL, Leemans A, Bai CH, Lee CH, Tsai YF, Chiu HC, Chen WH (2008) Gender differences and age-related white matter changes of the human brain: a diffusion tensor imaging study. Neuroimage 39(2):566-577. https://doi.org/10.1016/j.neuroimage.2007.09.017
- Hu, R., Qiu, D., Guo, Y., Zhao, Y., Leatherday, C., Wu, J., & Allen, J. W. (2019). Variability of Resting-State Functional MRI Graph Theory Metrics across 3T Platforms. Journal of neuroimaging : official journal of the American Society of Neuroimaging, 29(3), 344–347. https://doi.org/10.1111/jon.12603
- Hugo, J., & Ganguli, M. (2014). Dementia and cognitive impairment: epidemiology, diagnosis, and treatment. Clinics in geriatric medicine, 30(3), 421–442. https://doi.org/10.1016/j.cger.2014.04.001
- Jacobi, H., Faber, J., Timmann, D., & Klockgether, T. (2021). Update cerebellum and cognition. Journal of neurology, 10.1007/s00415-021-10486-w. Advance online publication. https://doi.org/10.1007/s00415-021-10486-w
- Jeurissen, B., Descoteaux, M., Mori, S., & Leemans, A. (2019). Diffusion MRI fiber tractography of the brain. NMR in biomedicine, 32(4), e3785. https://doi.org/10.1002/nbm.3785
- Judas, M., Rados, M., Jovanov-Milosevic, N., Hrabac, P., Stern-Padovan, R., & Kostovic, I. (2005). Structural, immunocytochemical, and mr imaging properties of periventricular crossroads of growing cortical pathways in preterm infants. AJNR. American journal of neuroradiology, 26(10), 2671–2684.
- Kee Hyung Park, Lee, J. Y., Na, D. L., Kim, S. Y., Cheong, H. K., Moon, S. Y., Shim, Y. S., Park, K. W., Ku, B. D., Choi, S. H., Joo, H., Lee, J. S., Go, S. M., Kim, S. H., Kim, S., Cha, K. R., Lee, J., & Seo, S. W. (2011). Different associations of periventricular and deep white matter lesions with cognition, neuropsychiatric symptoms, and daily activities in dementia. Journal of geriatric psychiatry and neurology, 24(2), 84–90. https://doi.org/10.1177/0891988711402351
- Kennedy, D. P., & Adolphs, R. (2012). The social brain in psychiatric and neurological disorders. Trends in cognitive sciences, 16(11), 559–572. https://doi.org/10.1016/j.tics.2012.09.006
- Keřkovský, M., Stulík, J., Dostál, M., Kuhn, M., Lošák, J., Praksová, P., Hulová, M., Bednařík, J., Šprláková-Puková, A., & Mechl, M. (2019). Structural and functional MRI correlates of T2 hyperintensities of brain white matter in young neurologically asymptomatic adults. European radiology, 29(12), 7027–7036. https://doi.org/10.1007/s00330-019-06268-8
- Kim, C., Johnson, N. F., Cilles, S. E., & Gold, B. T. (2011). Common and distinct mechanisms of cognitive flexibility in prefrontal cortex. The Journal of neuroscience : the official journal of the Society for Neuroscience, 31(13), 4771–4779. https://doi.org/10.1523/JNEUROSCI.5923-10.2011
- Kiviniemi, V., Kantola, J. H., Jauhiainen, J., Hyvärinen, A., & Tervonen, O. (2003). Independent component analysis of nondeterministic fMRI signal sources. NeuroImage, 19(2 Pt 1), 253–260. https://doi.org/10.1016/s1053-8119(03)00097-1
- Kloppenborg, R. P., Nederkoorn, P. J., Geerlings, M. I., & van den Berg, E. (2014). Presence and progression of white matter hyperintensities and cognition: a meta-analysis. Neurology, 82(23), 2127–2138. https://doi.org/10.1212/WNL.0000000000000505
- Kohama, S. G., Rosene, D. L., & Sherman, L. S. (2012). Age-related changes in human and non-human primate white matter: from myelination disturbances to cognitive decline. Age (Dordrecht, Netherlands), 34(5), 1093–1110. https://doi.org/10.1007/s11357-011-9357-7
- Kulaga-Yoskovitz, J., Bernhardt, B.C., Hong, S., Mansi, T., Liang, K.E., van der Kouwe, A.J.W., Smallwood, J., Bernasconi, A., Bernasconi, N. (2015) Multi-contrast submillimetric 3Tesla hippocampal subfield segmentation protocol and dataset. Sci Data. 2, 150059.
- Kwong, K. K., Belliveau, J. W., Chesler, D. A., Goldberg, I. E., Weisskoff, R. M., Poncelet, B. P., Kennedy, D. N., Hoppel, B. E., Cohen, M. S., & Turner, R. (1992). Dynamic magnetic resonance imaging of human brain activity during primary sensory

stimulation. Proceedings of the National Academy of Sciences of the United States of America, 89(12), 5675–5679. https://doi.org/10.1073/pnas.89.12.5675

- Langen, C. D., Zonneveld, H. I., White, T., Huizinga, W., Cremers, L., de Groot, M., Ikram, M. A., Niessen, W. J., & Vernooij, M. W. (2017). White matter lesions relate to tract-specific reductions in functional connectivity. Neurobiology of aging, 51, 97–103. https://doi.org/10.1016/j.neurobiolaging.2016.12.004
- Lebel, C., & Deoni, S. (2018). The development of brain white matter microstructure. NeuroImage, 182, 207–218. https://doi.org/10.1016/j.neuroimage.2017.12.097
- Liao, X., Vasilakos, A. V., & He, Y. (2017). Small-world human brain networks: Perspectives and challenges. Neuroscience and biobehavioral reviews, 77, 286–300. https://doi.org/10.1016/j.neubiorev.2017.03.018
- Liu, H., Wang, L., Geng, Z., Zhu, Q., Song, Z., Chang, R., & Lv, H. (2016). A voxel-based morphometric study of age- and sex-related changes in white matter volume in the normal aging brain. Neuropsychiatric disease and treatment, 12, 453–465. https://doi.org/10.2147/NDT.S90674
- Liu, H., Yang, Y., Xia, Y., Zhu, W., Leak, R. K., Wei, Z., Wang, J., & Hu, X. (2017). Aging of cerebral white matter. Ageing research reviews, 34, 64–76. https://doi.org/10.1016/j.arr.2016.11.006
- Liu, Y., Liang, M., Zhou, Y., He, Y., Hao, Y., Song, M., Yu, C., Liu, H., Liu, Z., & Jiang, T. (2008). Disrupted small-world networks in schizophrenia. Brain : a journal of neurology, 131(Pt 4), 945–961. https://doi.org/10.1093/brain/awn018
- Lundgaard, I., Luzhynskaya, A., Stockley, J. H., Wang, Z., Evans, K. A., Swire, M., Volbracht, K., Gautier, H. O., Franklin, R. J., Charles Ffrench-Constant, Attwell, D., & Káradóttir, R. T. (2013). Neuregulin and BDNF induce a switch to NMDA receptor-dependent myelination by oligodendrocytes. PLoS biology, 11(12), e1001743. https://doi.org/10.1371/journal.pbio.1001743
- Lv, H., Wang, Z., Tong, E., Williams, L. M., Zaharchuk, G., Zeineh, M., Goldstein-Piekarski, A. N., Ball, T. M., Liao, C., & Wintermark, M. (2018). Resting-State Functional MRI: Everything That Nonexperts Have Always Wanted to Know. AJNR. American journal of neuroradiology, 39(8), 1390–1399. https://doi.org/10.3174/ajnr.A5527
- Mac Donald, C. L., Dikranian, K., Song, S. K., Bayly, P. V., Holtzman, D. M., & Brody, D. L. (2007). Detection of traumatic axonal injury with diffusion tensor imaging in a mouse model of traumatic brain injury. Experimental neurology, 205(1), 116–131. https://doi.org/10.1016/j.expneurol.2007.01.035
- MacPherson, S. E., Cox, S. R., Dickie, D. A., Karama, S., Starr, J. M., Evans, A. C., Bastin, M. E., Wardlaw, J. M., & Deary, I. J. (2017). Processing speed and the relationship between Trail Making Test-B performance, cortical thinning and white matter microstructure in older adults. Cortex; a journal devoted to the study of the nervous system and behavior, 95, 92–103. https://doi.org/10.1016/j.cortex.2017.07.021
- Madden, D. J., Parks, E. L., Tallman, C. W., Boylan, M. A., Hoagey, D. A., Cocjin, S. B., Packard, L. E., Johnson, M. A., Chou, Y. H., Potter, G. G., Chen, N. K., Siciliano, R. E., Monge, Z. A., Honig, J. A., & Diaz, M. T. (2017). Sources of disconnection in neurocognitive aging: cerebral white-matter integrity, resting-state functional connectivity, and white-matter hyperintensity volume. Neurobiology of aging, 54, 199–213. https://doi.org/10.1016/j.neurobiolaging.2017.01.027
- Maillard, P., Fletcher, E., Singh, B., Martinez, O., Johnson, D. K., Olichney, J. M., Farias, S. T., & DeCarli, C. (2019). Cerebral white matter free water: A sensitive biomarker of cognition and function. Neurology, 92(19), e2221–e2231. https://doi.org/10.1212/WNL.0000000000007449
- Mandonnet, E., Sarubbo, S., & Petit, L. (2018). The Nomenclature of Human White Matter Association Pathways: Proposal for a Systematic Taxonomic Anatomical Classification. Frontiers in neuroanatomy, 12, 94. https://doi.org/10.3389/fnana.2018.00094
- Marrosu, F., Portas, C., Mascia, M. S., Casu, M. A., Fà, M., Giagheddu, M., Imperato, A., & Gessa, G. L. (1995). Microdialysis measurement of cortical and hippocampal acetylcholine release during sleep-wake cycle in freely moving cats. Brain research, 671(2), 329–332. https://doi.org/10.1016/0006-8993(94)01399-3
- Marquine, M. J., Attix, D. K., Goldstein, L. B., Samsa, G. P., Payne, M. E., Chelune, G. J., & Steffens, D. C. (2010). Differential patterns of cognitive decline in anterior and posterior white matter hyperintensity progression. Stroke, 41(9), 1946–1950. https://doi.org/10.1161/STROKEAHA.110.587717
- Mascalchi, M., Bianchi, A., Basile, M., Gulino, P., Trifan, M. R., Difeo, D., Bartolini, E., Defilippi, C., & Diciotti, S. (2016). Effectiveness of 3D T2-Weighted FLAIR FSE Sequences with Fat Suppression for Detection of Brain MR Imaging Signal Changes in Children. AJNR. American journal of neuroradiology, 37(12), 2376–2381. https://doi.org/10.3174/ajnr.A4915
- McLachlan RS (2009) A brief review of the anatomy and physiology of the limbic system. Can J Neurol Sci 36 Suppl 2:S84-S87.
- Mercadante, A. A., & Tadi, P. (2020). Neuroanatomy, Gray Matter. In StatPearls. StatPearls Publishing.
- Meynert, T. (1888). Psychiatrie: Clinique des Maladies du Cerveau Antérieur Basée sur sa Structure, ses Fonctions et sa Nutrition. Trans. G. Cousot. Bruxelles: A. Manceaux.
- Mohr, J. P., Pessin, M. S., Finkelstein, S., Funkenstein, H. H., Duncan, G. W., & Davis, K. R. (1978). Broca aphasia: pathologic and clinical. Neurology, 28(4), 311–324. https://doi.org/10.1212/wnl.28.4.311
- Mok, V., Wong, K. K., Xiong, Y., Wong, A., Schmidt, R., Chu, W., Hu, X., Leung, E. Y., Chen, S., Chen, Y., Tang, W. K., Chen, X., Ho, C. L., Wong, K. S., & Wong, S. T. (2011). Cortical and frontal atrophy are associated with cognitive impairment in age-related confluent white-matter lesion. Journal of neurology, neurosurgery, and psychiatry, 82(1), 52–57. https://doi.org/10.1136/jnnp.2009.201665
- Moran, C., Phan, T. G., & Srikanth, V. K. (2012). Cerebral small vessel disease: a review of clinical, radiological, and histopathological phenotypes. International journal of stroke : official journal of the International Stroke Society, 7(1), 36–46. https://doi.org/10.1111/j.1747-4949.2011.00725.x
- Nasrallah, F. A., Yeow, L. Y., Biswal, B., & Chuang, K. H. (2015). Dependence of BOLD signal fluctuation on arterial blood CO2 and O2: Implication for resting-state functional connectivity. NeuroImage, 117, 29–39. https://doi.org/10.1016/j.neuroimage.2015.05.035
- Nieto-Castanon, A. (2020) Handbook of functional connectivity Magnetic Resonance Imaging methods in CONN. Hilbert Press

- Nordahl, C. W., Ranganath, C., Yonelinas, A. P., Decarli, C., Fletcher, E., & Jagust, W. J. (2006). White matter changes compromise prefrontal cortex function in healthy elderly individuals. Journal of cognitive neuroscience, 18(3), 418–429. https://doi.org/10.1162/089892906775990552
- Nyquist, P. A., Bilgel, M., Gottesman, R., Yanek, L. R., Moy, T. F., Becker, L. C., Cuzzocreo, J. L., Prince, J., Wasserman, B. A., Yousem, D. M., Becker, D. M., Kral, B. G., & Vaidya, D. (2015). Age differences in periventricular and deep white matter lesions. Neurobiology of aging, 36(4), 1653–1658. https://doi.org/10.1016/j.neurobiolaging.2015.01.005
- O'Donnell, L. J., & Westin, C. F. (2011). An introduction to diffusion tensor image analysis. Neurosurgery clinics of North America, 22(2), 185–viii. https://doi.org/10.1016/j.nec.2010.12.004
- O'Sullivan, M., Jones, D. K., Summers, P. E., Morris, R. G., Williams, S. C., & Markus, H. S. (2001). Evidence for cortical "disconnection" as a mechanism of age-related cognitive decline. Neurology, 57(4), 632–638. https://doi.org/10.1212/wnl.57.4.632
- Patel A, Biso GMNR, Fowler JB (2020) Neuroanatomy, Temporal Lobe. In StatPearls. StatPearls Publishing
- Porcu M, Craboledda D, Garofalo P, Barberini L, Sanfilippo R, Zaccagna F, Wintermark M, Montisci R, Saba L (2019a) Reorganization of brain networks following carotid endarterectomy: an exploratory study using resting state functional connectivity with a focus on the changes in Default Mode Network connectivity. Eur J Radiol 110:233-241. https://doi.org/10.1016/j.ejrad.2018.12.007
- Porcu, M., Wintermark, M., Suri, J. S., & Saba, L. (2019). The influence of the volumetric composition of the intracranial space on neural activity in healthy subjects: a resting-state functional magnetic resonance study. The European journal of neuroscience, 10.1111/ejn.14627. Advance online publication. https://doi.org/10.1111/ejn.14627
- Porcu, M., Operamolla, A., Scapin, E., Garofalo, P., Destro, F., Caneglias, A., Suri, J. S., Falini, A., Defazio, G., Marrosu, F., & Saba, L. (2020a). Effects of White Matter Hyperintensities on Brain Connectivity and Hippocampal Volume in Healthy Subjects According to Their Localization. Brain connectivity, 10(8), 436–447. https://doi.org/10.1089/brain.2020.0774
- Porcu, M., Garofalo, P., Craboledda, D., Suri, J. S., Suri, H. S., Montisci, R., Sanfilippo, R., & Saba, L. (2020b). Carotid artery stenosis and brain connectivity: the role of white matter hyperintensities. Neuroradiology, 62(3), 377–387. https://doi.org/10.1007/s00234-019-02327-5
- Porcu, M., Sanfilippo, R., Montisci, R., Balestrieri, A., Suri, J. S., Wintermark, M., & Saba, L. (2020c). White-matter hyperintensities in patients with carotid artery stenosis: An exploratory connectometry study. The neuroradiology journal, 33(6), 486–493. https://doi.org/10.1177/1971400920959323
- Porcu, M., Wintermark, M., Suri, J. S., & Saba, L. (2020d). The influence of the volumetric composition of the intracranial space on neural activity in healthy subjects: a resting-state functional magnetic resonance study. The European journal of neuroscience, 51(9), 1944–1961. https://doi.org/10.1111/ejn.14627
- Porcu, M., Cocco, L., Puig, J., Mannelli, L., Yang, Q., Suri, J. S., Defazio, G., & Saba, L. (2021a). Global Fractional Anisotropy: Effect on Resting-state Neural Activity and Brain Networking in Healthy Participants. Neuroscience, 472, 103–115. https://doi.org/10.1016/j.neuroscience.2021.07.021Salat D. H. (2011). The declining infrastructure of the aging brain. Brain connectivity, 1(4), 279–293. https://doi.org/10.1089/brain.2011.0056
- Porcu, M., Cocco, L., Cocozza, S., Pontillo, G., Operamolla, A., Defazio, G., Suri, J. S., Brunetti, A., & Saba, L. (2021b). The association between white matter hyperintensities, cognition and regional neural activity in healthy subjects. The European journal of neuroscience, 54(4), 5427–5443. https://doi.org/10.1111/ejn.15403
- Power JD, Mitra A, Laumann TO, Snyder AZ, Schlaggar BL (2014) Petersen SE. Methods to detect, characterize, and remove motion artifact in resting state fMRI. Neuroimage 84:320-341. https://doi.org/10.1016/j.neuroimage.2013.08.048
- Prins, N. D., & Scheltens, P. (2015). White matter hyperintensities, cognitive impairment and dementia: an update. Nature reviews. Neurology, 11(3), 157–165. https://doi.org/10.1038/nrneurol.2015.10
- Raichle M. E. (2015). The brain's default mode network. Annual review of neuroscience, 38, 433–447. https://doi.org/10.1146/annurev-neuro-071013-014030
- Raichle, M. E., MacLeod, A. M., Snyder, A. Z., Powers, W. J., Gusnard, D. A., & Shulman, G. L. (2001). A default mode of brain function. Proceedings of the National Academy of Sciences of the United States of America, 98(2), 676–682. https://doi.org/10.1073/pnas.98.2.676
- Rawji, K. S., & Yong, V. W. (2013). The benefits and detriments of macrophages/microglia in models of multiple sclerosis. Clinical & developmental immunology, 2013, 948976. https://doi.org/10.1155/2013/948976
- Reginold, W., Sam, K., Poublanc, J., Fisher, J., Crawley, A., & Mikulis, D. J. (2018). Impact of white matter hyperintensities on surrounding white matter tracts. Neuroradiology, 60(9), 933–944. https://doi.org/10.1007/s00234-018-2053-x
- Rehman, A., & Al Khalili, Y. (2020). Neuroanatomy, Occipital Lobe. In StatPearls. StatPearls Publishing.
- Reitan, R. M. (1992) Trail making test A & B. Reitan Neuropsychology Laboratory
- Reitan, R. M. & Wolfson, D. (1988) Traumatic brain injury. Vol. II. Recovery and rehabilitation. Tucson, AZ: Neuropsy-chology Press.
- Reijmer, Y. D., Schultz, A. P., Leemans, A., O'Sullivan, M. J., Gurol, M. E., Sperling, R., Greenberg, S. M., Viswanathan, A., & Hedden, T. (2015). Decoupling of structural and functional brain connectivity in older adults with white matter hyperintensities. NeuroImage, 117, 222–229. https://doi.org/10.1016/j.neuroimage.2015.05.054
- Riphagen, J. M., Gronenschild, E., Salat, D. H., Freeze, W. M., Ivanov, D., Clerx, L., Verhey, F., Aalten, P., & Jacobs, H. (2018). Shades of white: diffusion properties of T1- and FLAIR-defined white matter signal abnormalities differ in stages from cognitively normal to dementia. Neurobiology of aging, 68, 48–58. https://doi.org/10.1016/j.neurobiolaging.2018.03.029
- Romero, J. E., Coupé, P., & Manjón, J. V. (2017). HIPS: A new hippocampus subfield segmentation method. NeuroImage, 163, 286–295. https://doi.org/10.1016/j.neuroimage.2017.09.049
- Sabayan, B., van der Grond, J., Westendorp, R. G., van Buchem, M. A., & de Craen, A. J. (2015). Accelerated progression of white matter hyperintensities and subsequent risk of mortality: a 12-year follow-up study. Neurobiology of aging, 36(6), 2130–2135. https://doi.org/10.1016/j.neurobiolaging.2015.03.003

- Sachdev, P. S., Parslow, R., Wen, W., Anstey, K. J., & Easteal, S. (2009). Sex differences in the causes and consequences of white matter hyperintensities. Neurobiology of aging, 30(6), 946–956. https://doi.org/10.1016/j.neurobiolaging.2007.08.023
- Salvadó, G., Brugulat-Serrat, A., Sudre, C. H., Grau-Rivera, O., Suárez-Calvet, M., Falcon, C., Fauria, K., Cardoso, M. J., Barkhof, F., Molinuevo, J. L., Gispert, J. D., & ALFA Study (2019). Spatial patterns of white matter hyperintensities associated with Alzheimer's disease risk factors in a cognitively healthy middle-aged cohort. Alzheimer's research & therapy, 11(1), 12. https://doi.org/10.1186/s13195-018-0460-1
- Schilling, K. G., Yeh, F. C., Nath, V., Hansen, C., Williams, O., Resnick, S., Anderson, A. W., & Landman, B. A. (2019). A fiber coherence index for quality control of B-table orientation in diffusion MRI scans. Magnetic resonance imaging, 58, 82–89. https://doi.org/10.1016/j.mri.2019.01.018
- Schmahmann, J. D., & Sherman, J. C. (1998). The cerebellar cognitive affective syndrome. Brain : a journal of neurology, 121 (Pt 4), 561–579. https://doi.org/10.1093/brain/121.4.561
- Schmahmann, J. D., Smith, E. E., Eichler, F. S., & Filley, C. M. (2008). Cerebral white matter: neuroanatomy, clinical neurology, and neurobehavioral correlates. Annals of the New York Academy of Sciences, 1142, 266–309. https://doi.org/10.1196/annals.1444.017
- Schmidt, R., Ropele, S., Enzinger, C., Petrovic, K., Smith, S., Schmidt, H., Matthews, P. M., & Fazekas, F. (2005). White matter lesion progression, brain atrophy, and cognitive decline: the Austrian stroke prevention study. Annals of neurology, 58(4), 610–616. https://doi.org/10.1002/ana.20630
- Schmidt, R., Berghold, A., Jokinen, H., Gouw, A. A., van der Flier, W. M., Barkhof, F., Scheltens, P., Petrovic, K., Madureira, S., Verdelho, A., Ferro, J. M., Waldemar, G., Wallin, A., Wahlund, L. O., Poggesi, A., Pantoni, L., Inzitari, D., Fazekas, F., Erkinjuntti, T., & LADIS Study Group (2012). White matter lesion progression in LADIS: frequency, clinical effects, and sample size calculations. Stroke, 43(10), 2643–2647. https://doi.org/10.1161/STROKEAHA.112.662593
- Shan, Y., Tan, S., Wang, Y., Li, K., Zhang, L., Liao, S., Zhou, L., Deng, Z., Hu, X., Li, H., Men, X., Zhang, B., Peng, L., Kang, Z., Zou, Y., & Lu, Z. (2017). Risk Factors and Clinical Manifestations of Juxtacortical Small Lesions: A Neuroimaging Study. Frontiers in neurology, 8, 497. https://doi.org/10.3389/fneur.2017.00497
- Sivakumar, L., Riaz, P., Kate, M., Jeerakathil, T., Beaulieu, C., Buck, B., Camicioli, R., & Butcher, K. (2017). White matter hyperintensity volume predicts persistent cognitive impairment in transient ischemic attack and minor stroke. International journal of stroke : official journal of the International Stroke Society, 12(3), 264–272. https://doi.org/10.1177/1747493016676612
- Smith, S. M., & Nichols, T. E. (2009). Threshold-free cluster enhancement: addressing problems of smoothing, threshold dependence and localisation in cluster inference. NeuroImage, 44(1), 83–98. https://doi.org/10.1016/j.neuroimage.2008.03.061
- Soares, J. M., Marques, P., Alves, V., & Sousa, N. (2013). A hitchhiker's guide to diffusion tensor imaging. Frontiers in neuroscience, 7, 31. https://doi.org/10.3389/fnins.2013.00031
- Song, S. K., Yoshino, J., Le, T. Q., Lin, S. J., Sun, S. W., Cross, A. H., & Armstrong, R. C. (2005). Demyelination increases radial diffusivity in corpus callosum of mouse brain. NeuroImage, 26(1), 132–140. https://doi.org/10.1016/j.neuroimage.2005.01.028
- Springo, Z., Tarantini, S., Toth, P., Tucsek, Z., Koller, A., Sonntag, W. E., Csiszar, A., & Ungvari, Z. (2015). Aging Exacerbates Pressure-Induced Mitochondrial Oxidative Stress in Mouse Cerebral Arteries. The journals of gerontology. Series A, Biological sciences and medical sciences, 70(11), 1355–1359. https://doi.org/10.1093/gerona/glu244
- Stadelmann, C., Timmler, S., Barrantes-Freer, A., & Simons, M. (2019). Myelin in the Central Nervous System: Structure, Function, and Pathology. Physiological reviews, 99(3), 1381–1431. https://doi.org/10.1152/physrev.00031.2018
- Stahon, K. E., Bastian, C., Griffith, S., Kidd, G. J., Brunet, S., & Baltan, S. (2016). Age-Related Changes in Axonal and Mitochondrial Ultrastructure and Function in White Matter. The Journal of neuroscience : the official journal of the Society for Neuroscience, 36(39), 9990–10001. https://doi.org/10.1523/JNEUROSCI.1316-16.2016
- Strassburger, T. L., Lee, H. C., Daly, E. M., Szczepanik, J., Krasuski, J. S., Mentis, M. J., Salerno, J. A., DeCarli, C., Schapiro, M. B., & Alexander, G. E. (1997). Interactive effects of age and hypertension on volumes of brain structures. Stroke, 28(7), 1410–1417. https://doi.org/10.1161/01.str.28.7.1410
- Sugiyama, I., Tanaka, K., Akita, M., Yoshida, K., Kawase, T., & Asou, H. (2002). Ultrastructural analysis of the paranodal junction of myelinated fibers in 31-month-old-rats. Journal of neuroscience research, 70(3), 309–317. https://doi.org/10.1002/jnr.10386
- Sun, J., Tong, S., & Yang, G. Y. (2012). Reorganization of Brain Networks in Aging and Age-related Diseases. Aging and disease, 3(2), 181–193.
- Tamura, Y., & Araki, A. (2015). Diabetes mellitus and white matter hyperintensity. Geriatrics & gerontology international, 15 Suppl 1, 34–42. https://doi.org/10.1111/ggi.12666
- Teipel SJ, Bokde AL, Meindl T, Amaro E Jr, Soldner J, Reiser MF, Herpertz SC, Möller HJ, Hampel H (2010) White matter microstructure underlying default mode network connectivity in the human brain. Neuroimage 49(3):2021-2032. https://doi.org/10.1016/j.neuroimage.2009.10.067
- Thau, L., Reddy, V., & Singh, P. (2021). Anatomy, Central Nervous System. In StatPearls. StatPearls Publishing.
- The LADIS Study Group, Poggesi, A., Pantoni, L., Inzitari, D., Fazekas, F., Ferro, J., O'Brien, J., Hennerici, M., Scheltens, P., Erkinjuntti, T., Visser, M., Langhorne, P., Chabriat, H., Waldemar, G., Wallin, A., & Wahlund, A. (2011). 2001-2011: A Decade of the LADIS (Leukoaraiosis And DISability) Study: What Have We Learned about White Matter Changes and Small-Vessel Disease?. Cerebrovascular diseases (Basel, Switzerland), 32(6), 577–588. https://doi.org/10.1159/000334498
- Tomasi, D., & Volkow, N. D. (2010). Functional connectivity density mapping. Proceedings of the National Academy of Sciences of the United States of America, 107(21), 9885–9890. https://doi.org/10.1073/pnas.1001414107
- Tononi, G., Sporns, O., & Edelman, G. M. (1994). A measure for brain complexity: relating functional segregation and integration in the nervous system. Proceedings of the National Academy of Sciences of the United States of America, 91(11), 5033–5037. https://doi.org/10.1073/pnas.91.11.5033
- Tubi, M. A., Feingold, F. W., Kothapalli, D., Hare, E. T., King, K. S., Thompson, P. M., Braskie, M. N., & Alzheimer's Disease Neuroimaging Initiative (2020). White matter hyperintensities and their relationship to cognition: Effects of segmentation algorithm. NeuroImage, 206, 116327.

- Tzourio-Mazoyer, N., Landeau, B., Papathanassiou, D., Crivello, F., Etard, O., Delcroix, N., Mazoyer, B., & Joliot, M. (2002). Automated anatomical labeling of activations in SPM using a macroscopic anatomical parcellation of the MNI MRI single-subject brain. NeuroImage, 15(1), 273–289. https://doi.org/10.1006/nimg.2001.0978
- Uddin, L. Q., Yeo, B., & Spreng, R. N. (2019). Towards a Universal Taxonomy of Macro-scale Functional Human Brain Networks. Brain topography, 32(6), 926–942. https://doi.org/10.1007/s10548-019-00744-6
- Ungvari, Z., Kaley, G., de Cabo, R., Sonntag, W. E., & Csiszar, A. (2010). Mechanisms of vascular aging: new perspectives. The journals of gerontology. Series A, Biological sciences and medical sciences, 65(10), 1028–1041. https://doi.org/10.1093/gerona/glq113
- van Hemmen J, Saris IMJ, Cohen-Kettenis PT, Veltman DJ, Pouwels PJW, Bakker J (2017) Sex Differences in White Matter Microstructure in the Human Brain Predominantly Reflect Differences in Sex Hormone Exposure. Cereb Cortex 27(5):2994-3001. https://doi.org/10.1093/cercor/bhw156
- Vazzana, R., Bandinelli, S., Lauretani, F., Volpato, S., Lauretani, F., Di Iorio, A., Abate, M., Corsi, A. M., Milaneschi, Y., Guralnik, J. M., & Ferrucci, L. (2010). Trail Making Test predicts physical impairment and mortality in older persons. Journal of the American Geriatrics Society, 58(4), 719–723. https://doi.org/10.1111/j.1532-5415.2010.02780.x
- Vernooij, M. W., Ikram, M. A., Vrooman, H. A., Wielopolski, P. A., Krestin, G. P., Hofman, A., Niessen, W. J., Van der Lugt, A., & Breteler, M. M. (2009). White matter microstructural integrity and cognitive function in a general elderly population. Archives of general psychiatry, 66(5), 545–553. https://doi.org/10.1001/archgenpsychiatry.2009.5
- von Bohlen und Halbach, O., & Unsicker, K. (2002). Morphological alterations in the amygdala and hippocampus of mice during ageing. The European journal of neuroscience, 16(12), 2434–2440. https://doi.org/10.1046/j.1460-9568.2002.02405.x
- Wade RG, Teh I, Andersson G, Yeh FC, Wiberg M, Bourke G (2021) Fractional anisotropy thresholding for deterministic tractography of the roots of the brachial plexus. Sci Rep 11(1):80. https://doi.org/10.1038/s41598-020-79840-8
- Walhovd, K. B., Johansen-Berg, H., & Káradóttir, R. T. (2014). Unraveling the secrets of white matter--bridging the gap between cellular, animal and human imaging studies. Neuroscience, 276(100), 2–13. https://doi.org/10.1016/j.neuroscience.2014.06.058
- Wang, Z., Williams, V. J., Stephens, K. A., Kim, C. M., Bai, L., Zhang, M., & Salat, D. H. (2020). The effect of white matter signal abnormalities on default mode network connectivity in mild cognitive impairment. Human brain mapping, 41(5), 1237–1248. https://doi.org/10.1002/hbm.24871
- Wang, Y., Meng, R., Liu, G., Cao, C., Chen, F., Jin, K., Ji, X., & Cao, G. (2019). Intracranial atherosclerotic disease. Neurobiology of disease, 124, 118–132. https://doi.org/10.1016/j.nbd.2018.11.008
- Warbrick T, Rosenberg J, Shah NJ (2017) The relationship between BOLD fMRI response and the underlying white matter as measured by fractional anisotropy (FA): A systematic review. Neuroimage 153:369-381. https://doi.org/10.1016/j.neuroimage.2016.12.075
- Wardlaw, J. M., Smith, E. E., Biessels, G. J., Cordonnier, C., Fazekas, F., Frayne, R., Lindley, R. I., O'Brien, J. T., Barkhof, F., Benavente, O. R., Black, S. E., Brayne, C., Breteler, M., Chabriat, H., Decarli, C., de Leeuw, F. E., Doubal, F., Duering, M., Fox, N. C., Greenberg, S., … STandards for ReportIng Vascular changes on nEuroimaging (STRIVE v1) (2013). Neuroimaging standards for research into small vessel disease and its contribution to ageing and neurodegeneration. The Lancet. Neurology, 12(8), 822–838. https://doi.org/10.1016/S1474-4422(13)70124-8
- Wardlaw, J. M., Valdés Hernández, M. C., & Muñoz-Maniega, S. (2015). What are white matter hyperintensities made of? Relevance to vascular cognitive impairment. Journal of the American Heart Association, 4(6), 001140. https://doi.org/10.1161/JAHA.114.001140
- Wassenaar, T. M., Yaffe, K., van der Werf, Y. D., & Sexton, C. E. (2019). Associations between modifiable risk factors and white matter of the aging brain: insights from diffusion tensor imaging studies. Neurobiology of aging, 80, 56–70. https://doi.org/10.1016/j.neurobiolaging.2019.04.006
- Watts, D. J., & Strogatz, S. H. (1998). Collective dynamics of 'small-world' networks. Nature, 393(6684), 440–442. https://doi.org/10.1038/30918
- Weaver AH (2005) Reciprocal evolution of the cerebellum and neocortex in fossil humans. Proc Natl Acad Sci U S A 102(10):3576-3580. https://doi.org/10.1073/pnas.0500692102
- Whitfield-Gabrieli S, Nieto-Castanon A (2012) Conn: a functional connectivity toolbox for correlated and anticorrelated brain networks. Brain Connect. 2(3):125-141. https://doi.org/10.1089/brain.2012.0073
- Williamson, J. M., & Lyons, D. A. (2018). Myelin Dynamics Throughout Life: An Ever-Changing Landscape?. Frontiers in cellular neuroscience, 12, 424. https://doi.org/10.3389/fncel.2018.00424
- Wycoco, V., Shroff, M., Sudhakar, S., & Lee, W. (2013). White matter anatomy: what the radiologist needs to know. Neuroimaging clinics of North America, 23(2), 197–216. https://doi.org/10.1016/j.nic.2012.12.002
- Winklewski, P. J., Sabisz, A., Naumczyk, P., Jodzio, K., Szurowska, E., & Szarmach, A. (2018). Understanding the Physiopathology Behind Axial and Radial Diffusivity Changes-What Do We Know?. Frontiers in neurology, 9, 92. https://doi.org/10.3389/fneur.2018.00092
- Worsley, K. J., Marrett, S., Neelin, P., Vandal, A. C., Friston, K. J., & Evans, A. C. (1996). A unified statistical approach for determining significant signals in images of cerebral activation. Human brain mapping, 4(1), 58–73. https://doi.org/10.1002/(SICI)1097-0193(1996)4:1<58::AID-HBM4>3.0.CO;2-O
- Wright, C. B., Festa, J. R., Paik, M. C., Schmiedigen, A., Brown, T. R., Yoshita, M., DeCarli, C., Sacco, R., & Stern, Y. (2008). White matter hyperintensities and subclinical infarction: associations with psychomotor speed and cognitive flexibility. Stroke, 39(3), 800–805. https://doi.org/10.1161/STROKEAHA.107.484147
- Xing, Y., Yang, J., Zhou, A., Wang, F., Wei, C., Tang, Y., & Jia, J. (2021). White Matter Fractional Anisotropy Is a Superior Predictor for Cognitive Impairment Than Brain Volumes in Older Adults With Confluent White Matter Hyperintensities. Frontiers in psychiatry, 12, 633811. https://doi.org/10.3389/fpsyt.2021.633811
- Yang AC, Tsai SJ, Liu ME, Huang CC, Lin CP (2016) The Association of Aging with White Matter Integrity and Functional Connectivity Hubs. Front Aging Neurosci. 8:143. Published 2016 Jun 15. https://doi.org/10.3389/fnagi.2016.00143

- Yang, T., Sun, Y., Lu, Z., Leak, R. K., & Zhang, F. (2017). The impact of cerebrovascular aging on vascular cognitive impairment and dementia. Ageing research reviews, 34, 15–29. https://doi.org/10.1016/j.arr.2016.09.007
- Yeh FC (2020) Shape analysis of the human association pathways. Neuroimage 223:117329. https://doi.org/10.1016/j.neuroimage.2020.117329
- Yeh FC, Verstynen TD, Wang Y, Fernández-Miranda JC, Tseng WY (2013) Deterministic diffusion fiber tracking improved by quantitative anisotropy. PLoS One 8(11):e80713. https://doi.org/10.1371/journal.pone.0080713
- Yeo, B. T., Krienen, F. M., Sepulcre, J., Sabuncu, M. R., Lashkari, D., Hollinshead, M., Roffman, J. L., Smoller, J. W., Zöllei, L., Polimeni, J. R., Fischl, B., Liu, H., & Buckner, R. L. (2011). The organization of the human cerebral cortex estimated by intrinsic functional connectivity. Journal of neurophysiology, 106(3), 1125–1165. https://doi.org/10.1152/jn.00338.2011
- Young, V. G., Halliday, G. M., & Kril, J. J. (2008). Neuropathologic correlates of white matter hyperintensities. Neurology, 71(11), 804–811. https://doi.org/10.1212/01.wnl.0000319691.50117.54
- Yu W, Krook-Magnuson E (2015) Cognitive Collaborations: Bidirectional Functional Connectivity Between the Cerebellum and the Hippocampus. Frontiers in systems neuroscience, 9, 177. https://doi.org/10.3389/fnsys.2015.00177
- Yuan, P., & Raz, N. (2014). Prefrontal cortex and executive functions in healthy adults: a meta-analysis of structural neuroimaging studies. Neuroscience and biobehavioral reviews, 42, 180–192. https://doi.org/10.1016/j.neubiorev.2014.02.005
- Zang, Y., Jiang, T., Lu, Y., He, Y., & Tian, L. (2004). Regional homogeneity approach to fMRI data analysis. NeuroImage, 22(1), 394–400. https://doi.org/10.1016/j.neuroimage.2003.12.030
- Zang, Y. F., He, Y., Zhu, C. Z., Cao, Q. J., Sui, M. Q., Liang, M., Tian, L. X., Jiang, T. Z., & Wang, Y. F. (2007). Altered baseline brain activity in children with ADHD revealed by resting-state functional MRI. Brain & development, 29(2), 83–91. https://doi.org/10.1016/j.braindev.2006.07.002
- Zatorre, R. J., Fields, R. D., & Johansen-Berg, H. (2012). Plasticity in gray and white: neuroimaging changes in brain structure during learning. Nature neuroscience, 15(4), 528–536. https://doi.org/10.1038/nn.3045
- Zhang J. (2010). Diffusion tensor imaging of white matter pathology in the mouse brain. Imaging in medicine, 2(6), 623–632. https://doi.org/10.2217/iim.10.60
- Zhu, Y., Lu, T., Xie, C., Wang, Q., Wang, Y., Cao, X., Su, Y., Wang, Z., & Zhang, Z. (2020). Functional Disorganization of Small-World Brain Networks in Patients With Ischemic Leukoaraiosis. Frontiers in aging neuroscience, 12, 203. https://doi.org/10.3389/fnagi.2020.00203
- Zhuang, F. J., Chen, Y., He, W. B., & Cai, Z. Y. (2018). Prevalence of white matter hyperintensities increases with age. Neural regeneration research, 13(12), 2141–2146. https://doi.org/10.4103/1673-5374.241465
- Zou, Q. H., Zhu, C. Z., Yang, Y., Zuo, X. N., Long, X. Y., Cao, Q. J., Wang, Y. F., & Zang, Y. F. (2008). An improved approach to detection of amplitude of low-frequency fluctuation (ALFF) for resting-state fMRI: fractional ALFF. Journal of neuroscience methods, 172(1), 137–141. https://doi.org/10.1016/j.jneumeth.2008.04.012
- Zuo, X. N., Kelly, C., Adelstein, J. S., Klein, D. F., Castellanos, F. X., & Milham, M. P. (2010). Reliable intrinsic connectivity networks: test-retest evaluation using ICA and dual regression approach. NeuroImage, 49(3), 2163–2177. https://doi.org/10.1016/j.neuroimage.2009.10.080
- Zuo, X. N., & Xing, X. X. (2014). Test-retest reliabilities of resting-state FMRI measurements in human brain functional connectomics: a systems neuroscience perspective. Neuroscience and biobehavioral reviews, 45, 100–118. https://doi.org/10.1016/j.neubiorev.2014.05.009